DESIGN TOOLS AND PREDICTIONS FOR NONLINEAR ELASTIC SOLIDS IN SOFT MACHINE DESIGN

BY

CAROLYN N. DARLING

THESIS

Submitted in partial fulfillment of the requirements
for the degree of Master of Science in Mechanical Engineering
in the Graduate College of the
University of Illinois at Urbana-Champaign, 2020

Urbana, Illinois

Adviser:

Randy H. Ewoldt

ABSTRACT

Soft machine design is a new frontier for using and designing rheologically complex materials, however we lack a systematic design toolbox for such efforts.

We study existing design tools (Chapter 1), identify limitations (Chapter 1), and present new design tools (Chapter 2) for rheologically-complex soft solids. We identify material properties and features that may be vital for optimal soft machine performance, such as intrinsic nonlinearities, variable stiffness, and strain to break. Keeping these properties in mind, we explore new design-based organizations of knowledge, including design motivated constitutive modeling and Ashby-style material selection charts. As a result, we develop new Ashby-style diagrams with properties not typically reported, include soft materials that tend to be missing from material databases, and organize knowledge in a way that streamlines material selection for soft machines. Soft robot actuators, grippers, and skins, as well as medical devices, are just a few of the many soft systems that may benefit from the proposed soft machine design tools.

After discussing limitations of the current state of soft machine design and making contributions to soft machine design tools that support the 'design with' materials, we study mathematical models to support the 'design of' nonlinear elastic functional solids for soft machines (Chapter 3). We study the behavior of magnetorheological elastomers (MRE's), and specifically the effect that nonlinearity and softness have on the variable shear stiffness response of MRE's. We find surprising results, where a higher degree of nonlinearity can either stiffen or soften the variable shear stiffness response depending on competing magnetic and nonlinear elastic free energy contributions. We define three different regimes where we expect the elastic nonlinearity of a MRE to have a different effect on the variable shear stiffness of the composite. These functional materials are building blocks for soft

machine design and the variable stiffness is often studied aiming to increase material functionality.

There are many constitutive models for nonlinear elastic solids that are often used in design. These constitutive equations have been studied thoroughly under a typical deformation, such as uniaxial stretch and simple shear independently. However, a common deformation in MRE's is a combination of an imposed uniaxial stretch when a magnetic field is induced and external simple shear deformation. We study these constitutive models under an initial uniaxial stretch (pre-strain) and imposed simple shear to understand the effect on shear stiffness (Chapter 4). Surprisingly, we find that many of the constitutive models that were studied shear soften in compression. Some models eventually shear stiffen in compression when a finite elastic strain is achieved. We find that these predictions align with bio-polymer networks and semi-flexible fibers that also shear soften in compression. However, these models do not capture the behavior of biological tissues that shear stiffen in compression. We provide insight to the constitutive model predictions by referencing single chain models and making a connection to the chain extension ratio.

Throughout this thesis, we aim to make a contribution to knowledge through studies that support the 'design with' nonlinear elastic solids and the 'design of' nonlinear elastic solids specific to soft machine design.

To my family.

ACKNOWLEDGMENTS

I would like to thank my family and friends for their unconditional support throughout my time in graduate school. I am also very thankful for my advisor Randy Ewoldt for his exceptional support and guidance, and for inspiring a passion for learning. I am very grateful to my desk neighbor Gaurav Chaudhary for welcoming me into the group, challenging me, and encouraging me. Thank you to Tanver Hossain for reading this work and providing feedback. Many thanks to other past and present members of the Ewoldt group, namely, Samya Sen and Yilin Wang.

TABLE OF CONTENTS

LIST OF TABLES

LIST OF FIGURES

CHAPTER 1

A REVIEW: SOFT MACHINE DESIGN

1.1 Introduction

In a traditional sense, a machine or robot is imagined as a complex system of many rigid components attached by joints that function together in a highly controlled manner. Humans have successfully built these traditional rigid machines for centuries. The Mars rover that was launched in 2011 by NASA, the first successful airplane invented in 1903 by the Wright brothers, and the wheel and axle first invented around 3500 B.C. are all examples of these successful traditional machines throughout human history. Thus, the design process and design tools are well-developed for traditional machine design as discussed in many popular books such as *Mechanical Engineering Design* by *Joseph Shigley* and *Material Selection in Mechanical Design* by *Michael F. Ashby* [2, 13].

However, emerging applications in assistive devices, soft robotics, medicine, aerospace, exploration, and wearable electronics require a final design that is flexible and able to conform to its surroundings to operate in many different environments. This requires the use of soft solids, gels, foams, functional composites, and/or rheologically complex fluids in the final design, creating a new frontier for using rheologically complex materials. While the machine design process and design tools have been well-developed for traditional machines, these new soft machine applications require a new systematic soft machine design process, new soft machine design tools, and new soft materials to create successful machines using vastly different rheologically complex materials, such as nonlinear elastic solids.

In this chapter, the current state of soft machine design is reviewed and limitations are discussed. Evaluating the current state of soft machine design is a preliminary step to creating successful design tools that will be discussed

in later chapters.

1.2 Soft machine design process

There is no single unique machine design solution for a given problem, so a 'good' solution may be difficult to develop and many design iterations may occur. However, to be successful at machine design, it is a requirement to make appropriate design decisions at the appropriate time. To support making a 'good' design decision and overcoming several competing and difficult-to-define design objectives, the designer should use creative thinking, available design tools, and follow a systematic design process [2, 14]. In regards to designing soft machines, the designer is often guided by intuition and bio-inspiration instead of a systematic process, which can be problematic since design decisions should be made at the appropriate time in order to consider all design possibilities for the development of successful soft machines [15].

To the best of my knowledge, the only thoroughly defined soft robotic design process was introduced in 2018 and can be seen in Figure 1.1 [1]. It can be applied to soft machines in general and was designed for soft robotics specifically. A case study is also included on designing a gecko-inspired, climbing soft robot. The design process includes steps of (i) defining a task, (ii) searching for a solution, (iii) conceptual design, (iv) mechanical modeling, (v) embodiment design, and (vi) final realization. Where the conceptual design step is dependent on the pool of soft elements that include actuators, pumps, valves, sensors, etc., and the embodiment design step is dependent on the types of fabrication that include casting methods, 3D printing, etc. This design process mainly differs from traditional machine design processes, such as Shigley's machine design process shown in Figure 1.2, by considering bio-inspired design, rheologically complex materials, soft elements, and different fabrication methods.

A method for designing bio-inspired robots was also proposed in 2014 and can be seen in Figure 1.3 [3]. While this method was designed for bio-inspired robots specifically, it can be applied to many soft machines in general, given that many natural biological machines are soft. The structure of this design process has three significant steps that include (i) inspire, (ii) abstract, and (iii) implement. While there is variance in this bio-inspired robotic design

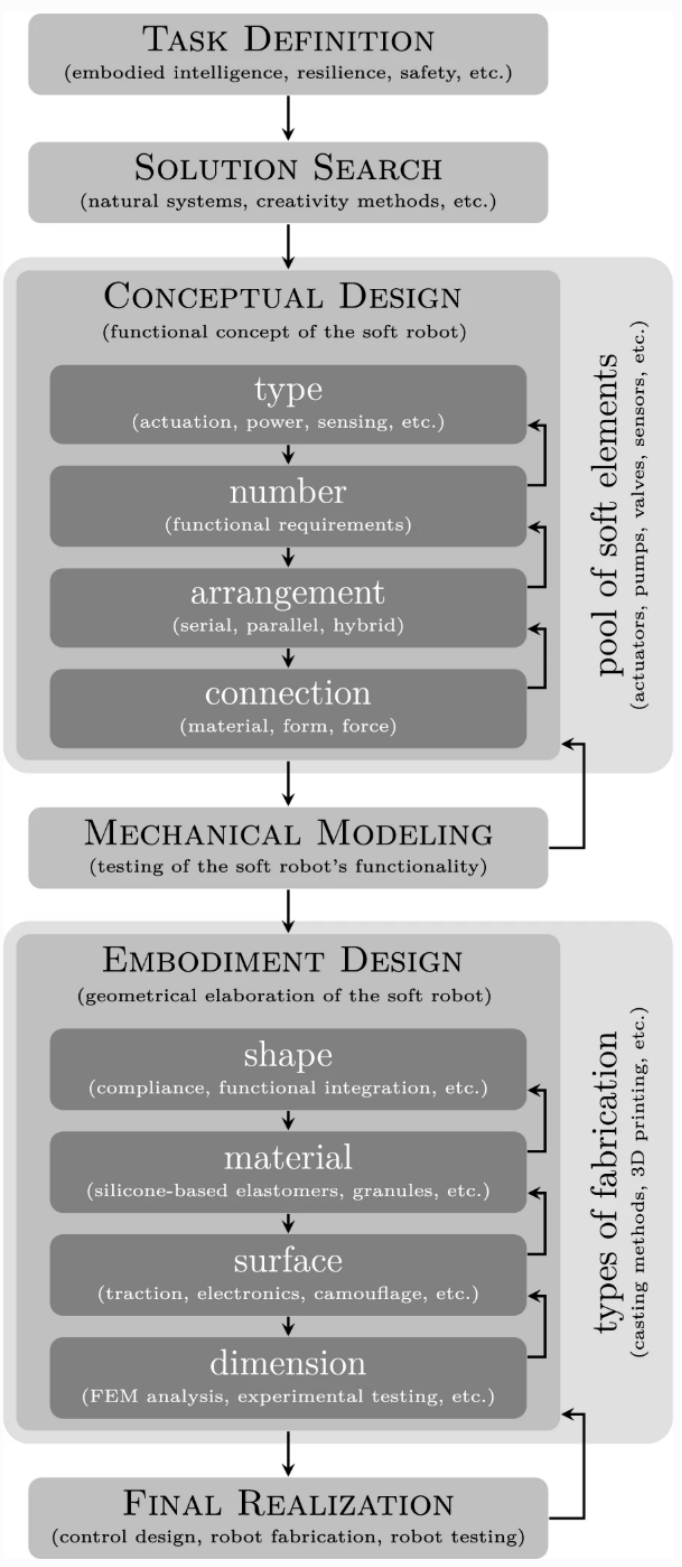

Figure 1.1: Systematic soft robot design methodology proposed by Schiller and Seibel (image from Figure 1 in [1]).

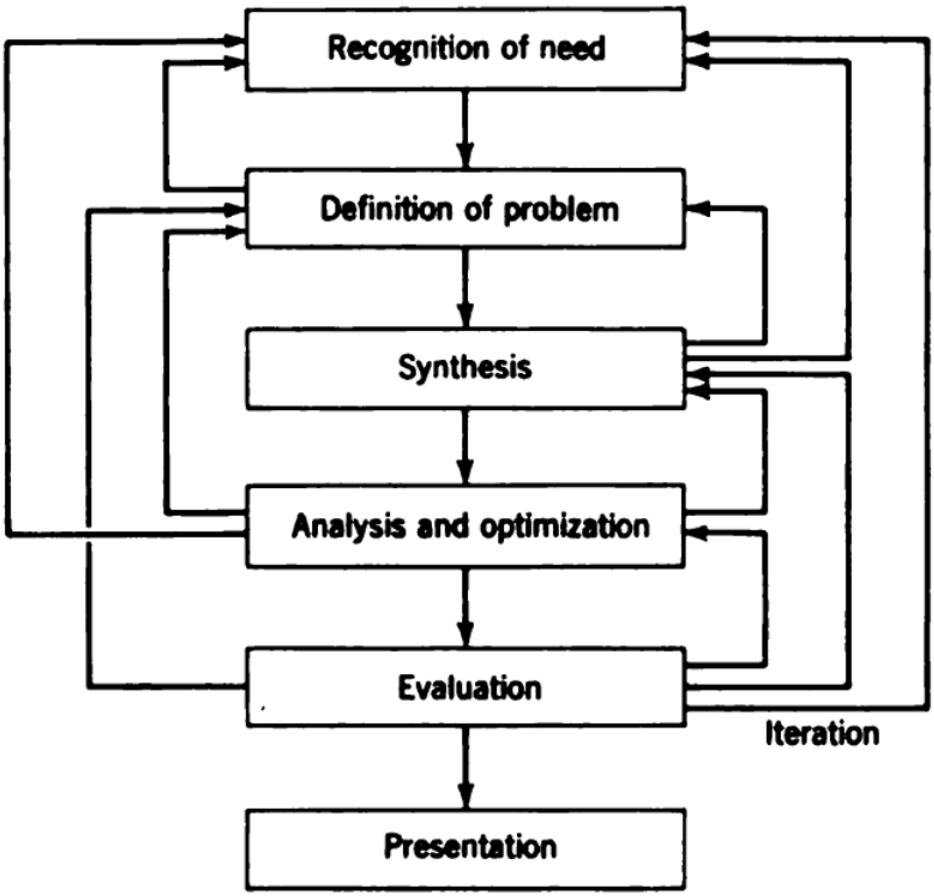

Figure 1.2: Systematic traditional machine design methodology proposed by Shigley (image from [2]).

process from the previously discussed soft robotic design process, there is still a strong dependence on the available rheologically complex materials, soft elements, and fabrication methods.

A thorough design process for origami machines was also developed that can be applied to structurally compliant soft robots, shown in Figure 1.4 [4]. While this soft machine design does not use rheologically complex materials, the morphology of the soft machine creates a compliant and soft robot.

1.2.1 Limitations

While there are a few existing design processes that can be applied to soft machine design, a design process does not yet exist that is specifically meant for soft machine design. This leaves the designer often relying on intuition for

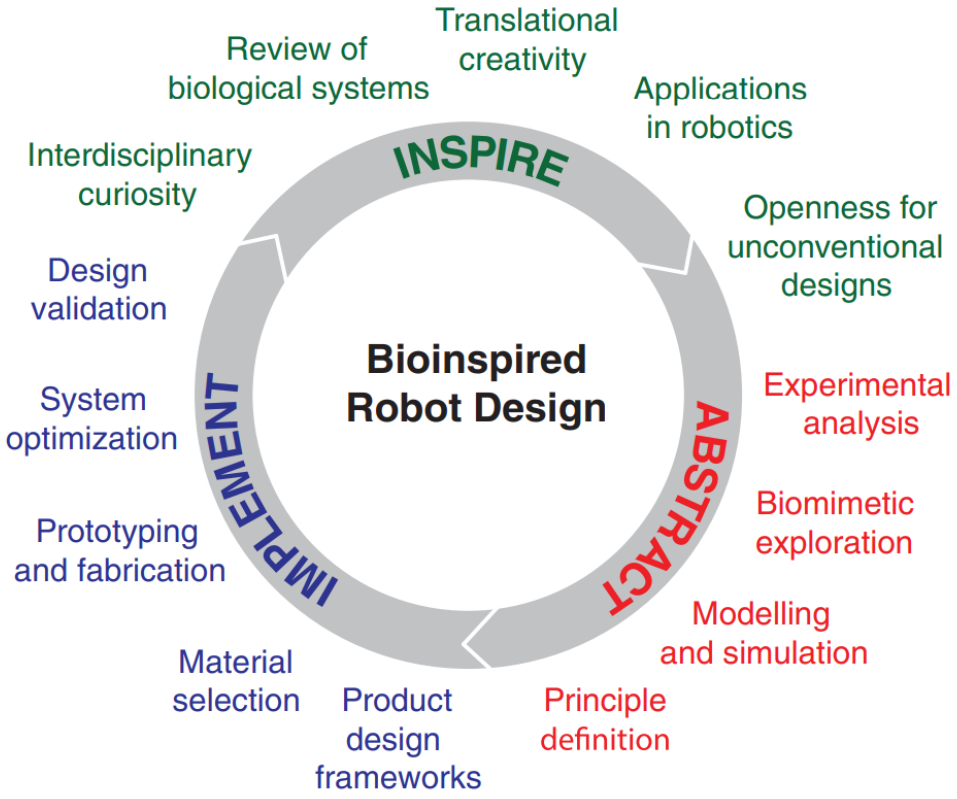

Figure 1.3: Inspire–abstract–implement (IAI) bio-inspired design paradigm proposed by Mirko Kovač (image from Figure 1 in [3]).

important design decisions, rather than a clear and repeatable design process. It is beneficial to have some ambiguity in a systematic process to leave room for design creativity, but it is also beneficial to have a clear design process defined for repeatability and to support knowledge sharing initiatives.

There are similarities between each of the defined design processes. All of these design processes have a focus on bio-inspired design, rheologically complex material selection, soft elements, soft fabrication methods, and morphology, which are not included in the traditional machine design processes. This suggests that these are key areas where design tools may need to be developed to support a designer in creating a 'good' soft machine design.

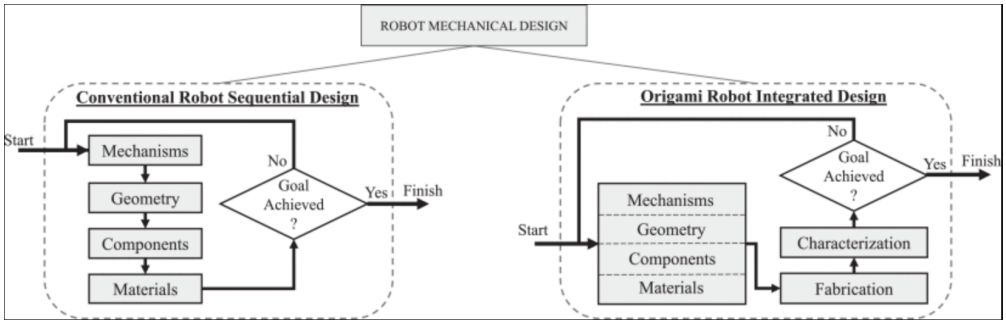

Figure 1.4: Comparing traditional and origami robot design processes proposed by Zhakypov and Paik (image from Figure 1 in [4]).

1.3 Design tools

Design tools support the designer in making 'good' design choices. Through a literature review focusing on soft machine design, common design tools support the user in the areas of (i) material selection, (ii) constitutive equations and modeling, and (iii) fabrication methods.

1.4 Material selection design tools

1.4.1 Significant mechanical and rheological properties

Since material selection plays a prominent role in soft machine design, it is important to evaluate the most significant material properties to select a 'good' material for the final design. Since the materials are rheologically complex and of a different category than materials selected for traditional machine design, it is expected that there should be differences in significant material properties. The materials used in traditional and soft machines also serve different purposes. The material used in soft machines has desired functionality and is expected to deform. Whereas the material used in traditional machines acts more as a connection between two joints and is not expected to have functionality. Intuitively, the significant properties of the rheologically complex materials may be function-valued, where the significant properties of the traditional materials may be set to a specific value and retained at the value. This already highlights the complexity of material selection for soft machines.

Table 1.1: Significant material properties for soft machine design.

Significant Material Property List	
Variable	**Property**
G_0 [Pa]	Shear elastic modulus [16, 17]
G' [Pa]	Shear storage modulus [7]
G'' [Pa]	Shear loss modulus [7]
$\Delta G/G_0$ [Pa/Pa]	Variable stiffness [6, 7]
ε_{max} [mm/mm]	Elongation to break [16, 17]
$\eta(\dot{\gamma})$ [Pa.s]	Viscosity [7]
U [J/m^3]	Strain energy density [7]
b, β [-]	Nonlinearity [18]
ρ [g/mm^3]	Density [19]
t [s]	Response time to stimulus [6]
ρ [Ω.mm]	Electrical resistivity [19]
ϵ_r [-]	Dielectric constant [16, 19]
k [W/m.K]	Thermal conductivity [16, 19]
μ [cm.g.s]	Magnetic permeability [6]
σ_y [Pa]	Yield stress [20, 21]
τ_{thixo} [s]	Thixotropic recovery [20, 21]
$G(t)$ [Pa]	LVE relaxation modulus [22]
$H(\tau)$ [Pa]	LVE relaxation specturm [22]

Through a literature survey, some repetitive and significant material properties for the material selection in soft machines were found. These properties can be seen in Table 1.1.

As expected, many of the significant properties are function-valued and will change with deformation, frequency, or another activation stimulus. The significant properties that are not function-valued, such as G_0 and β, are used as parameters for function-valued predictive models. While soft machine materials are selected based on these interesting rheological properties, it is important for the designer to understand when some of these properties may hold more significance over others. This is dependent on the desired actuation method, sensing capabilities, and performance. The actuation method can include stimuli from mechanical, chemical, light, electrical, magnetic, temperature, and pressure sources [16]. For example, if the actuation method is a magnetic field then the magnetic permeability of the material should hold more significance over the electrical resistivity. Table 1.1 is a list of the most common and important properties, and does not encompass all possible relevant properties for a soft machine design. Throughout this thesis, we

will focus on the significant material properties of shear elastic modulus G_0, variable shear stiffness $\Delta G/G_0$, strain energy density U, and nonlinearity b, β.

While significant properties are chosen based on the desired actuation method, sensing capabilities, and performance, there are still many other important factors and considerations depending on the application [16]. These considerations include, but are not limited to:

- Fabrication: Manufacturing processability [16, 17, 19]
- Aesthetics: Transparency, tactile perception [23]
- Life-time: Sustainability, biodegradability, self-healing [16, 23]
- Comfort: Porosity, adhesion [16, 23]

1.4.2 Common materials

With these significant factors and function-valued properties in mind, the designer can begin selecting rheologically complex materials for a soft machine design using design tools that support the 'design with' soft materials [20]. Commonly selected materials can be seen in Table 1.2 and mainly consist of elastomers, hydrogels, and fillers. There is not a wide variety of materials that are used in soft machines, and this opens opportunities for rheologists, chemists, and material scientists/engineers to create new materials for soft machine design using proper design tools to support the 'design of' soft materials.

1.4.3 Material selection charts and databases

Rheological and material properties should be evaluated in order to select a 'good' material, and material property databases and references are a design tool that helps the user find these properties. There are many material property databases and handbooks that exist. However, most are designed for purposes other than soft machine design and may not contain the most significant properties for soft machine design. The most relevant databases and handbooks include information on biological materials, soft robotic materials, and polymers. Table 1.3 references some of these useful databases,

Table 1.2: Common materials for soft machine design.

Common Material List		
Actuation	**Material description**	**Material**
Pressure	Siloxane-based copolymer [16]	PDMS [16, 7, 24] Ecoflex [7, 24]
Electric	Electroactive polymers, compliant electrodes [16]	Acrylic elastomers [16] Silicones [16, 7] Polyurethanes [16, 7]
Thermal	Liquid-crystal polymers [16]	
Light	Liquid-crystal polymers [16]	
Magnetic	Magnetic fillers embedded in polymer networks [16]	PDMS [25] PEGDA [25] Colloidal nanocrystal clusters (CNC's) [25] Iron [26] EcoFlex [26] Aluminum [26] PEG [27] NdFeB particles [27] CI [28] Elastomers [28]
Chemical	Hydrogels [16]	Alginate [29] PAAm [29] PEG [27]

textbooks, and handbooks. The journal article that is referenced contains a very detailed review of many more material property databases.

Material selection charts are design tools that use these properties found in material property databases, and organize knowledge in a streamlined way that is effective in aiding the user in the design process. These material property charts (also known as Ashby diagrams) are common for rigid materials with significant rigid properties, but are far less common for rheologically complex materials with significant rheological properties. To the best of our knowledge, the only material property charts that are focused on nonlinear elastic solids used in soft machine designs are shown in Figures 1.5, 1.6, 1.7, and 1.8. These material selection charts can be difficult to design when many significant properties are function-valued.

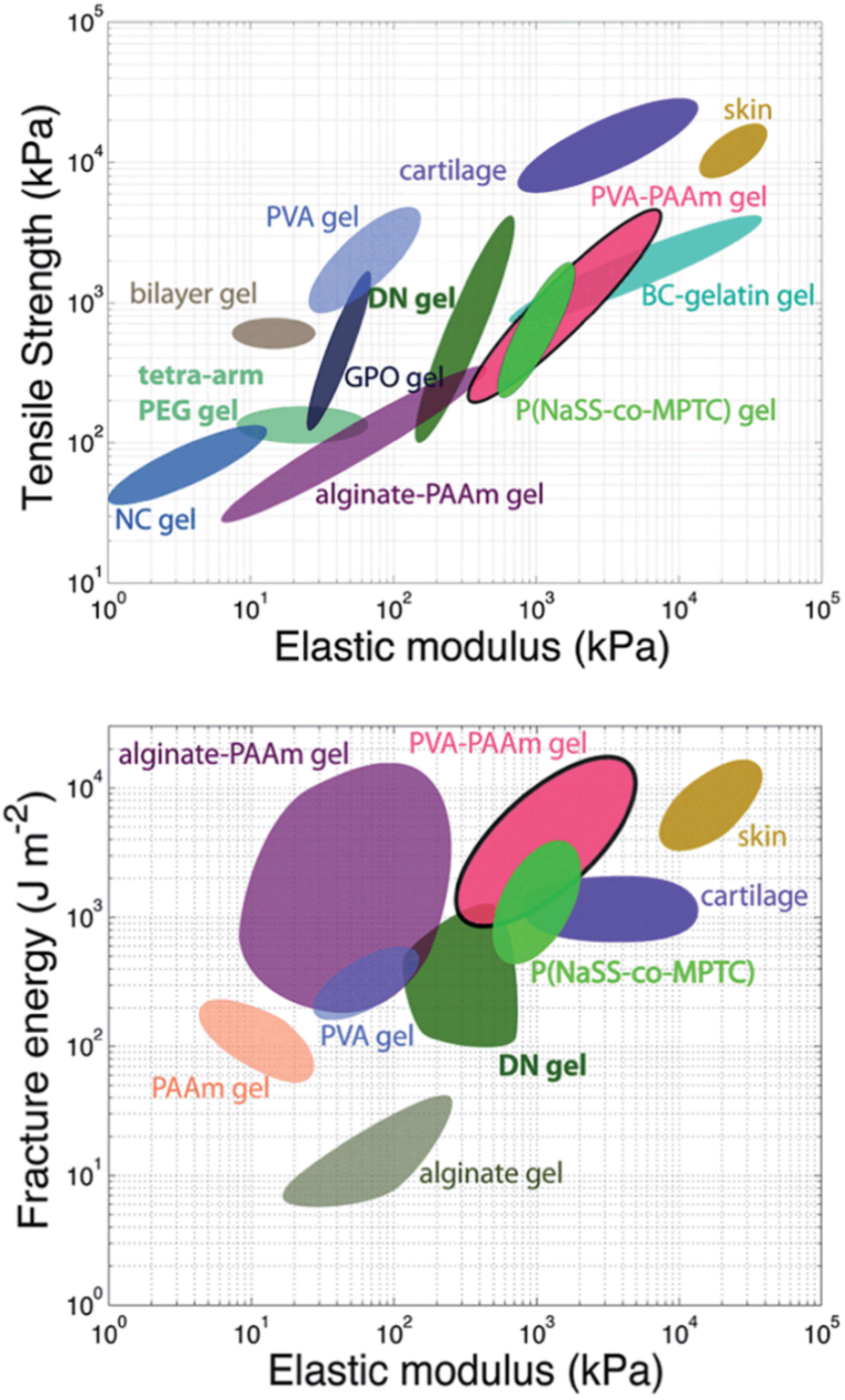

Figure 1.5: Material selection charts for soft materials (image from Figure 4 in [5]).

Table 1.3: Material databases and references relevant to soft machine design.

Soft Machine Material Databases and References	
Type	**Reference**
Shared resources [30]	Soft robotics toolkit
Journal [31]	Soft robotics
Journal [32]	Bioinspiration and biomimetics
Journal [33]	IEEE
Journal [34]	Nature
Handbook [35]	Handbook of biomaterial properties
Database [36]	Materials data book
Database [37]	National institute for material science PoLyInfo polymer database
Database [38]	CROW polymer database
Database [39]	MatWeb material property database
Database [40]	Citrine Informatics' Citrination platform
Database [41]	MakeItFrom material property database
Textbook [13]	Material Selection in Mechanical Design
Software [42]	Granta design
Journal article [43]	P.S. Ramalhete, A.M.R. Senos, C. Aguiar, "Digital tools for material selection in product design", *Materials and Design*, Volume 31, Issue 5, 2010, Pages 2275-2287, https://doi.org/10.1016/j.matdes.2009.12.013.

1.4.4 Limitations

There are very few material selection charts that have been developed for soft materials and are able to be applied to soft machine design. Many of the existing material selection charts include materials with an elastic modulus above 10^9 Pa! This is not considered soft according to the *Soft Robotics Journal* [44]. There are only a handful of material selection charts that include soft materials and the soft materials that are included in the material property charts are limited. Therefore, there is also a need for softer materials to be developed and characterized to expand the design space for soft machine design. In later chapters, we develop new design tools to support the 'design with' and 'design of' soft materials for soft machine design.

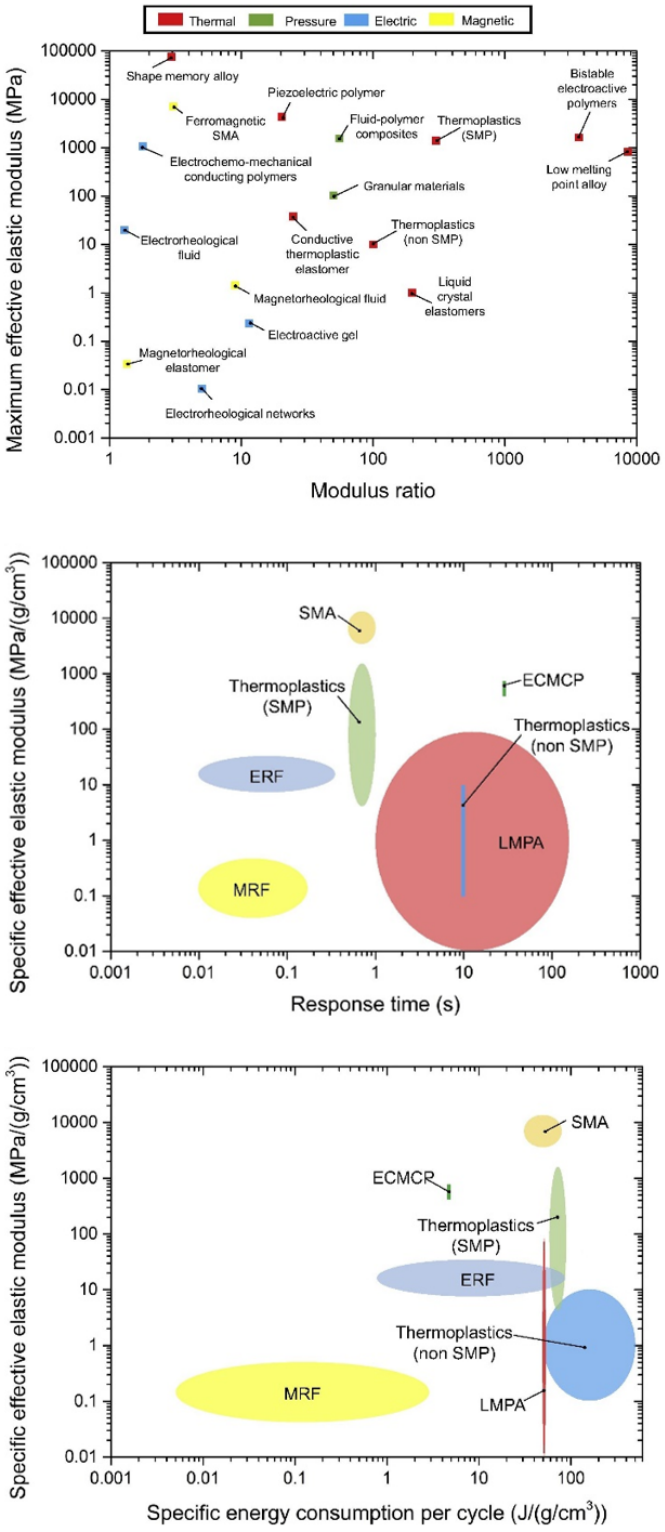

Figure 1.6: Material selection charts for functional materials with variable stiffness(image from Figure 1 in [6]).

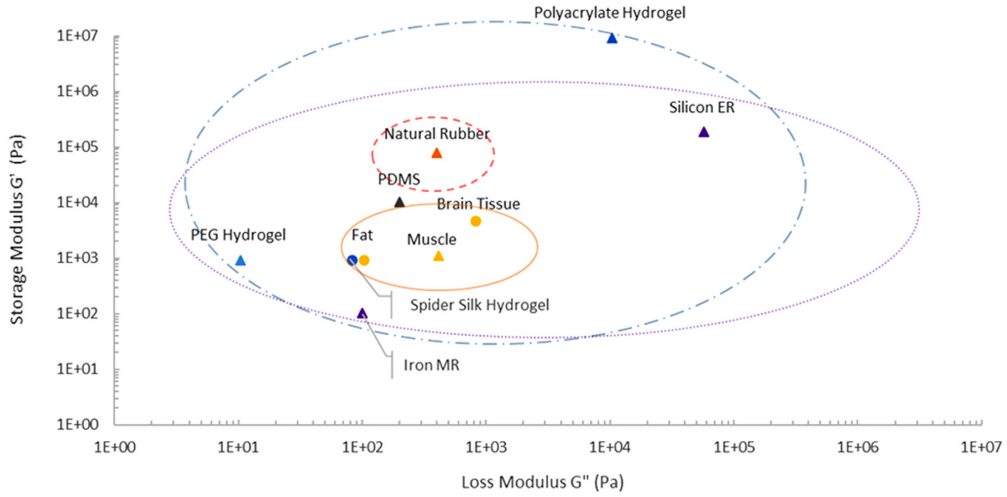

Figure 1.7: Material selection charts for rheologically complex materials (image from Figure 1 in [7]).

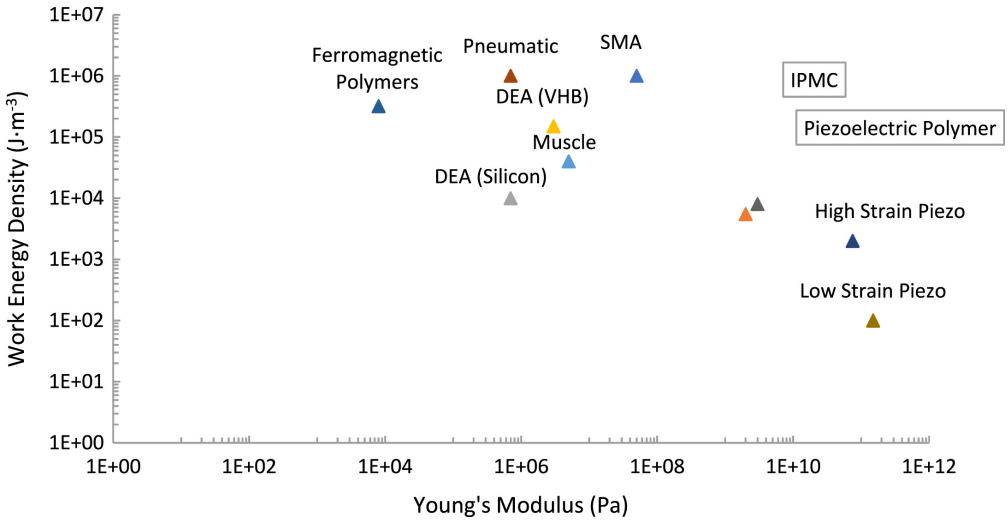

Figure 1.8: Material selection charts for functional soft actuators (image from Figure 2 in [7]).

1.5 Constitutive equations

Since these materials are rheologically complex and the material properties are function-valued, constitutive equations and predictive models are design tools that can provide more information on the material function beyond material selection charts. Common predictive models for materials in soft machine design focus on the material response to specific input stimuli, based on assumptions. For soft nonlinear elastomeric solids, hyperelastic constitutive equations derived from the strain energy density are used to make predictions

Table 1.4: Constitutive equations for hyperelastic materials. The material constant parameters are referenced as μ_i, K_i, C_p, m_p, α, and β. I_i and J are related to the invariants of the Left Cauchy-Green deformation tensor. λ_i are the principle stretches.

Hyperelastic constitutive equations [45, 46, 47]	
Name	**Equation**
Neo-Hookean	$U = \frac{\mu_1}{2}(I_1 - 3) + \frac{K_1}{2}(J-1)^2$
Mooney-Rivlin	$U = \frac{\mu_1}{2}(I_1 - 3) + \frac{\mu_2}{2}(I_2 - 3) + \frac{K_1}{2}(J-1)^2$
Ogden	$U = \sum_{p=1}^{N} \frac{C_p}{2m_p}(\lambda_1^{2m_p} + \lambda_2^{2m_p} + \lambda_3^{2m_p} - 3)$
Fung	$U = \frac{\mu}{2\alpha}(e^{\alpha(I_1-3)} - 1)$
Gent	$U = -\frac{\mu}{2\beta}\ln(1 - \beta(\lambda_1^2 + \lambda_2^2 + \lambda_3^2 - 3))$

[45]. Some common constitutive equations can be seen in Table 1.4. Common assumptions include incompressibility and isotropic material properties. The stress tensor can be found from the strain energy density function

$$\underline{\underline{\sigma}} = -p\underline{\underline{I}} + \beta_1\underline{\underline{B}} + \beta_{-1}\underline{\underline{B}}^{-1} \tag{1.1}$$

where p is the hydrostatic pressure, $\underline{\underline{I}}$ is the identity tensor, $\underline{\underline{B}}$ is the Finger tensor, and β_1 and β_{-1} are derived from the strain energy density function with respect to the first and second invariants of the Finger tensor $\underline{\underline{B}}$ [46]. The material response coefficients β_1 and β_{-1} are

$$\beta_1 = 2\frac{\partial U}{\partial I_1} \qquad\qquad \beta_{-1} = -2\frac{\partial U}{\partial I_2} \tag{1.2}$$

where I_1 and I_2 are the first and second invariants of the Finger tensor [46].

Moving a step further in the design process, after the material is selected and the material behavior is predicted with appropriate constitutive equations, design tools can be used to evaluate the entire soft system response. These are computational design tools such as Finite Element Analysis (FEA) that will use material properties, constitutive equations, and morphology to predict the behavior of an entire soft machine design. Finite element analysis

and soft actuators have been discussed in many articles [48].

1.5.1 Limitations

While many constitutive equations for soft materials are not newly developed, there are still some limitations. The number and interpretation of parameters needed for each constitutive model varies. It can be difficult to have meaningful intuition of the parameters that are used in each model. There is a need for a universal model with parameters that provide clear insight to the behavior of the soft materials. Also, while there are many successful models that predict material performance, a clear 'rule-book' does not exist that tells you under what deformations these constitutive equations may fail. Throughout this thesis, we relate common nonlinear elastic constitutive models to a universal nonlinear elastic model that gives clear insight into a materials response to deformation. We also investigate constitutive model performance under the unique deformation of a superposition of uniaxial stretch and simple shear.

1.6 Fabrication

An entire soft machine can be designed and modeled theoretically, but it is only valuable if it can be manufactured. Throughout history, most manufacturing processes focused on rigid materials. However, recent advancements in 3D printing allow for easy prototyping of rheologically complex materials in geometrically complex structures, contributing to the rise of soft machines.

Fabrication methods include soft lithography and 3D printing. The 3D printing technologies for materials for soft machine design consist of stereolithography (SLA), direct ink writing (DIW), embedded 3D printing, and pick-and-place 3D printing [8, 9, 49]. SLA allows for printing soft materials, DIW is capable of printing functional composites, embedded 3D printing allows for creating channels within a soft matrix, and pick-and-place 3D printing integrates hard control components into soft machines in a single platform. While these advances in fabrication methods have created opportunity for soft machine design, in such a new field there is still room for much development.

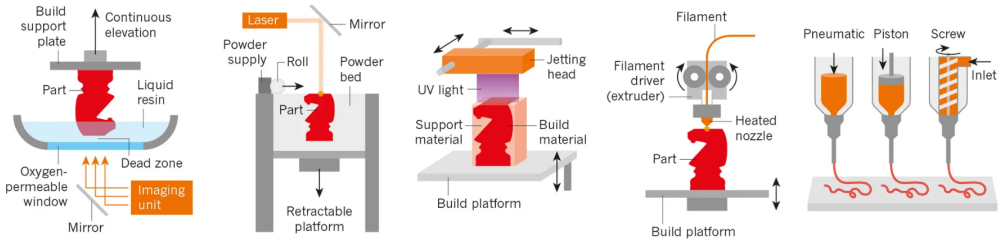

Figure 1.9: 3D printing methods (image from Figure 1 in [8]).

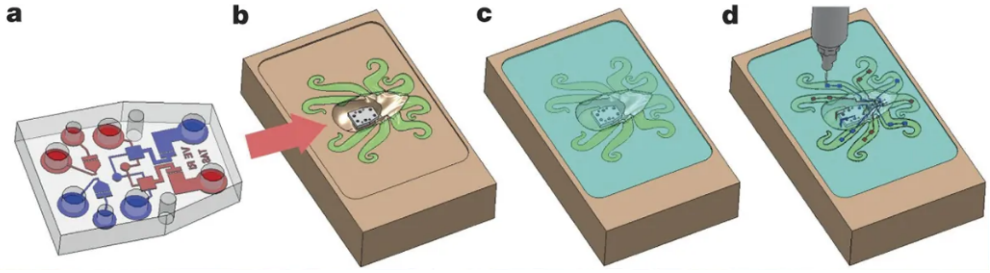

Figure 1.10: Embedded 3D printing method (image from Figure 1 in [9]).

1.7 Conclusions

Design tools for soft machine design have little to no development since the field is fairly new. Thus, there is an opportunity to develop design tools to support and advance the design of soft machines using rheologically complex materials. These design tools can exist by supporting the (i) 'design with' materials and the (ii) 'design of' materials. The next chapters will be focusing on developing both types of design tools for soft machine design, discussing predictive behavior of magnetorheological elastomers, and evaluating models for hyperelasticity.

CHAPTER 2

MATERIAL SELECTION DESIGN TOOLS FOR SOFT MACHINE DESIGN

2.1 Introduction

There are a limited number of design tools to support the soft machine design process as discussed in Chapter 1. We take initial steps to develop design tools that focus on material selection and universal modeling using significant properties and materials commonly used in soft machine design.

2.2 Methods

We develop material selection charts by collecting material data from journal articles, books, and material databases that are referenced in Tables 2.1-2.4. The design tool that is presented in Figure 2.3 was created by a previous graduate student Olivia Carey-De La Torre [10].

2.3 Proposed material selection charts

We propose an Ashby style material selection chart to support soft machine design that includes information on strain to break ε_{break} and elastic modulus E for soft materials, as shown in Figure 2.1. We include common materials used in soft machine design such as elastomers and gels. We also include biological materials which are typically soft and fibers that form extremely soft fibrous networks. The material properties used in this Ashby diagram were determined to be of significant importance to soft machine design, as discussed in Chapter 1.

We propose an Ashby style material selection chart that shows the stiffness variation $\frac{E_{max}}{E_{min}}$ for many soft functional materials that are commonly used as

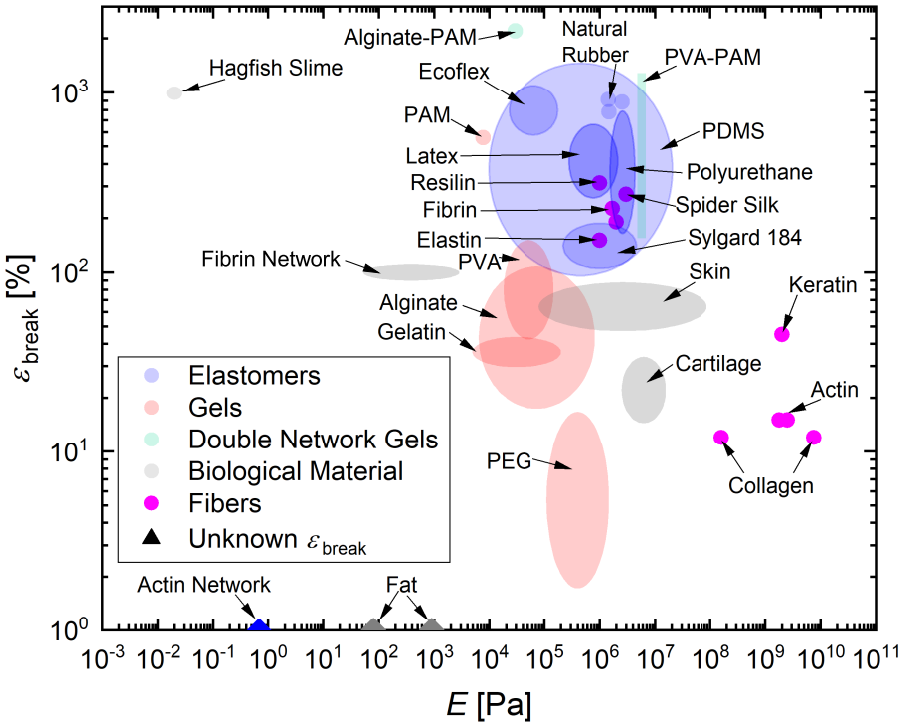

Figure 2.1: Ashby style material selection chart showing the elastic modulus E versus the strain to break ε_{break} for many soft materials and materials common in soft machine design. The materials with an unknown strain to break ε_{break} include actin networks and fat. The references for each material in this Ashby diagram can be seen in Table 2.1.

soft machine actuators, as shown in Figure 2.2. This material selection chart can support soft machine design with functional materials and considers the stiffness activation mechanisms of an electric field, magnetic field, vacuum jamming, temperature, and light.

2.4 Universal nonlinear parameter

Nonlinear elastic solids, such as PDMS, are common in soft machine design and there are many constitutive models that can predict the nonlinear elastic behavior of these materials. However, as discussed in Chapter 1, it can be difficult to gather intuition on a materials deformation behavior based on

Table 2.1: Table of material references used to make the elastic modulus E versus strain to break ε_{break} Ashby style material selection chart.

Material	**Reference**
Hagfish slime	[50, 51, 52]
Fat	[53]
Cartilage	[54]
Skin	[55, 56]
Fibrin Network	[57, 58]
Fibrin Elastin Resilin Keratin Collagen Spider silk Actin	[59]
PEG	[60, 61]
Alginate Gelatin PAM Alginate-PAM	[62, 63]
Actin gel	[64]
PVA	[65, 66]
PVA-PAM	[5, 67]
Ecoflex	[68, 69, 70]
Natural rubber	[36]
PDMS	[71, 72]
Polyurethane	[36, 73]
Latex	[74]
Sylgard 184	[75, 76]

the nonlinearity fitting parameter used for each constitutive model. It is also unclear how a nonlinearity parameter used in one constitutive model relates to a nonlinearity parameter used in a different constitutive model.

Addressing these constitutive modeling issues, a previous graduate student, Olivia Carey-De La Torre, defined a universal nonlinear parameter b to be used to describe nonlinear elastic response in shear [10]

$$\sigma(\gamma) = G_0\gamma(1 + b\gamma^2). \tag{2.1}$$

If $b > 0$ the material shows a stiffening response in shear and if $b < 0$ the

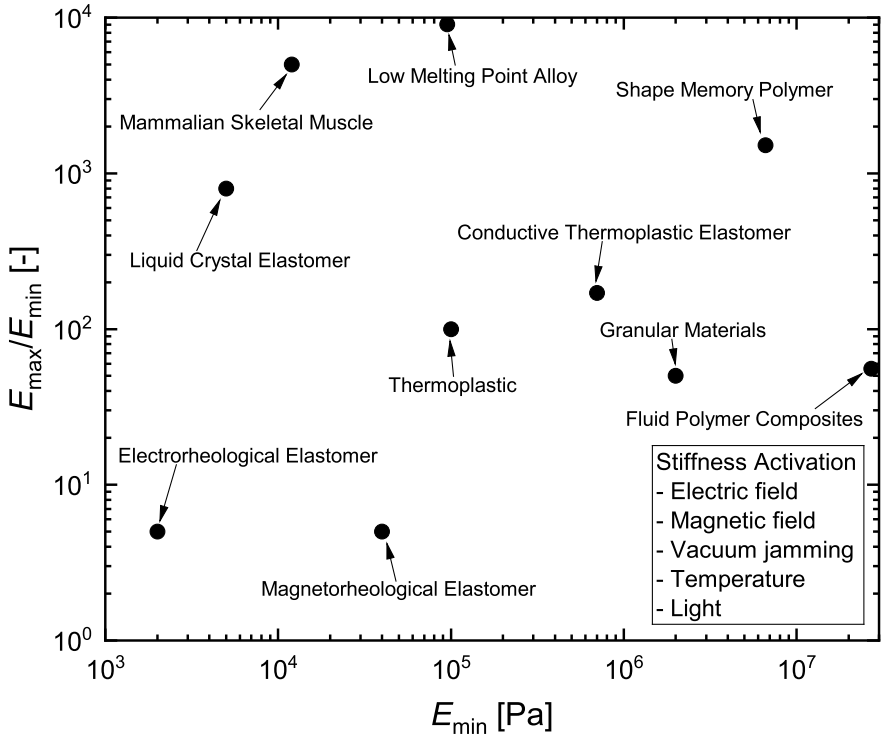

Figure 2.2: Ashby style material selection chart showing the elastic modulus E versus the stiffness variation $\frac{E_{max}}{E_{min}}$ for many soft functional materials common in soft machine design. The references for each material in this Ashby diagram can be seen in Table 2.2.

material shows a softening response in shear [10]. Therefore, intuition on the material performance is easy to gather from this proposed universal nonlinear elastic parameter [10].

This universal nonlinear elastic parameter b can also be related to parameters in many other constitutive models. Olivia Carey-De La Torre previously found the relation of the universal nonlinear parameter b to parameters in the Neo-Hookean and Fung models [10], as shown in Table 2.3. We additionally find the universal nonlinear relations for the Gent and nonlinear chain network models. A more detailed discussion of these nonlinear elastic equations can be seen in Chapter 4.

Table 2.2: Table of material references used to make the minimum elastic modulus E_{min} versus stiffness ratio $\frac{Emax}{E_{min}}$ Ashby style material selection chart.

Material	**Reference**
Electrorheological elastomer	[6]
Magnetorheological elastomer	[6, 77]
Thermoplastic	[6]
Liquid crystal elastomer	[6, 78]
Mammalian skeletal muscle	[79, 80]
Low melting point alloy	[6]
Shape memory polymer	[79, 6]
Conductive thermoplastic elastomer	[6, 81]
Granular materials	[6]
Fluid polymer composites	[6]

2.4.1 Gent model universal relation

The Gent model is a hyperelastic constitutive equation and the elastic potential is [46]

$$U = -\frac{G_0}{2\beta}\ln(1-\beta(I_1-3)). \tag{2.2}$$

Assuming simple shear deformation, the shear stress is calculated from the elastic potential as

$$\sigma(\gamma) = \frac{G_0\gamma}{1-\beta\gamma^2} \tag{2.3}$$

where the shear calculation method is described in Chapter 4, equations 4.6-4.8.

To relate the universal nonlinear parameter b to the Gent model nonlinear parameter β, we take a Taylor Expansion about $\gamma = 0$ (small shear deformations),

$$\sigma(\gamma) \approx \sigma(\gamma)|_{\gamma=0} + \left.\frac{\partial\sigma}{\partial\gamma}\right|_{\gamma=0}\frac{\gamma}{1!} + \left.\frac{\partial^2\sigma}{\partial\gamma^2}\right|_{\gamma=0}\frac{\gamma^2}{2!} + \left.\frac{\partial^3\sigma}{\partial\gamma^3}\right|_{\gamma=0}\frac{\gamma^3}{3!} + \dots \tag{2.4}$$

The derivatives of the Gent model and their values at $\gamma = 0$ are defined as

follows,

$$\sigma(\gamma)|_{\gamma=0} = 0, \tag{2.5}$$

$$\frac{\partial \sigma}{\partial \gamma} = \frac{G_0}{1-\beta\gamma^2} + \frac{2\beta G_0 \gamma^2}{(1-\beta\gamma^2)^2}, \tag{2.6}$$

$$\frac{\partial \sigma}{\partial \gamma}|_{\gamma=0} = G_0, \tag{2.7}$$

$$\frac{\partial^2 \sigma}{\partial \gamma^2} = \frac{6\beta G_0 \gamma}{(1-\beta\gamma^2)^2} + \frac{8\beta^2 G_0 \gamma^3}{(1-\beta\gamma^2)^3}, \tag{2.8}$$

$$\frac{\partial^2 \sigma}{\partial \gamma^2}|_{\gamma=0} = 0, \tag{2.9}$$

$$\frac{\partial^3 \sigma}{\partial \gamma^3} = \frac{6\beta G_0}{(1-\beta\gamma^2)^2} + \frac{48\beta^2 G_0 \gamma^2}{(1-\beta\gamma^2)^3} + \frac{48\beta^3 G_0 \gamma^4}{(1-\beta\gamma^2)^4}, \tag{2.10}$$

and

$$\frac{\partial^3 \sigma}{\partial \gamma^3}|_{\gamma=0} = 6\beta G_0. \tag{2.11}$$

Plugging in equations 2.5-2.11 into equation 2.4 yields

$$\sigma(\gamma) \approx G_0 \gamma \left(1 + \beta\gamma^2\right). \tag{2.12}$$

Then by comparing equation 2.12 to equation 2.1, we find that

$$b = \beta. \tag{2.13}$$

2.4.2 Nonlinear chain network model universal relation

The nonlinear chain network model is a hyperelastic constitutive equation and the elastic potential is defined as [46]

$$U = \frac{3G_0}{\left[1 + \frac{2}{(1-\beta)^2}\right]} \left[\frac{I_1}{6} + \beta^{-1}\left(1 - \frac{\beta I_1}{3}\right)^{-1}\right]. \tag{2.14}$$

Assuming simple shear deformation, the shear stress is calculated from the elastic potential as

$$\sigma(\gamma) = G_0\gamma\left[1+\frac{2}{(1-\beta)^2}\right]^{-1}\left[1+\frac{18}{(\beta\gamma^2+3\beta-3)^2}\right] \tag{2.15}$$

where the shear calculation method is described in Chapter 4, equations 4.6-4.8.

To relate the universal nonlinear parameter b to the nonlinear chain network model nonlinear parameter β, we take a Taylor Expansion about $\gamma = 0$ (small shear deformations) as shown in equation 2.4.

The derivatives of the nonlinear chain network model and their values at $\gamma = 0$ are defined as follows,

$$\sigma(\gamma)|_{\gamma=0} = 0, \tag{2.16}$$

$$\frac{\partial\sigma}{\partial\gamma} = \left[\frac{G_0}{1+\frac{2}{(1-\beta)^2}}\right]\left[1+\frac{18}{(\beta\gamma^2+3\beta-3)^2}-\frac{72\beta\gamma^2}{(\beta\gamma^2+3\beta-3)^3}\right], \tag{2.17}$$

$$\frac{\partial\sigma}{\partial\gamma}|_{\gamma=0} = G_0, \tag{2.18}$$

$$\frac{\partial^2\sigma}{\partial\gamma^2} = \left[\frac{216G_0}{1+\frac{2}{(1-\beta)^2}}\right]\left[\frac{-\beta\gamma}{(\beta\gamma^2+3\beta-3)^3}+\frac{2\beta^2\gamma^3}{(\beta\gamma^2+3\beta-3)^4}\right], \tag{2.19}$$

$$\frac{\partial^2\sigma}{\partial\gamma^2}|_{\gamma=0} = 0, \tag{2.20}$$

$$\frac{\partial^3\sigma}{\partial\gamma^3} = \left[\frac{216G_0}{1+\frac{2}{(1-\beta)^2}}\right]\left[\frac{-\beta}{(\beta\gamma^2+3\beta-3)^3}+\frac{1302\beta^2\gamma^2}{(\beta\gamma^2+3\beta-3)^4}-\frac{16\beta^3\gamma^4}{(\beta\gamma^2+3\beta-3)^5}\right], \tag{2.21}$$

and

$$\frac{\partial^3\sigma}{\partial\gamma^3}|_{\gamma=0} = \frac{-8\beta G_0}{(\beta-1)(\beta^2-2\beta+3)}. \tag{2.22}$$

Table 2.3: Common constitutive equations for hyperelastic incompressible materials and their relation to the universal nonlinear parameter b.

Nonlinear elastic constitutive equations and their universal relation [45, 46, 10, 47]		
Name	**Equation**	**Universal nonlinear relation**
Neo-Hookean	$U = \frac{G_0}{2}(I_1 - 3)$ G_0 is a material property	$b = 0$
Fung	$U = \frac{G_0}{2\alpha}(e^{\alpha(I_1-3)} - 1)$ G_0, α are material properties	$b = \alpha$
Gent	$U = -\frac{G_0}{2\beta}\ln(1 - \beta(I_1 - 3))$ G_0, β are material properties	$b = \beta$
Nonlinear chain network	$U = \frac{3G_0}{\left[1+\frac{2}{(1-\beta)^2}\right]}\left[\frac{I_1}{6} + \beta^{-1}\left(1 - \frac{\beta I_1}{3}\right)^{-1}\right]$ G_0, β are material properties	$b = \frac{4}{3}\frac{\beta}{(1-\beta)(\beta^2-2\beta+3)}$

Plugging in equations 2.16-2.22 into equation 2.4 yields

$$\sigma(\gamma) \approx G_0\gamma\left(1 - \frac{4}{3}\frac{\beta}{(\beta-1)(\beta^2-2\beta+3)}\gamma^2\right). \tag{2.23}$$

Then by comparing equation 2.23 to equation 2.1, we find that

$$b = \frac{4}{3}\frac{\beta}{(1-\beta)(\beta^2-2\beta+3)}. \tag{2.24}$$

2.4.3 Constitutive models in universal terms

We include Table 2.3 that summarizes some nonlinear elastic constitutive models and their relation to the nonlinear universal parameter. The Neo-Hookean and Fung model universal relations were found by Olivia Carey-De La Torre [10] and the Gent and nonlinear chain network model universal relations are a new contribution.

2.4.4 Material selection chart with universal nonlinearity

Olivia Carey-De La Torre proposed a final representation of the universal nonlinear term b as an Ashby style material selection chart shown in Figure 2.3. Many soft materials are included in the Ashby diagram and it relates to common nonlinear elastic constitutive models used in soft machine design. Therefore, this work adds to the design tools for material selection for soft machine design.

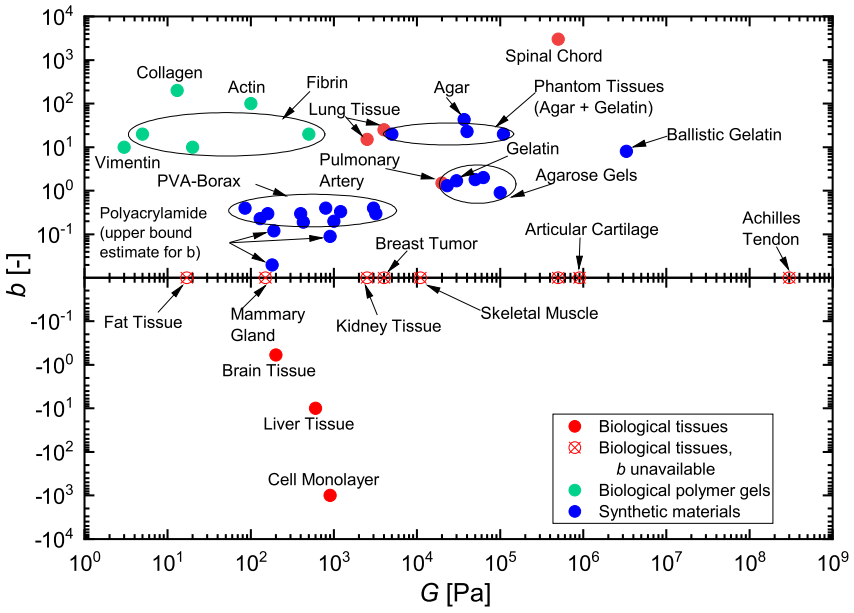

Figure 2.3: This figure was created by Olivia Carey-De La Torre [10]. This is an Ashby style material selection chart showing the shear modulus G versus inherent nonlinearity b for many soft materials common in soft machine design. The references for each material in this Ashby diagram can be seen in Table 2.4.

2.5 Conclusions

In this work, we began to add to the design toolbox for soft machine design by developing relevant material selection charts and finding universal relations for additional nonlinear elastic constitutive models.

Table 2.4: Table of material references used to make the shear modulus G versus universal nonlinearity term b Ashby style material selection chart.

Material	**Reference**
Achilles tendon Articular cartilage Skeletal muscle Cardiac muscle Breast tumor Kidney tissue Liver tissue Mammary gland Fat	[80]
Actin Fibrin Collagen Vimentin Polyacrylamide	[82]
Fibrin	[58]
Polyacrylamide	[83]
Agarose	[84]
Agar Gelatin Phantom tissues	[85]
Ballistic gelatin	[86]
Lung tissue	[87]
Brain tissue	[88, 89]
Cell monolayer	[90]
Liver tissue	[88]
Spinal chord	[89]

CHAPTER 3

EXPLORING MATHEMATICAL MODELS FOR THE DESIGN OF A NEW MATERIAL CONCEPT

3.1 Introduction

From a thorough investigation of the current state of soft machine design, it is clear that functional materials with variable stiffness are important for soft machine design and there are limited design tools that support the 'design of' these functional materials. In this chapter, we make predictions for the variable shear stiffness of magnetorheological elastomers (MRE's) when a magnetic field is introduced. For a given magnetic particle, particle distribution, particle concentration, and magnetic field, we can predict the variable shear stiffness of the composite as a function of the initial softness and nonlinearity of the composite material. Nonlinear MRE performance has not been studied previously as an effect of elastic softness and nonlinearity. We find that the elastic nonlinearity can cause a shear stiffening or softening response and we provide an explanation for this effect. This model could provide insight to the strong stiffening effect observed in a magnetic fibrin composite [57]. We study the underlying magnetic and elastic contributions and make conclusions on the effects that these individual contributions have on the overall variable shear stiffness. We create a 'design of' tool that shows the variable stiffness as a function of the initial softness and nonlinearity. We explain how this design tool can be used in a complete design framework to create a bottlebrush PDMS composite material for soft machine design [91].

The predictions that are made for the variable shear stiffness of the composite material follow the theory of mechanical behavior of magnetorheological elastomers (MRE) proposed by *Ivaneyko, Toshchevikov, Saphiannikova,* and *Heinrich* [11]. However, that proposed theory assumed a linear elasticity model in shear for the elastomer matrix. For our predictions, we include a nonlinear hyperelastic model proposed by *Dobrynin* and *Carrillo* [12] as the

elastic contribution from the elastomer matrix background.

For our research contribution, we combine the theory of mechanical behavior of magnetorheological elastomers and the nonlinear hyperelastic model to study the role of nonlinear elastic contributions to the variable shear stiffness of magnetorheological elastomers to gain insight to the underlying physics.

There have been many studies on modeling MRE's [92]. Some work has been published that makes predictions for MRE's with a linear elastic matrix material that resembles a Hookean solid [93, 94, 95]. Other research attempts to capture the nonlinear elastic effects using a Neo-Hookean or Mooney-Rivlin model [96, 97, 98, 99, 100, 101]. However, these models can predict a linear or nonlinear response depending on the type of deformation. Under any shear deformation, both the Neo-Hookean and Mooney-Rivlin models predict a linear stress-strain relationship. There is some published work on modeling MRE's with nonlinear elastic shear models, such as the Ogden model [102]. However, to the best of our knowledge, this work does not discuss the effects of the degree of nonlinearity and softness of the elastomeric matrix on the MRE response, the variable shear stiffness, or the performance under a superposition of uniaxial extension and simple shear. The theoretical study in this Chapter contributes to knowledge on MRE performance by studying the effects of nonlinearity and softness of the matrix on the variable shear stiffness under compression induced by a magnetic field and an applied shear deformation.

Our predictions assume an incompressible material, affine deformation, and that all particles are the same, spherical, rigid, and cannot penetrate [11, 12]. Additionally, our predictions consider an unconfined material shown in Case 1 in Figure 3.1. Measurements of variable stiffness that would be expected from a rheometer with a fixed gap height would correlate to predictions made considering Case 2 in Figure 3.1. Case 2 is beyond the scope of this thesis, as it involves a more complex distribution of strains throughout the material.

Since we are considering an unconfined material, we generally expect the material to compress or extend in the direction of the magnetic field due to dipole-dipole interactions to reach an equilibrium strain before the material is introduced to a shear deformation [11]. Therefore, the variable shear stiffness would be dependent on both the uniaxial deformation and the shear deformation. In this thesis, we consider an isotropic distribution of particles

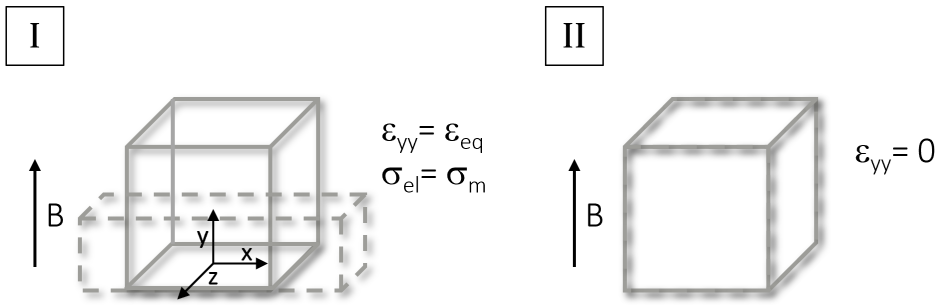

Figure 3.1: **Case 1:** Unconfined material **Case 2:** Confined material.

with a simple cubic lattice structure that compresses due to dipole-dipole interactions. However, other distributions of particles cause extension [11, 97].

3.2 Macroscopic and microscopic deformation

Assuming an unconfined incompressible material, the displacement equations are a superposition of uniaxial deformation and simple shear [46, 11],

$$\begin{aligned} x &= x_o\,(1+\varepsilon)^{-1/2} + y_o(1+\varepsilon)\gamma \\ y &= y_o\,(1+\varepsilon) \\ z &= z_o\,(1+\varepsilon)^{-1/2} \end{aligned} \tag{3.1}$$

where x_o, y_o, and z_o are the initial positions with respect to each coordinate axis, and x, y, and z are the positions with respect to each coordinate axis after deformation. Also, γ is the shear strain imposed after the uniaxial engineering strain ε.

Assuming affine deformation, the macroscopic deformation of the material can be related to the changing distance vector between each i^{th} and j^{th} particle $\overrightarrow{R_{ij}}$ *(Equation 21 in [11])*,

$$\begin{aligned} R_{ij,x} &= R^0_{ij,x}\,(1+\varepsilon)^{-1/2} + R^0_{ij,y}(1+\varepsilon)\gamma \\ R_{ij,y} &= R^0_{ij,y}\,(1+\varepsilon) \\ R_{ij,z} &= R^0_{ij,z}\,(1+\varepsilon)^{-1/2}\,. \end{aligned} \tag{3.2}$$

The finger tensor $\underline{\underline{B}}$ is calculated from the deformation gradient tensor $\underline{\underline{F}}$

$$\underline{\underline{F}} = \begin{bmatrix} \frac{\partial x}{\partial x_o} & \frac{\partial x}{\partial y_o} & \frac{\partial x}{\partial z_o} \\ \frac{\partial y}{\partial x_o} & \frac{\partial y}{\partial y_o} & \frac{\partial y}{\partial z_o} \\ \frac{\partial z}{\partial x_o} & \frac{\partial z}{\partial y_o} & \frac{\partial z}{\partial z_o} \end{bmatrix} \qquad \underline{\underline{F}} = \begin{bmatrix} (1+\varepsilon)^{-\frac{1}{2}} & \gamma(1+\varepsilon) & 0 \\ 0 & 1+\varepsilon & 0 \\ 0 & 0 & (1+\varepsilon)^{-\frac{1}{2}} \end{bmatrix} \tag{3.3}$$

$$\underline{\underline{B}} = \underline{\underline{F}} \cdot \underline{\underline{F}}^T = \begin{bmatrix} (1+\varepsilon)^{-1} + \gamma^2(1+\varepsilon)^2 & \gamma(1+\varepsilon)^2 & 0 \\ \gamma(1+\varepsilon)^2 & (1+\varepsilon)^2 & 0 \\ 0 & 0 & (1+\varepsilon)^{-1} \end{bmatrix} \tag{3.4}$$

and applies to both the macroscopic deformation and the deformation between each particle.

Now that the deformation of the material from superimposed uniaxial and simple shear deformation is understood, the variable shear stiffness can be derived from the balance of elastic and magnetic free energy under this extension and shear deformation.

3.3 Theory of mechanical behavior of MRE's

This section reviews the theory of mechanical behavior of magnetorheological elastomers discussed in the literature by *Ivaneyko, Toshchevikov, Saphiannikova,* and *Heinrich* [11].

3.3.1 Free energy

The material free energy has contributions from elastic energy and magnetic potential energy. The elastic energy stems from the elastic entropy of the polymer chains and the magnetic potential energy is due to the interactions between the magnetic particles and the applied magnetic field [11]. We define the free energy per unit volume as *(Equation 7 in [11])*

$$F(\gamma, \varepsilon) = u_{el}(\gamma, \varepsilon) + u_m(\gamma, \varepsilon). \tag{3.5}$$

3.3.2 Magnetic free energy

The magnetic contribution to the free energy is dependent on the magnetic field strength, saturation magnetization, particle magnetic permeability, volume fraction, and medium permeability. To understand the particle magnetization, we reference the Frohlich-Kennely equation [103],

$$M = \frac{M_s(\mu_{ini} - 1)(B/\mu_o)}{M_s + (\mu_{ini} - 1)(B/\mu_o)} \tag{3.6}$$

where M is the particle magnetization, M_s is the saturation magnetization, μ_{ini} is the relative particle magnetic permeability, B is the magnetic flux density, and μ_o is the vacuum permeability.

The magnetic free energy per unit volume is [104]

$$u_m(\gamma, \varepsilon) = -\frac{\mu_r \mu_o N}{4\pi V} \sum_i \left[\frac{3(\overrightarrow{m_i} \bullet \overrightarrow{R_{ij}})(\overrightarrow{m_j} \bullet \overrightarrow{R_{ij}})}{\left|\overrightarrow{R_{ij}}\right|^5} - \frac{(\overrightarrow{m_i} \bullet \overrightarrow{m_j})}{\left|\overrightarrow{R_{ij}}\right|^3} \right], \tag{3.7}$$

where μ_r is the relative permeability of the medium, μ_o is the permeability of the vacuum, $\frac{N}{V}$ is the number of magnetic particles per unit volume, $\overrightarrow{m_i}$ and $\overrightarrow{m_j}$ are the dipole moments of the i^{th} and j^{th} magnetic particles, and $\overrightarrow{R_{ij}}$ is the distance vector between the i^{th} and j^{th} particles. The elastomeric medium is assumed to be nonmagnetic so we assume that $\mu_r = 1$. The infinite rectangular lattice model does not depend on the interactions with every i^{th} and j^{th} particle due to symmetry. Therefore, we can take the summation of interactions with every i^{th} particle with respect to one reference particle and multiply by N, the number of magnetic particles.

For our predictions, we assume that $\overrightarrow{m_i}$ and $\overrightarrow{m_j}$ are parallel to the direction of the magnetic field and we do not account for rotation of the dipoles. The absolute values of $\overrightarrow{m_i}$ and $\overrightarrow{m_j}$ are $m_i = m_j = v_o M$ where $v_o = \frac{4}{3}\pi r^3$ and r is the radius of the magnetic particles. Therefore, we can simplify equation 3.7 to [11]

$$u_m(\gamma, \varepsilon) = -\frac{u_o v_o^2 N}{V} \left(\frac{M}{M_s}\right)^2 \sum_i \left[\frac{3\left(\overrightarrow{R_{ij}}\right)_y^2 - \left|\overrightarrow{R_{ij}}\right|^2}{\left|\overrightarrow{R_{ij}}\right|^5} \right], \tag{3.8}$$

where $u_o = \frac{\mu_o M_s^2}{4\pi}$.

A dimensionless parameter α is introduced to easily represent the distri-

bution of magnetic particles in the matrix [11],

$$\alpha = \frac{L_y^0}{L_x^0} = \frac{L_y^0}{L_z^0} \tag{3.9}$$

where $\alpha = 1$ represents an isotropic distribution, $\alpha < 1$ represents a chain-like distribution, and $\alpha > 1$ represents a plane-like distribution as shown in Figure 3.2 *(Figure 2 in [11])*. In this thesis, we are considering an isotropic distribution of particles where $\alpha = 1$.

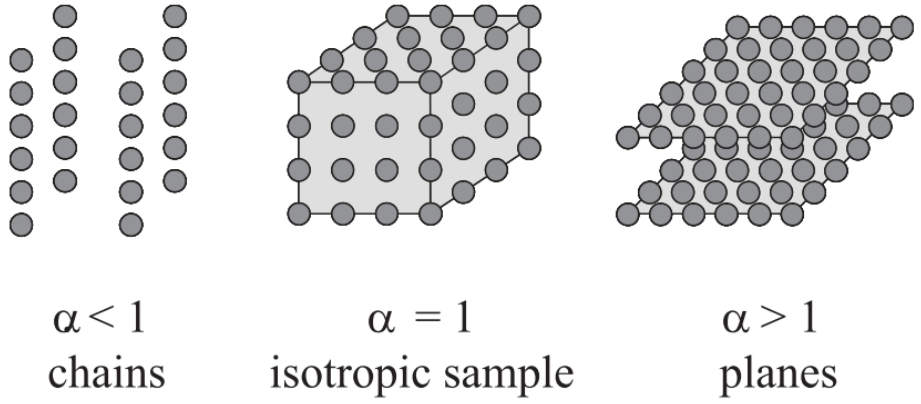

Figure 3.2: The various rectangular lattice distributions of particles before a magnetic field is induced and external shear is applied (image from Figure 2 in [11]). In this thesis, we are considering the isotropic sample where $\alpha = 1$.

In equation 3.8, the index i references all i^{th} particles in the entire material with respect to the j^{th} particle. However, the index i can be represented as the vector $i = (i_x, i_y, i_z)$, where i_x, i_y, i_z are the number of simple cubic lattice structures between the i^{th} and j^{th} particles in each coordinate direction. Then, we can define the distance between all particles as $\overrightarrow{R_{ij}} = (L_x i_x, L_y i_y, L_z i_z)$. Where L_x, L_y, L_z are the distances between each particle in a single rectangular lattice with respect to each coordinate direction as shown in Figure 3.3 [11].

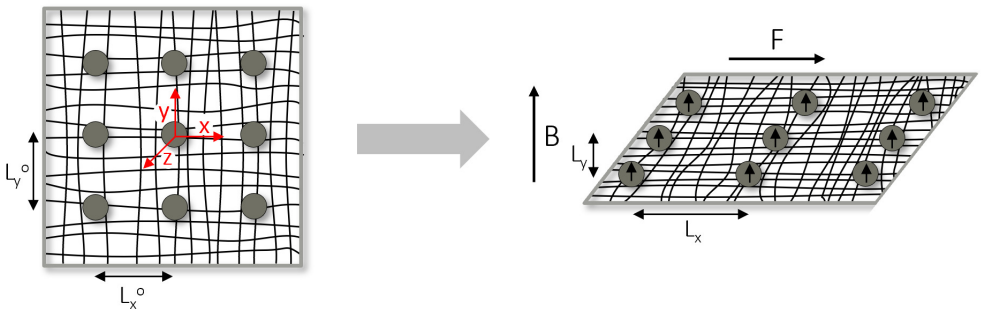

Figure 3.3: The distribution of particles before and after a magnetic field is induced and external shear is applied.

Then equation 3.8 can be rewritten as *(Equation 24 and 25 in [11])*

$$u_m(\gamma,\varepsilon) = -\,u_o\phi^2\left(\frac{M}{M_s}\right)^2\alpha(1+\varepsilon)^{3/2} \cdot \sum_{(i_x i_y i_z)\neq 0}\left[\frac{(2-\gamma^2)\alpha^2(1+\varepsilon)^3 i_y^2 - i_x^2 - i_z^2 - 2\gamma\alpha i_y i_x(1+\varepsilon)^{\frac{3}{2}}}{\left[(1+\gamma^2)\alpha^2(1+\varepsilon)^3 i_y^2 + i_x^2 + i_z^2 + 2\gamma\alpha i_y i_x(1+\varepsilon)^{\frac{3}{2}}\right]^{\frac{5}{2}}}\right] \tag{3.10}$$

where $\phi = \frac{v_o}{L_x^o L_y^o L_z^o}$ and $\frac{N}{V} = \frac{1}{L_x L_y L_z}$. Equation 3.10 represents the magnetic potential energy inside the composite material that contributes to the total free energy of the material.

The summation in equation 3.10 relates to the number of rectangular lattice structures in the finite material that need to be referenced for the magnetic free energy to converge. The magnetic free energy convergence can be seen in Figure 3.4. The increase in the number of cells by unity changes the value of the magnetic free energy by only 0.1% when 17 lattice structures are referenced. Therefore, if 17+ of the nearest lattice structures are referenced, the percent error of the magnetic free energy would be 0.1% or less. We reference seventeen of the nearest lattice structure particles to validate our calculations for the equilibrium strain with the literature.

The magnetic stress contribution can be found by taking the first derivative of the magnetic free energy per unit volume with respect to the uniaxial strain

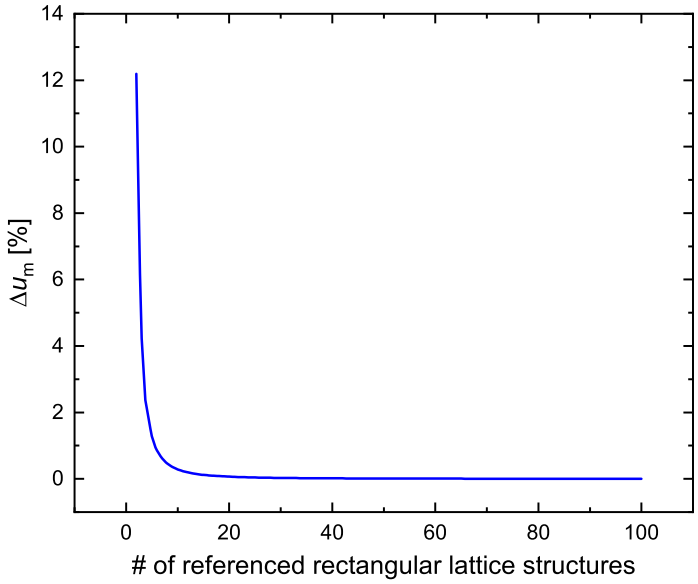

Figure 3.4: The number of neighboring square lattice structure particles interacting with the reference particle and the effect on the percent change of magnetic free energy considering an isotropic distribution of particles $\alpha = 1$. This figure is created by referencing equation 3.10, where $\gamma, \varepsilon = 0$.

[11],

$$\sigma_{m,yy} = \frac{\partial u_m(\gamma,\varepsilon)}{\partial \varepsilon}\Big|_{\gamma=0}. \tag{3.11}$$

Then the magnetic stress in the direction of the magnetic field is [11]

$$\begin{aligned}\sigma_{m,yy} = &- u_o\phi^2 \left(\frac{M}{M_s}\right)^2 \alpha\sqrt{1+\varepsilon} \\ &\cdot \sum_{(i_x i_y i_z)\neq 0} \left[\frac{12\alpha^4(1+\varepsilon)^6 i_y^4 - 30\alpha^2 i_y^2(1+\varepsilon)^3(i_x+i_z)^2 + 3(i_x^2+i_z^2)^2}{2\left[\alpha^2(1+\varepsilon)^3 i_y^2 + i_x^2 + i_z^2\right]^{7/2}}\right].\end{aligned} \tag{3.12}$$

Figure 3.5 shows how $\sigma_{m,yy}$ increases due to compression ($\varepsilon < 0$) for an isotropic simple cubic lattice particle distribution.

The shear modulus is also derived from the free energy. The magnetic shear modulus can be obtained by solving the equation $G_m = \frac{\partial^2 u_m}{\partial \gamma^2}\Big|_{\gamma=0}$ [11].

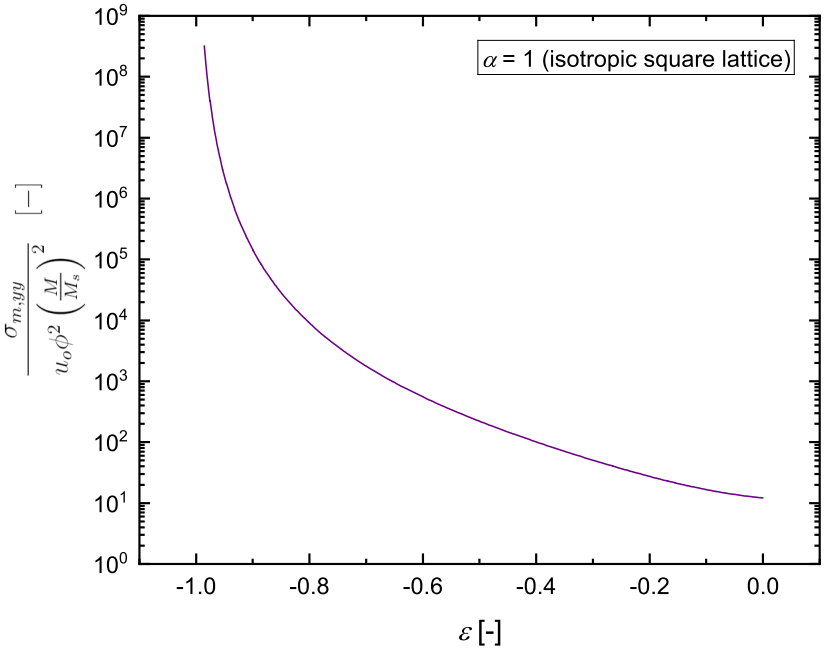

Figure 3.5: The relationship between uniaxial strain and the magnetic shear stress considering an isotropic distribution of particles $\alpha = 1$ and 30 neighboring square lattice structures. This figure is created by referencing equation 3.12.

Then the magnetic shear modulus is

$$G_m = u_o\phi^2\left(\frac{M}{M_s}\right)^2 3\alpha^3(1+\varepsilon)^{\frac{9}{2}} \cdot \sum_{(i_x i_y i_z)\neq 0} \frac{i_y^2\left[4\alpha^4 i_y^4(1+\varepsilon)^6 + 3\alpha^2 i_y^2(i_z^2 - 9i_x^2)(1+\varepsilon)^3 - i_z^4 + 3i_z^2 i_x^2 + 4i_x^4\right]}{\left[\alpha^2 i_y^2(1+\varepsilon)^3 + i_z^2 + i_x^2\right]^{\frac{9}{2}}}. \tag{3.13}$$

Figure 3.6 shows stiffening of $G_{m,yx}$ due to compressive strain ε, for an isotropic square lattice of particles. The stiffening results primarily from decreasing the distance between the magnetic dipoles aligned with the compression axis.

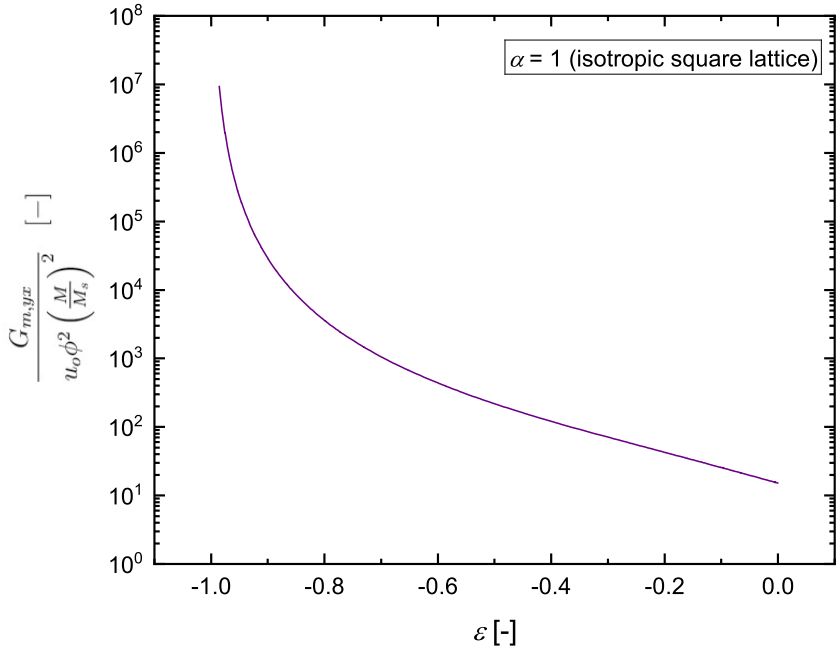

Figure 3.6: The relationship between uniaxial strain and the magnetic shear modulus considering an isotropic distribution of particles $\alpha = 1$ and 30 neighboring square lattice structures. This figure is created by referencing equation 3.13.

3.3.3 Elastic free energy

Assuming a linear approximation, the elastic free energy resembles a Hookean material. The free energy per unit volume under uniaxial or simple shear is

$$u_{el} = \frac{E_0\varepsilon^2}{2} \qquad u_{el} = \frac{G_0\gamma^2}{2}. \tag{3.14}$$

The elastic stress is found by taking the first derivative of the elastic free energy with respect to strain and the shear modulus is found by taking the second derivative with respect to strain,

$$\sigma_{el,yy} = \frac{\partial u_{el}}{\partial\varepsilon} = E_0\varepsilon \qquad \sigma_{el,yx} = \frac{\partial u_{el}}{\partial\gamma} = G_0\gamma \tag{3.15}$$

$$E_{el} = \frac{\partial u_{el}^2}{\partial^2\varepsilon} = \ E_0 \qquad G_{el} = \frac{\partial u_{el}^2}{\partial^2\gamma} = G_0. \tag{3.16}$$

Using a linear approximation for the elastomer matrix gives a modulus

that is independent of strain. This is not the typical behavior for elastomer materials under large deformation, which resemble a hyperelastic material response.

3.3.4 Equilibrium elongation

When a magnetic field is applied, the particles inside of the MRE interact due to dipole moments induced by, and aligned with, the magnetic field. This interaction is an attraction force in the direction of the applied magnetic field, thus causing the material to compress until the material reaches a steady state where the magnetic stress is balanced by the elastic stress. The equilibrium strain $\varepsilon = \varepsilon_{eq}$ can be found by solving the equation $\sigma_{el,yy} = \sigma_{m,yy}$ and referencing 17 neighboring rectangular lattice structures [11],

$$\begin{aligned} 0 =& E_0\varepsilon_{eq} + u_o\phi^2\left(\frac{M}{M_s}\right)^2 \alpha\sqrt{1+\varepsilon_{eq}} \\ &\cdot \sum_{(i_x i_y i_z)\neq 0}\left[\frac{12\alpha^4(1+\varepsilon_{eq})^6 i_y^4 - 30\alpha^2 i_y^2(1+\varepsilon_{eq})^3(i_x+i_z)^2 + 3(i_x^2+i_z^2)^2}{2\left[\alpha^2(1+\varepsilon_{eq})^3 i_y^2 + i_x^2 + i_z^2\right]^{7/2}}\right]. \end{aligned} \tag{3.17}$$

We compare our results to the results from the literature [11] to validate that our approach and calculations are correct. The equilibrium strain results from our calculations and from literature [11] can be seen in Figures 3.7 and 3.8. Our results correlate with the results from the literature validating that our approach and calculations for the equilibrium strain are correct.

3.3.5 Shear Modulus

After the equilibrium strain is calculated, the total shear modulus can be found as the sum of the magnetic and elastic contributions $G = G_{el} + G_m$,

$$\begin{aligned} G =& G_0 + u_o\phi^2\left(\frac{M}{M_s}\right)^2 3\alpha^3(1+\varepsilon_{eq})^{\frac{9}{2}} \\ &\cdot \sum_{(i_x i_y i_z)\neq 0} \frac{i_y^2\left[4\alpha^4 i_y^4(1+\varepsilon_{eq})^6 + 3\alpha^2 i_y^2(i_z^2 - 9i_x^2)(1+\varepsilon_{eq})^3 - i_z^4 + 3i_z^2 i_x^2 + 4i_x^4\right]}{\left[\alpha^2 i_y^2(1+\varepsilon_{eq})^3 + i_z^2 + i_x^2\right]^{\frac{9}{2}}}. \end{aligned} \tag{3.18}$$

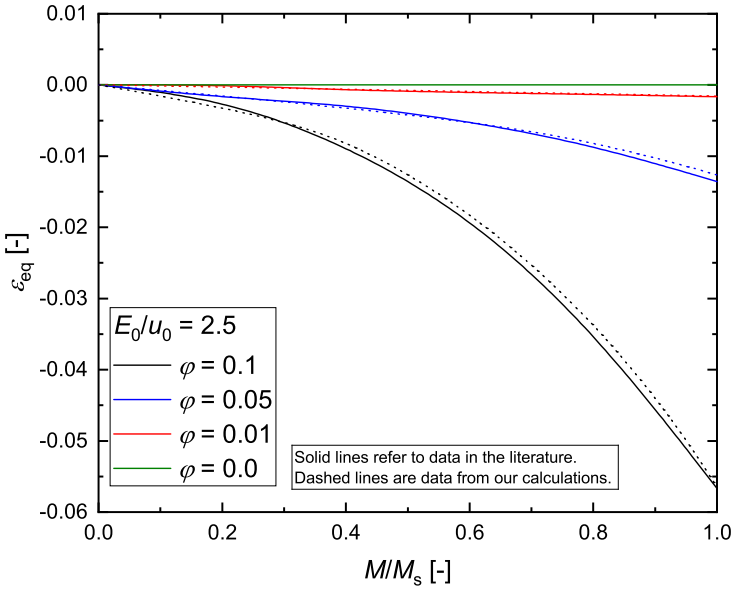

Figure 3.7: The uniaxial equilibrium strain resulting from the particle magnetization. The dashed lines are our calculations and the solid lines refer to the data in the literature [11]. This figure is created by referencing equation 3.17.

We compare our results for the shear modulus to the results from the literature [11] to validate that our approach and calculations are correct. The variable shear stiffness results from our calculations and from literature can be seen in Figures 3.9 and 3.10. Our results correlate with the results from the literature [11]. Thus, our approach and calculations are valid for the shear modulus and we can update the elastic free energy contribution with a nonlinear elastic model to include a more realistic nonlinear elastic free energy contribution.

3.4 Nonlinear elastic free energy

The predictive elastic contribution to the free energy is dependent on the constitutive model that is selected to describe the elastomer matrix background behavior under a superposition of extension and shear. We are assuming a hyperelastic and incompressible material response. Some common hyperelastic constitutive models include the Neo-Hookean, Mooney-Rivlin,

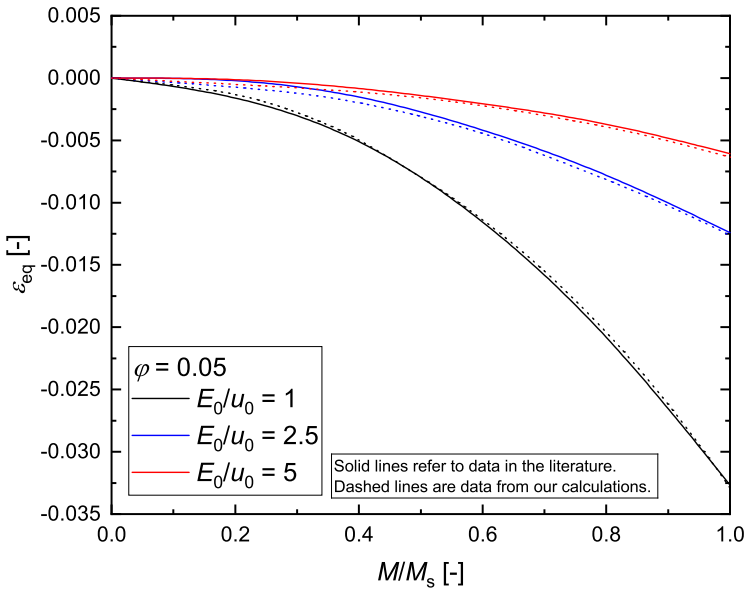

Figure 3.8: The uniaxial equilibrium strain resulting from the particle magnetization. The dashed lines are our calculations and the solid lines refer to the data in the literature [11]. This figure is created by referencing equation 3.17.

Arruda-Boyce, Ogden, Fung, and Gent models [45, 46]. In Chapter 4, we discuss the performance of these models in extension and shear.

For our material predictions in this chapter, we are using a hyperelastic constitutive model described in a paper by *Andrey V. Dobrynin* and *Jan-Michael Y. Carrillo* [12] that has a similar material response to the Fung and Gent models under the superposition of extension and shear. This constitutive model was selected because it is used in a design framework for designing tuneable bottle-brush PDMS and can capture a dramatic strain stiffening response when the finite elastic limit is approached. PDMS is the most common material used in soft machine designs [91]. Therefore, using this constitutive model allows us to make predictions of variable shear stiffness and additionally gives insight to parameters used in the fabrication of bottlebrush PDMS. This model has also been shown to accurately predict the nonlinear response of semi-flexible networks such as actin and fibrin [105], which can relate to previous work in our group with fibrin material [57].

The strain energy density function that describes the hyperelastic behavior

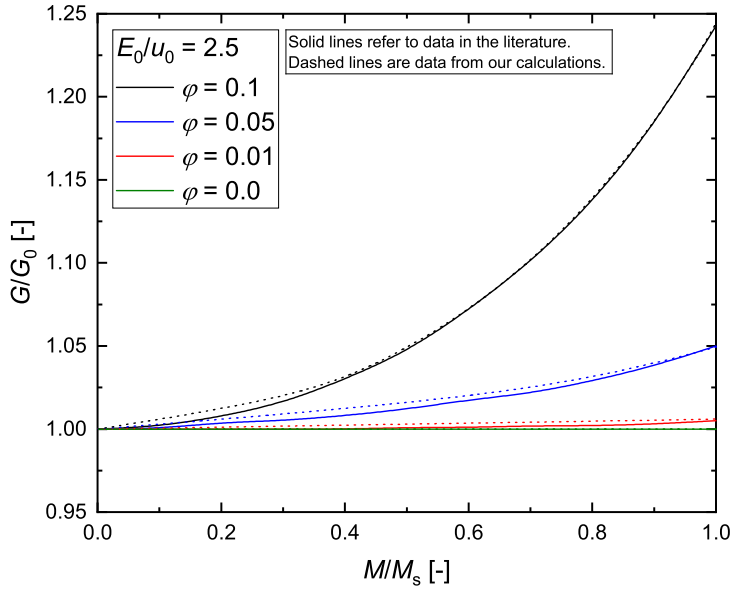

Figure 3.9: The variable shear stiffness resulting from the induced magnetic field. The dashed lines are our calculations and the solid lines refer to the data in the literature [11]. This figure is created by referencing equation 3.18 after the equilibrium strain ε_{eq} is found from equation 3.17.

and free energy per unit volume is [12]

$$u_{el}(I_1) = 3G_0 \left[1 + \frac{2}{(1-\beta)^2}\right]^{-1} \left[\frac{I_1}{6} + \beta^{-1}\left(1 - \frac{\beta I_1}{3}\right)^{-1}\right], \tag{3.19}$$

where G_0 is the initial shear modulus, β is the nonlinear parameter, and I_1 is the first invariant of the finger tensor. The nonlinear parameter β is related to the underlying polymer chain extension by $\beta = \frac{R}{R_{max}}$. For the superposition of extension and shear, $I_1 = (1+\varepsilon)^2 + 2(1+\varepsilon)^{-1} + \gamma^2(1+\varepsilon)^2$ [46].

This hyperelastic constitutive equation assumes affine deformation, incompressibility, an isotropic network, and that the free energy is equal to a sum of contributions from strands between cross-links [12].

The elastic stress contribution is derived from the free energy per unit

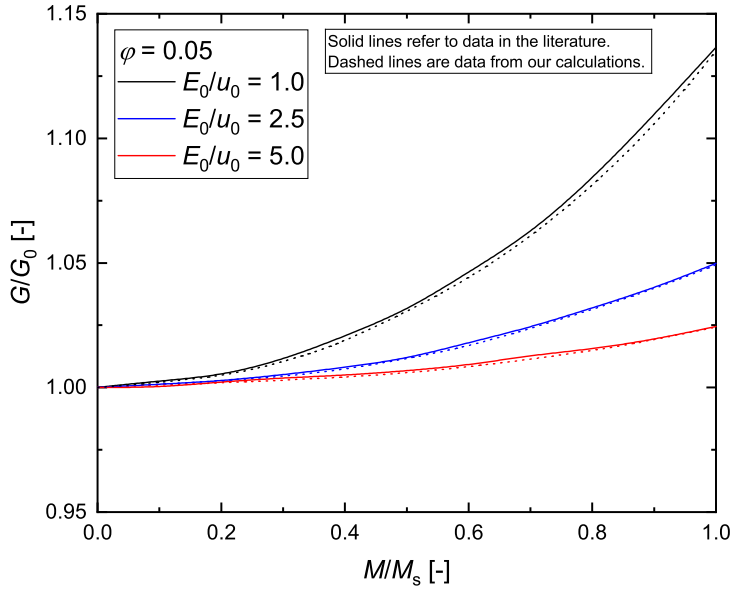

Figure 3.10: The variable shear stiffness resulting from the induced magnetic field. The dashed lines are our calculations and the solid lines refer to the data in the literature [11]. This figure is created by referencing equation 3.18 after the equilibrium strain ε_{eq} is found from equation 3.17.

volume [45],

$$\sigma_{el,ij} = 2\left[\frac{\partial u_{el}(I_1)}{\partial I_1}B_{ij} - \frac{I_1\delta_{ij}}{3}\frac{\partial u_{el}(I_1)}{\partial I_1}\right]\Big|_{\gamma=0}. \tag{3.20}$$

Then the elastic stress in the uniaxial direction as a function of the uniaxial strain is [12]

$$\begin{aligned}\sigma_{el,yy} =& \frac{3G_0}{1+\frac{2}{(1-\beta)^2}}\left((1+\varepsilon)^2-(1+\varepsilon)^{-1}\right)\\ &\left(1+2\left(1-\frac{\beta((1+\varepsilon)^2+2(1+\varepsilon)^{-1}+\gamma^2(1+\varepsilon)^2)}{3}\right)^{-2}\right).\end{aligned} \tag{3.21}$$

As the nonlinearity term β increases, the elastic normal stress rapidly increases at smaller magnitudes of strain as shown in Figure 3.11.

The elastic shear modulus can be obtained by solving the equation $G_{el} =$

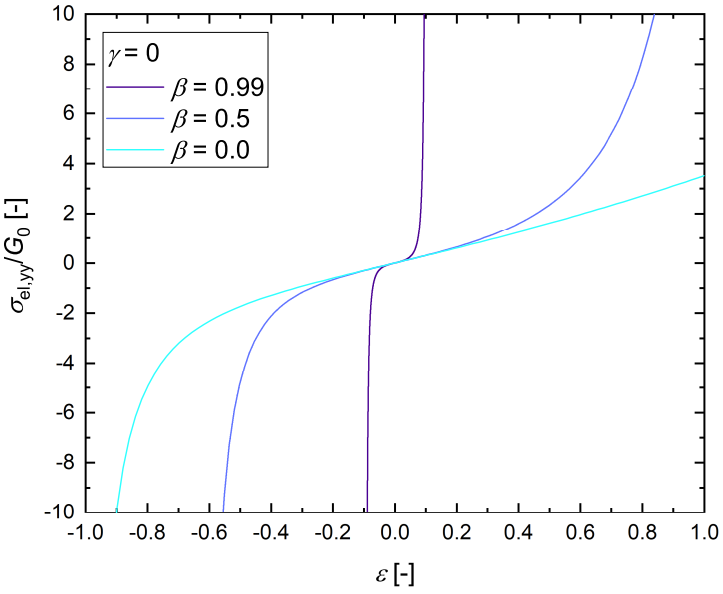

Figure 3.11: The resulting elastic normal stress as a function of the uniaxial strain for the model proposed by *Andrey V. Dobrynin* and *Jan-Michael Y. Carrillo* [12], and the dependence on the nonlinearity β and initial shear modulus G_0. This figure is created by referencing equation 3.21.

$\frac{\partial \sigma_{yx}}{\partial \gamma}\Big|_{\gamma=0}$. Then the elastic shear modulus is

$$G_{el} = \frac{G_0(1+\varepsilon)^2}{1+\frac{2}{(1-\beta)^2}}\left[1+\frac{18(1+\varepsilon)^2}{(\beta(1+\varepsilon)^3+2\beta-3(1+\varepsilon))^2}\right]. \tag{3.22}$$

Figures 3.12 and 3.13 show the elastic shear modulus as a function of strain ε and γ.

It is apparent that the shear modulus first decreases under compression before increasing again. This is will be discussed thoroughly in Chapter 4.

3.5 Nonlinear elastic MRE model

We combine the work presented on the mechanical behavior of MRE's by *Ivaneyko, Toshchevikov, Saphiannikova,* and *Heinrich* [11] with the hyper-elastic model work proposed by *Dobrynin* and *Carrillo* [12] to study the underlying material physics of the magnetic and elastic contributions to the

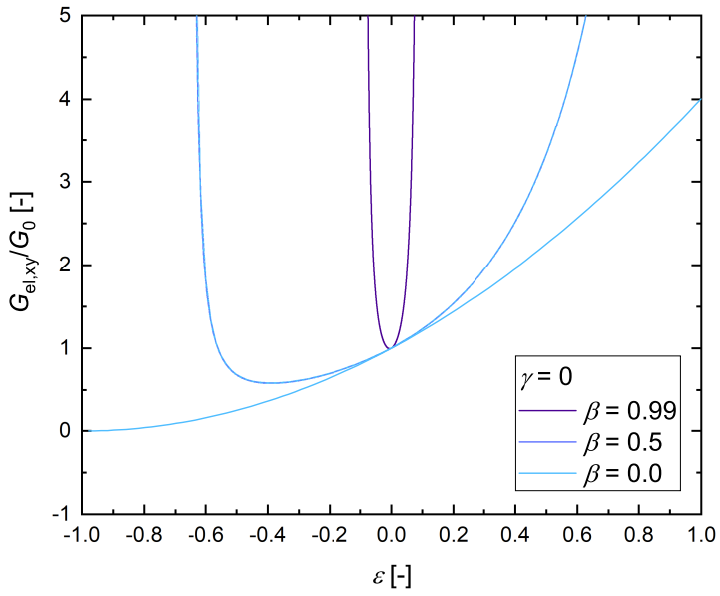

Figure 3.12: The resulting shear modulus as a function of the uniaxial strain for the model proposed by *Andrey V. Dobrynin* and *Jan-Michael Y. Carrillo* [12], and the dependence on the nonlinearity β and initial shear modulus G_0. This figure is created by referencing equation 3.22.

material variable shear stiffness.

The free energy per unit volume in equation 3.5 can be rewritten using the specific equations for the magnetic and elastic free energies per unit volume shown in equations 3.10 and 3.19. Therefore the free energy per unit volume is

$$\begin{aligned} F(\gamma,\varepsilon) =& 3G_0\left[1+\frac{2}{(1-\beta)^2}\right]^{-1}\left[\frac{(1+\varepsilon)^2+2(1+\varepsilon)^{-1}+\gamma^2(1+\varepsilon)^2}{6}\right. \\ &\left.+\beta^{-1}\left(1-\frac{\beta((1+\varepsilon)^2+2(1+\varepsilon)^{-1}+\gamma^2(1+\varepsilon)^2)}{3}\right)^{-1}\right] \\ &- u_o\phi^2\left(\frac{M}{M_s}\right)^2\alpha(1+\varepsilon)^{3/2} \\ &\cdot\sum_{(i_xi_yi_z)\neq 0}\left[\frac{(2-\gamma^2)\alpha^2(1+\varepsilon)^3i_y^2-i_x^2-i_z^2-2\gamma\alpha i_yi_x(1+\varepsilon)^{\frac{3}{2}}}{\left[(1+\gamma^2)\alpha^2(1+\varepsilon)^3i_y^2+i_x^2+i_z^2+2\gamma\alpha i_yi_x(1+\varepsilon)^{\frac{3}{2}}\right]^{\frac{5}{2}}}\right]. \end{aligned} \tag{3.23}$$

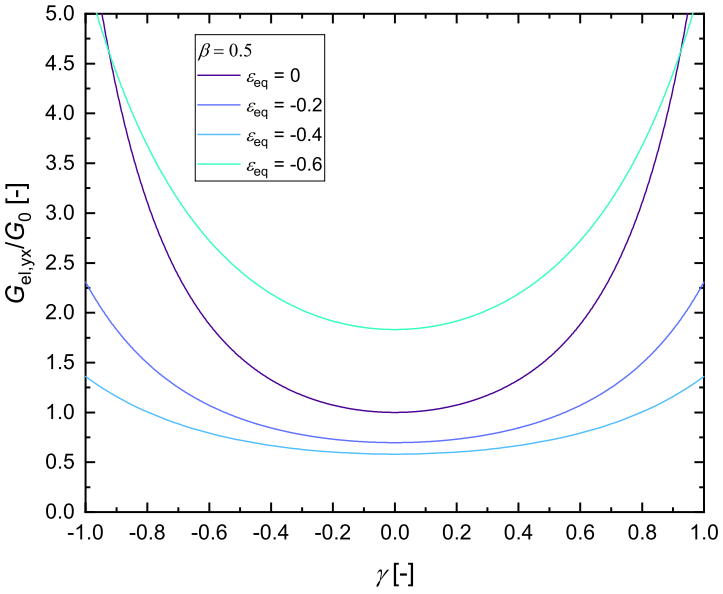

Figure 3.13: The resulting shear modulus as a function of the shear strain for the model proposed by *Andrey V. Dobrynin* and *Jan-Michael Y. Carrillo* [12], and the dependence on the equilibrium strain ε_{eq}. This figure is created by referencing equation 3.22.

The equilibrium strain can be solved by the equation $\sigma_{el,yy} = \sigma_{m,yy}$ using equations 3.21 and 3.12,

$$\begin{aligned} 0 =& \frac{G_0}{1+\frac{2}{(1-\beta)^2}} \left((1+\varepsilon_{eq})^2 - (1+\varepsilon_{eq})^{-1}\right) \\ & \left(1 + 2\left(1 - \frac{\beta((1+\varepsilon_{eq})^2 + 2(1+\varepsilon_{eq})^{-1} + \gamma^2(1+\varepsilon_{eq})^2)}{3}\right)^{-2}\right) \\ & + u_o\phi^2 \left(\frac{M}{M_s}\right)^2 \alpha\sqrt{1+\varepsilon_{eq}} \\ & \cdot \sum_{(i_x i_y i_z)\neq 0} \left[\frac{12\alpha^4(1+\varepsilon_{eq})^6 i_y^4 - 30\alpha^2 i_y^2(1+\varepsilon_{eq})^3(i_x+i_z)^2 + 3(i_x^2+i_z^2)^2}{2\left[\alpha^2(1+\varepsilon_{eq})^3 i_y^2 + i_x^2 + i_z^2\right]^{7/2}}\right]. \end{aligned} \tag{3.24}$$

This can be simplified to

$$\frac{u_o\phi^2\left(\frac{M}{M_s}\right)^2}{G_0} = f(\varepsilon_{eq}, \beta). \tag{3.25}$$

Then the shear modulus can be solved using the equilibrium strain and by the equation $G = G_{el} + G_m$ using equations 3.22 and 3.13,

$$G = \frac{G_0(1+\varepsilon_{eq})^2}{1+\frac{2}{(1-\beta)^2}}\left[1+\frac{18(1+\varepsilon_{eq})^2}{(\beta(1+\varepsilon_{eq})^3+2\beta-3(1+\varepsilon_{eq}))^2}\right] + u_o\phi^2\left(\frac{M}{M_s}\right)^2 3\alpha^3(1+\varepsilon_{eq})^{\frac{9}{2}} \cdot \sum_{(i_x i_y i_z)\neq 0} \frac{i_y^2\left[4\alpha^4 i_y^4(1+\varepsilon_{eq})^6+3\alpha^2 i_y^2(i_z^2-9i_x^2)(1+\varepsilon_{eq})^3-i_z^4+3i_z^2i_x^2+4i_x^4\right]}{\left[\alpha^2 i_y^2(1+\varepsilon_{eq})^3+i_z^2+i_x^2\right]^{\frac{9}{2}}}. \tag{3.26}$$

This can be simplified to

$$G = f(\varepsilon_{eq},\beta) + \frac{u_o\phi^2\left(\frac{M}{M_s}\right)^2}{G_0} f(\varepsilon_{eq}). \tag{3.27}$$

We define the variable shear stiffness as

$$\frac{\triangle G}{G_0} = \frac{G-G_0}{G_0} \tag{3.28}$$

and solve for the variable stiffness of the hyperelastic composite material as a function of imposed magnetic field and material composition. Then we can investigate the underlying magnetic contribution,

$$\frac{\triangle G_m}{G_0} = \frac{G_m}{G_0} \tag{3.29}$$

and elastic contribution,

$$\frac{\triangle G_{el}}{G_0} = \frac{G_{el}-G_0}{G_0} \tag{3.30}$$

to the overall variable stiffness and study the effect that the shear modulus and nonlinearity have on the variable shear stiffness.

3.6 Results and Discussion

Using the equations derived from the free energy of a hyperelastic MRE, we make predictions of the variable shear stiffness of a magnetorheological elas-

tomer for a given particle composition, an isotropic square lattice distribution ($\alpha = 1$), magnetic field strength, and volume fraction of particles. For our predicitons, we consider carbonyl iron nanoparticles with a saturation magnetization of $M_s = 1582$kA/m, magnetic permeability of $\mu_{ini} = 21.5$, volume fraction $\phi = 0.05$, and magnetic field strength of $B = 0.5$T [103]. Then using equations 3.23-3.26, the variable shear stiffness $\Delta G/G_0$ as a function of only β and G_0 is in Figures 3.23-3.26.

Figure 3.23 shows the total variable shear stiffness, while Figure 3.24 shows the magnetic contribution and Figures 3.25-3.26 show the elastic contribution to the total variable shear stiffness. It is clear from Figure 3.23 that a larger total variable shear stiffness is achievable with softer MRE's. However, there is an unclear trend in the total variable shear stiffness with respect to the nonlinear term β. For very stiff MRE's ($G_0 > 10^6 Pa$), β does not appear to have an impact on the total variable shear stiffness. For very soft MRE's ($G_0 < 10^4 Pa$), a smaller nonlinearity β causes a larger variable stiffness. In between these 'soft' and 'stiff' MRE's, there is also a 'semi-soft' region ($10^4 Pa < G_0 < 10^6 Pa$) where a larger nonlinearity β causes a slightly larger variable stiffness.

It is remarkable that stronger nonlinear elastic stiffening (large β) actually softens the MRE effect. We show that this behavior can be understood and explained by looking at the underlying magnetic and elastic contributions to the total variable shear stiffness with respect to G_0 and β. To the best of our knowledge, this has not been researched previously.

3.6.1 'Stiff' MRE

Referring to the 'stiff' MRE performance in Figure 3.23, we find that the log-log slope is equal to negative one and all nonlinear β terms overlap. Then this demonstrates that

$$\frac{\Delta G}{G_0} \sim G_0^{-1}. \tag{3.31}$$

In other words, ΔG is essentially constant if the material is sufficiently stiff. This occurs when ε_{eq} is sufficiently small that the particle distribution is essentially unchanged, and G_m is also unchanged.

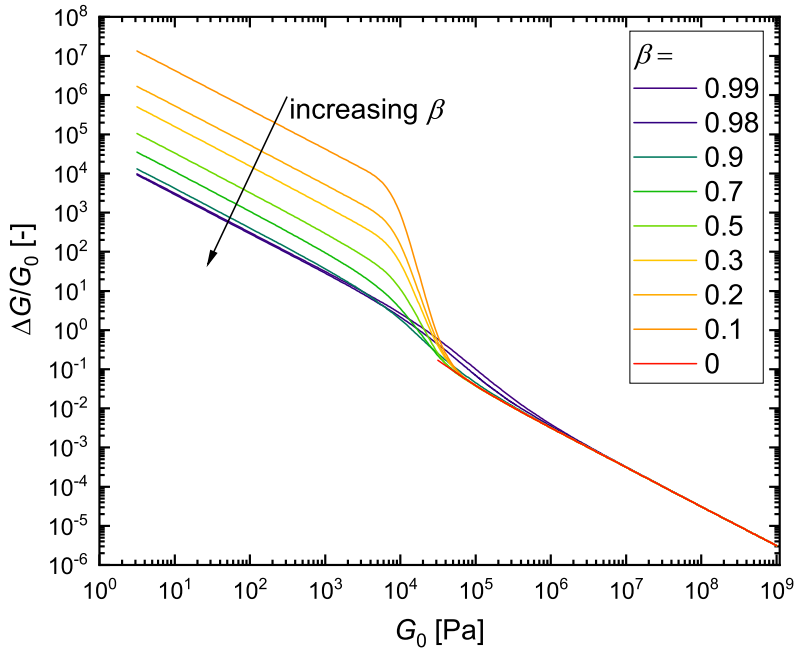

Figure 3.14: The total variable shear stiffness, including contributions from the magnetic and elastic free energy of a MRE, with respect to G_0 and β. We are considering an isotropic distribution of particles $\alpha = 1$, $\phi = 0.05$, $M_s = 1582$ kA/m, $\mu_{ini} = 21.5$, and $B = 0.5$ T. This figure is created by finding the equilibrium strain using equation 3.24 and referencing equations 3.26 and 3.28 to find the variable shear stiffness.

The magnetic contribution is

$$\frac{\Delta G_m}{G_0} = f(\varepsilon_{eq}) \tag{3.32}$$

and the elastic contribution is

$$\frac{\Delta G_{el}}{G_0} = f(\varepsilon_{eq}, \beta). \tag{3.33}$$

Since the total shear modulus is a summation of the magnetic and elastic contributions, we find that $f(\varepsilon_{eq}) + f(\varepsilon_{eq}, \beta) \sim G_0^{-1}$ for a 'stiff' MRE.

We aim to understand the underlying contributions that predict this 'stiff' MRE performance. The magnetic contribution shown in Figure 3.24 also shows that $\frac{\Delta G_m}{G_0} = f(\varepsilon_{eq}) \sim G_0^{-1}$. The elastic contribution shown in Fig-

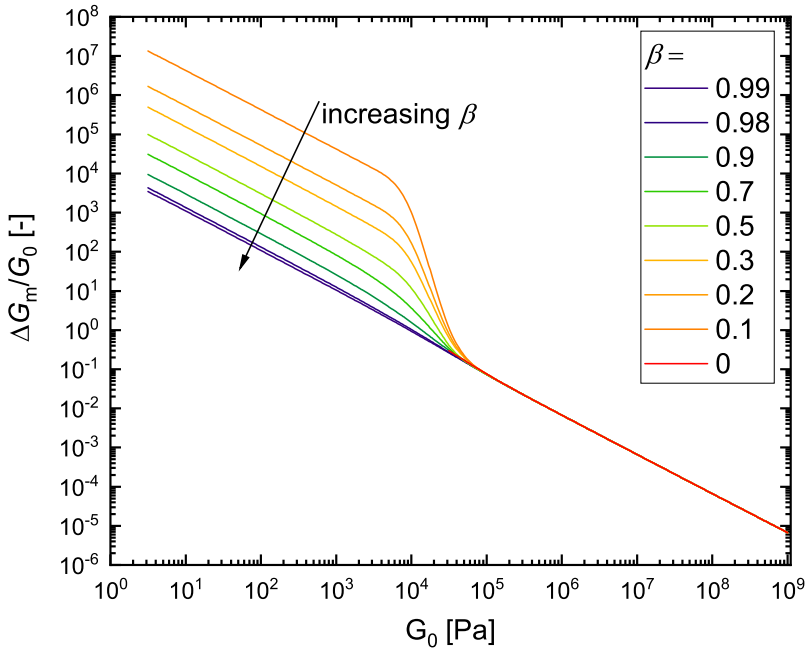

Figure 3.15: The magnetic variable shear stiffness, with respect to G_0 and β, and with a constant ϕ, M_s, μ_{ini}, and B. We are considering an isotropic distribution of particles $\alpha = 1$, $\phi = 0.05$, $M_s = 1582$ kA/m, $\mu_{ini} = 21.5$, and $B = 0.5$ T. This figure is created by finding the equilibrium strain using equation 3.24 and referencing equations 3.13 and 3.29 to find the variable shear stiffness.

ure 3.26 does not show any dependence on G_0. Therefore, the decrease in total variable shear stiffness with an increase in the shear modulus G_0 is due to the underlying magnetic contribution to variable stiffness. While the magnetic variable shear stiffness equation 3.13 has no dependence on G_0, it does have a dependence on ε_{eq}, and the ε_{eq} is dependent on G_0. The equilibrium strain ε_{eq} is due to the balance of magnetic and elastic stresses at very small strains for 'stiff' MRE's as shown in Figure 3.20. A larger G_0 contributes to the initial sharp increase in elastic normal stress with respect to strain. If G_0 is larger, the elastic normal stress will be equivalent to the magnetic normal stress and reach steady state at smaller equilibrium strains ε_{eq}. Therefore, a larger G_0 corresponds to a smaller ε_{eq} and approaches a constant ΔG_m, resulting in $\frac{\Delta G_m}{G_0} \sim G_0^{-1}$.

The dependence of variable shear stiffness on the MRE nonlinearity term

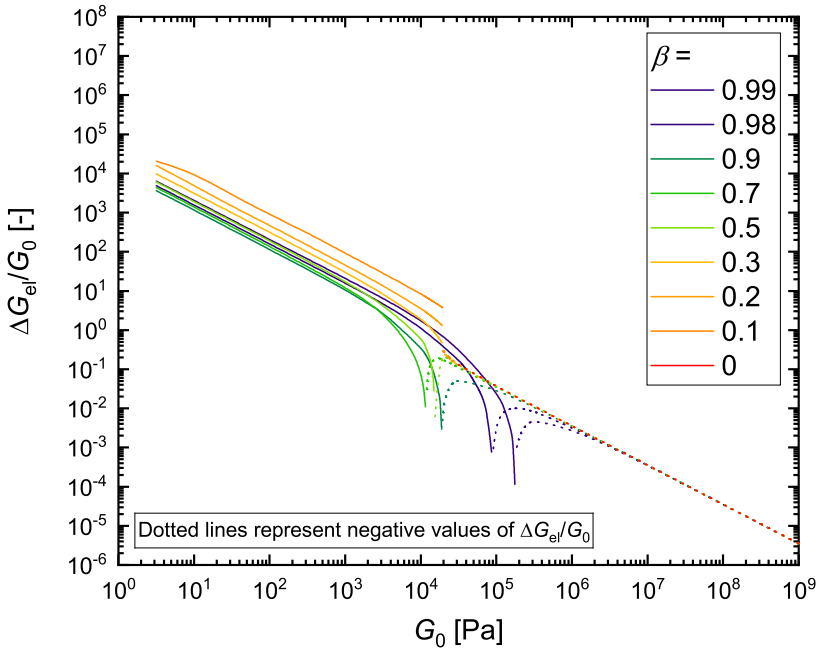

Figure 3.16: A log-log representation of the elastic variable shear stiffness with respect to G_0 and β. A larger point density should be used to fill in the gap between the solid lines and dotted lines. We are considering an isotropic distribution of particles $\alpha = 1$, $\phi = 0.05$, $M_s = 1582$ kA/m, $\mu_{ini} = 21.5$, and $B = 0.5$ T. This figure is created by finding the equilibrium strain using equation 3.24 and referencing equations 3.22 and 3.30 to find the variable shear stiffness.

β stems from the elastic contribution to the total variable shear stiffness. However, since equilibrium is achieved at extremely small strains ε_{eq}, the elastic shear modulus is not dependent on β and is $\approx G_0$. Then the elastic variable shear stiffness $\frac{\Delta G_{el}}{G_0} \approx \frac{G_0 - G_0}{G_0} = 0$, as shown in Figure 3.26. Considering equation 3.22 and taking the limit when ε_{eq} approaches zero, we find that the $\lim_{\varepsilon_{eq} \to 0} \frac{\Delta G_{el}}{G_0} = 0$ and the elastic variable shear stiffness is independent of β.

The total variable shear stiffness performance of 'stiff' MRE's is due to the magnetic contribution, since we have shown that the elastic variable shear stiffness is approximately zero at small equilibrium strains and independent

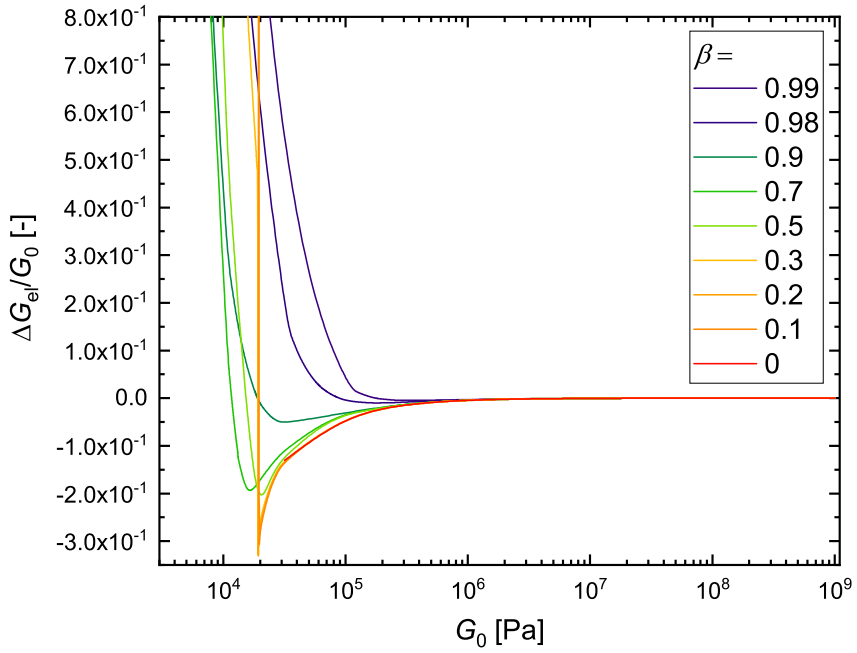

Figure 3.17: The elastic variable shear stiffness with respect to G_0 and β. We are considering an isotropic distribution of particles $\alpha = 1$, $\phi = 0.05$, $M_s = 1582$ kA/m, $\mu_{ini} = 21.5$, and $B = 0.5$ T. This figure is created by finding the equilibrium strain using equation 3.24 and referencing equations 3.22 and 3.30 to find the variable shear stiffness.

of β,

$$\frac{\Delta G}{G_0} \approx \frac{\Delta G_m}{G_0}. \tag{3.34}$$

This magnetic contribution to the total variable shear stiffness is the underlying reason that the variable shear stiffness increases as the initial shear modulus decreases. In this 'stiff' regime, the nonlinearity β of the MRE does not play a role in the MRE variable shear stiffness performance, but the shear modulus G_0 is significant.

3.6.2 'Soft' MRE

Considering the 'soft' MRE performance in Figure 3.23, we find that the slope is also equal to negative one, however the nonlinear β terms do not

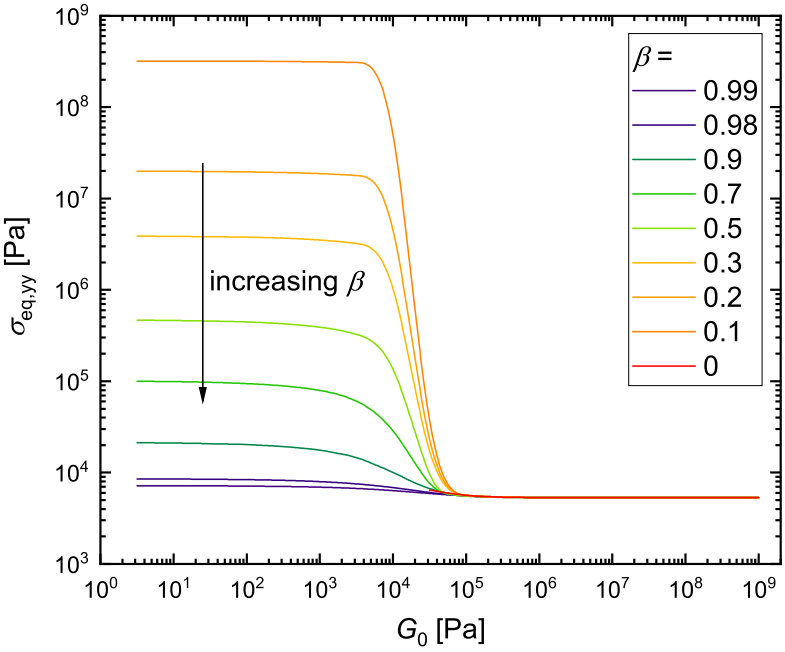

Figure 3.18: The equilibrium stress with respect to G_0 and β. We are considering an isotropic distribution of particles $\alpha = 1$, $\phi = 0.05$, $M_s = 1582$ kA/m, $\mu_{ini} = 21.5$, and $B = 0.5$ T. This figure is created by finding the equilibrium strain using equation 3.24 and referencing equation 3.21 to find the equilibrium stress.

overlap. Therefore, the total variable shear stiffness in this 'soft' regime can be represented as

$$\frac{\Delta G}{G_0} \sim G_0^{-1} \qquad \frac{\Delta G}{G_0} \approx f_m(\varepsilon_{eq}) + f_{el}(\varepsilon_{eq}, \beta), \tag{3.35}$$

where both the shear modulus G_0 and nonlinearity β effect the total variable shear stiffness of the 'soft' MRE.

The magnetic contribution shown in Figure 3.24 shows that $\frac{\Delta G_m}{G_0} = f(\varepsilon_{eq}) \sim G_0^{-1}$ and the elastic contribution shown in Figure 3.25 shows that $\frac{\Delta G_{el}}{G_0} = f(\varepsilon_{eq}, \beta) \sim G_0^{-1}$. Thus, both the magnetic and elastic contributions contribute the the increase in total variable shear stiffness with a decrease in G_0.

We look to Figure 3.28 to see the dependence of the equilibrium strain on G_0 and β. The shear modulus G_0 does not appear to effect the equilibrium

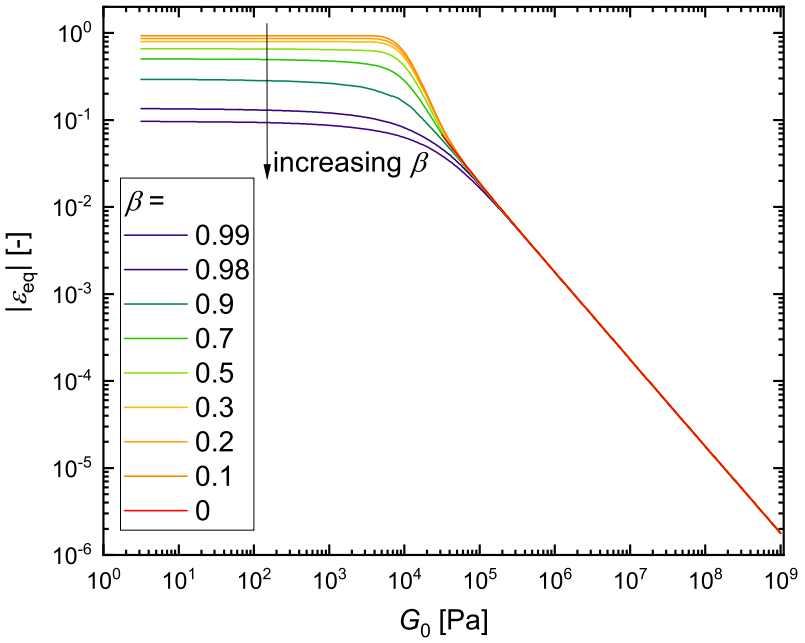

Figure 3.19: The equilibrium strain with respect to G_0 and β. We are considering an isotropic distribution of particles $\alpha = 1$, $\phi = 0.05$, $M_s = 1582$ kA/m, $\mu_{ini} = 21.5$, and $B = 0.5$ T. This figure is created by finding the equilibrium strain using equation 3.24.

strain ε_{eq} significantly, however the nonlinearity term β has a large effect on the equilibrium strain. This is due to the fact that the elastic normal stress does not reach a steady state where it is equivalent to the magnetic normal stress until the equilibrium strain approaches its finite elasticity limit as shown in Figure 3.21. As discussed previously, the finite strain in compression is heavily dependent on β but does not deviate significantly with a change in G_0. The MRE can achieve a significantly higher equilibrium strain ε_{eq} with a smaller nonlinear term β and shear modulus G_0.

The magnetic variable shear stiffness contribution $f(\varepsilon_{eq})$ does have a significant dependence on β and a mild dependence on G_0, since β and G_0 effect the equilibrium strain ε_{eq}. The magnetic contribution can be seen in Figure 3.24 where a larger magnetic variable shear stiffness can be achieved with a smaller nonlinearity term β, smaller shear modulus G_0, and complimentary larger equilibrium strain ε_{eq}.

The elastic variable shear stiffness contribution is dependent on both ε_{eq}

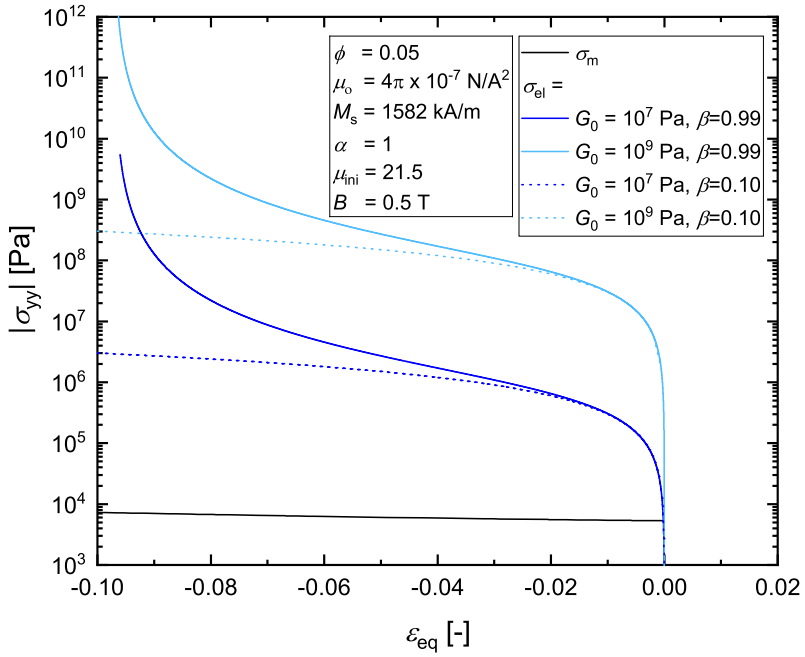

Figure 3.20: The normal stress contributions from the magnetic and equilibrium free energies with respect to the equilibrium strain ε_{eq} for 'stiff' MRE's. The equilibrium strain is found when $\sigma_m = \sigma_{el}$. We are considering an isotropic distribution of particles $\alpha = 1$, $\phi = 0.05$, $M_s = 1582$ kA/m, $\mu_{ini} = 21.5$, and $B = 0.5$ T. This figure is created by referencing equations 3.12 and 3.21 to find stress.

and β as shown in Figures 3.28 and 3.25. We already discussed how the equilibrium strain changes significantly with β and G_0 in this 'soft' region. As seen in equation 3.22, a larger equilibrium strain ε_{eq} causes a larger elastic variable shear stiffness contribution. However, a larger β also causes a larger elastic variable shear stiffness contribution. This creates an unclear trend in the effect that a MRE's nonlinearity can have on the elastic variable shear stiffness, because there is a trade-off between large equilibrium strains (which depend on small nonlinearity terms) and large nonlinearity terms. As shown in Figure 3.25, if β is less than 0.9, a larger variable stiffness can be achieved with a larger ε_{eq} and a smaller β. However, if the nonlinearity term β is approaching unity ($\beta > 0.9$), a larger elastic variable shear stiffness can be achieved with a smaller ε_{eq} and a larger β.

For the 'soft' MRE's, we have shown that the total variable shear stiffness is

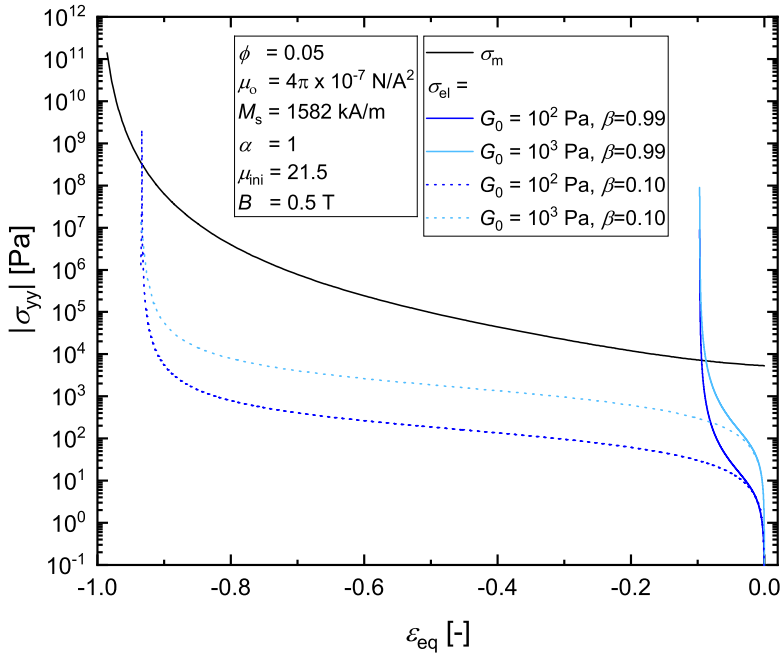

Figure 3.21: The normal stress contributions from the magnetic and equilibrium free energies with respect to the equilibrium strain ε_{eq} for 'soft' MRE's. The equilibrium strain is found when $\sigma_m = \sigma_{el}$. We are considering an isotropic distribution of particles $\alpha = 1$, $\phi = 0.05$, $M_s = 1582$ kA/m, $\mu_{ini} = 21.5$, and $B = 0.5$ T. This figure is created by referencing equations 3.12 and 3.21 to find stress.

dependent on both the magnetic contribution and elastic contribution. Both the magnetic and elastic variable shear stiffness contributions are $\sim G_0^{-1}$. However, the magnetic variable shear stiffness does have a larger contribution to the total variable shear stiffness than the elastic contribution. The shear modulus G_0 and nonlinearity β effect the total variable shear stiffness.

3.6.3 'Semi-soft' MRE

If we consider a MRE with a shear modulus of $10^4 < G_0 < 10^6$ Pa, as shown in Figure 3.23, the total variable shear stiffness increases with a decrease in G_0. However, there is an unclear trend with respect to the nonlinearity β.

Referring to the magnetic contribution in Figure 3.24, the magnetic variable shear stiffness increases with a decrease in G_0 and β, which is a similar

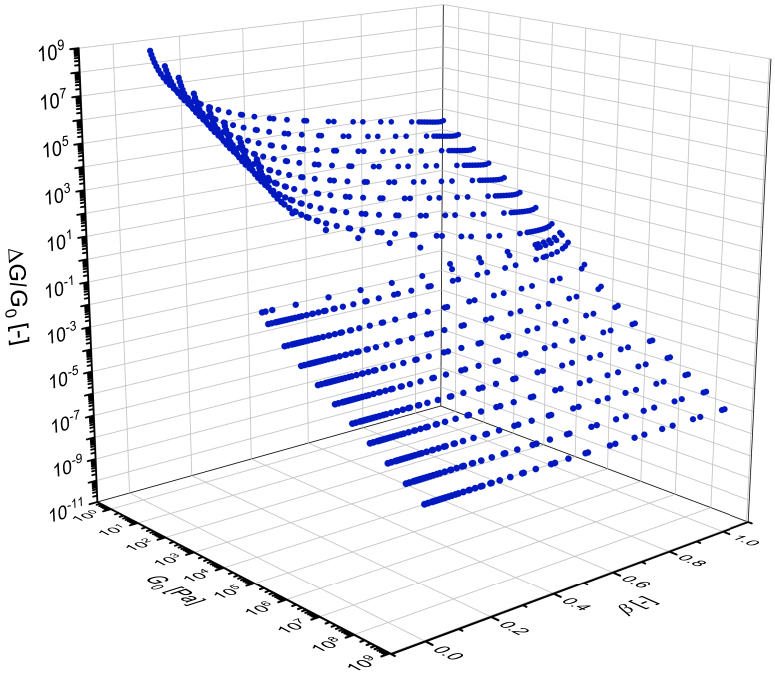

Figure 3.22: The total variable shear stiffness with respect to G_0 and β, including contributions from the magnetic and elastic free energy of a MRE, represented as a 'design of' surface plot tool. We are considering an isotropic distribution of particles $\alpha = 1$, $\phi = 0.05$, $M_s = 1582$ kA/m, $\mu_{ini} = 21.5$, and $B = 0.5$ T. This figure is created by finding the equilibrium strain using equation 3.24 and referencing equations 3.26 and 3.28 to find the variable shear stiffness.

behavior to the 'soft' MRE. However, the magnetic variable shear stiffness increases more rapidly with a small change in shear modulus G_0 for the 'semi-soft' MRE. This is due to the fact that the steady state strain that is achieved from the balance of the elastic and magnetic stresses has not yet approached the finite elastic strain limit. Thus, the equilibrium strain can continue to increase rapidly with a decrease in shear modulus until the equilibrium strain approaches the finite elastic strain limit. The magnetic contribution to the total variable shear stiffness is apparent from Figures 3.23 and 3.24.

Considering the elastic contribution in Figures 3.25 and 3.26, we see that large nonlinearity's approaching unity ($\beta \to 1$) have a large elastic variable shear stiffness. This is not a trend that we observed in 'soft' and 'stiff' MRE's. This is due to the change in elastic shear modulus G_{el} under com-

pression with respect to the equilibrium strain ε_{eq}, as shown in Figure 3.12. The elastic shear modulus with respect to equilibrium strain initially is equivalent to G_0 ('stiff' MRE's). Then the shear modulus begins to decrease under compression with an increasing equilibrium strain $|\varepsilon_{eq}|$ ('semi-soft' MRE's). Eventually, when the equilibrium strain approaches the finite elastic strain limit, the shear modulus begins to increase ('soft' MRE's). Thus, for 'semi-soft' MRE's with a nonlinearity β approaching unity, the finite elastic strain limit is approached at extremely small strains and the shear modulus very quickly increases and contributes to the elastic and total variable shear stiffness.

For 'semi-soft' MRE's, the magnetic variable shear stiffness is a large contribution to the total variable shear stiffness. The elastic variable shear stiffness is much smaller in magnitude and does not have a large contribution to the total variable shear stiffness, with the exception of 'semi-soft' MRE's with a nonlinearity approaching unity. Aside from the extremely nonlinear MRE's, the elastic contribution actually contributes a softening behavior since the elastic variable shear stiffness is < 1. This will be discussed in more detail in Chapter 4.

3.6.4 'Design of' tool

We present the MRE variable shear stiffness predictions in a surface plot shown in Figure 3.22. This surface plot could be used as a 'design of' tool when combined with the design framework proposed by *Mohammad Vatankhah-Varnosfaderani, Sergei S. Sheiko, et al.* for designing bottlebrush PDMS [91]. Based on a desired variable shear stiffness, this design tool could be used to find the initial shear modulus and nonlinear term that a material should have to obtain the variable shear stiffness. After selecting the necessary G_0 and β values, these parameters can be used directly in the design framework for designing bottlebrush PDMS [91]. Given G_0 and β, this design framework finds the degrees of polymerization of the side chains, the spacer between neighbouring side chains, and the strand backbone needed for fabrication.

3.6.5 Universal behavior

For our variable shear stiffness results, we described the predictive behavior of the MRE's referring to three different categories of 'stiff', 'soft', and 'semi-soft' MRE's. We defined these categories based on the shear modulus. However, this is not universal, and the shear modulus where these three different categories of predictive behavior may occur will vary depending on the magnetic particles, volume fraction, and magnetic field strength. These three regimes can be put into a more universal language by considering a ratio of magnetic and elastic contributions, as opposed to the shear modulus which only represents the elastic contribution. In equation 3.25, the equilibrium strain is found to be dependent on β and $\frac{u_o\phi^2\left(\frac{M}{M_s}\right)^2}{G_0}$. Then the nonlinear shear modulus is dependent on ε_{eq}, β, and $\frac{u_o\phi^2\left(\frac{M}{M_s}\right)^2}{G_0}$, as shown in equation 3.27. Therefore, the variable shear stiffness results should be reported as a function of $\frac{G_0}{u_o\phi^2\left(\frac{M}{M_s}\right)^2}$ as opposed to G_0 to show a universal behavior for all nonlinear MRE's with varying magnetic contributions and elastic contributions, as shown in Figures 3.23-3.28.

We consider the universal transition point between the 'soft' and 'semi-soft' MRE categories by defining a critical equilibrium strain and solving for a critical ratio of magnetic and elastic contributions $\frac{u_o\phi^2\left(\frac{M}{M_s}\right)^2}{G_0}$. The 'soft' MRE is defined by a dominating magnetic contribution which causes the nonlinear MRE to reach a finite elastic strain limit ($\varepsilon_{eq} \to 1$). Therefore, we define the 'soft' MRE regime by defining a critical equilibrium strain, $\varepsilon_{eq} \geq 0.9\varepsilon_{max}$. We can find ε_{max} by referring to equation 3.21 where a singularity is apparent when $\frac{\beta}{3}((1+\varepsilon_{max})^2 + 2(1+\varepsilon_{max})^{-1}) \to 1$. Then we find that

$$\beta = \frac{3}{(1+\varepsilon_{max})^2 + 2(1+\varepsilon_{max})^{-1}}. \tag{3.36}$$

We can now solve for the critical ratio of magnetic and elastic contributions by considering the equilibrium stress $\sigma_{el,yy} = \sigma_{m,yy}$ using $\varepsilon_{eq} = 0.9\varepsilon_{max}$ and $\beta = \frac{3}{(1+\varepsilon_{max})^2+2(1+\varepsilon_{max})^{-1}}$. Then we find that the critical transition point between the 'soft' and 'semi-soft' MRE behavior is

$$\frac{u_o\phi^2\left(\frac{M}{M_s}\right)^2}{G_0} = f(0.9\varepsilon_{max}, \beta). \tag{3.37}$$

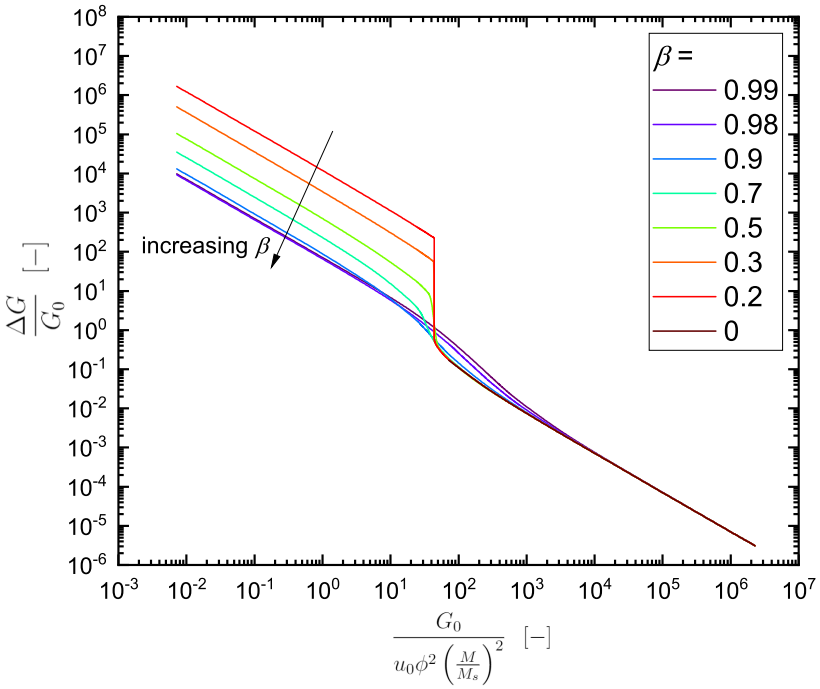

Figure 3.23: The total variable shear stiffness, including contributions from the magnetic and elastic free energy of a MRE, with respect to G_0 and β. We are considering an isotropic distribution of particles $\alpha = 1$ and predictions are universal and independent of ϕ, M_s, μ_{ini}, and B. This figure is created by finding the equilibrium strain using equation 3.24 and referencing equations 3.26 and 3.28 to find the variable shear stiffness.

However, the critical transition point is only dependent on β and not ε_{max} because we have shown the connection between β and ε_{max} in equation 3.36. Therefore, we solved for the critical transition point between the 'soft' and 'semi-soft' MRE in a universal language,

$$\frac{u_o\phi^2\left(\frac{M}{M_s}\right)^2}{G_0} = f(\beta). \tag{3.38}$$

We consider the universal transition point between the 'stiff' and 'semi-soft' MRE categories by defining a critical elastic shear stiffness deviation from linearity G_{el}/G_0 and solving for a critical ratio of magnetic and elastic contributions $\frac{u_o\phi^2\left(\frac{M}{M_s}\right)^2}{G_0}$. The 'stiff' MRE is defined by a dominating elastic contribution which causes the nonlinear MRE to behave as a linear MRE

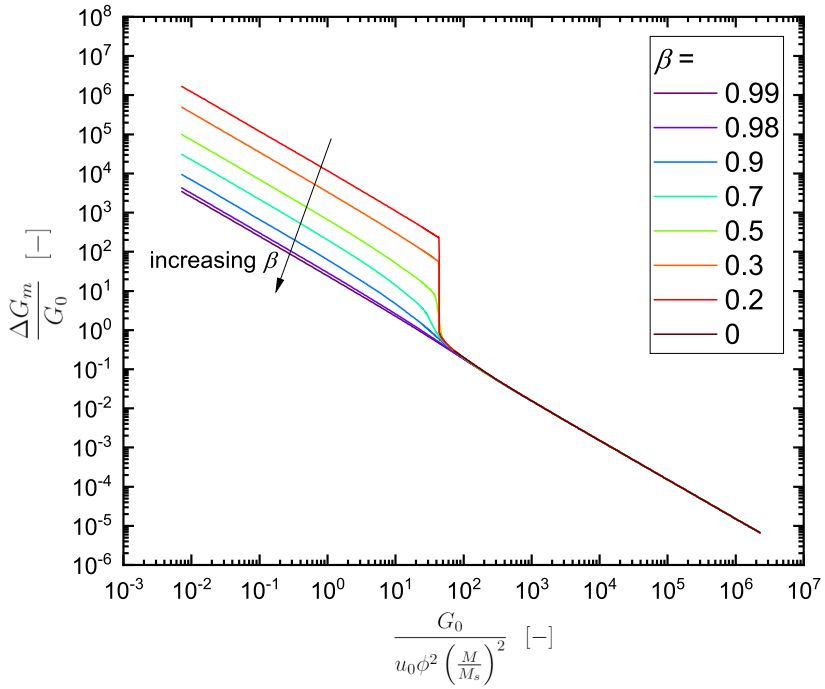

Figure 3.24: The magnetic variable shear stiffness, with respect to G_0 and β, and with a constant ϕ, M_s, μ_{ini}, and B. We are considering an isotropic distribution of particles $\alpha = 1$ and predictions are universal and independent of ϕ, M_s, μ_{ini}, and B. This figure is created by finding the equilibrium strain using equation 3.24 and referencing equations 3.13 and 3.29 to find the variable shear stiffness.

($G_{el} \rightarrow G_0$) and does not allow for significant movement of the magnetic particles. Therefore, we define the 'stiff' MRE regime by defining a critical elastic shear stiffness deviation from linearity $G_{el}/G_0 = 1.001$. Then we can solve for the combinations of β and ε_{eq} that define this transition point by considering equation 3.22.

$$\frac{G_{el}}{G_0} = f(\varepsilon_{eq}, \beta). \tag{3.39}$$

Then we can find the critical transition point in terms of a universal magnetic and elastic contribution by considering the equilibrium stress $\sigma_{el,yy} = \sigma_{m,yy}$ and using the combinations of β and ε_{eq} that define the critical elastic shear stiffness deviation from linearity $G_{el}/G_0 = 1.001$. Then we find the critical

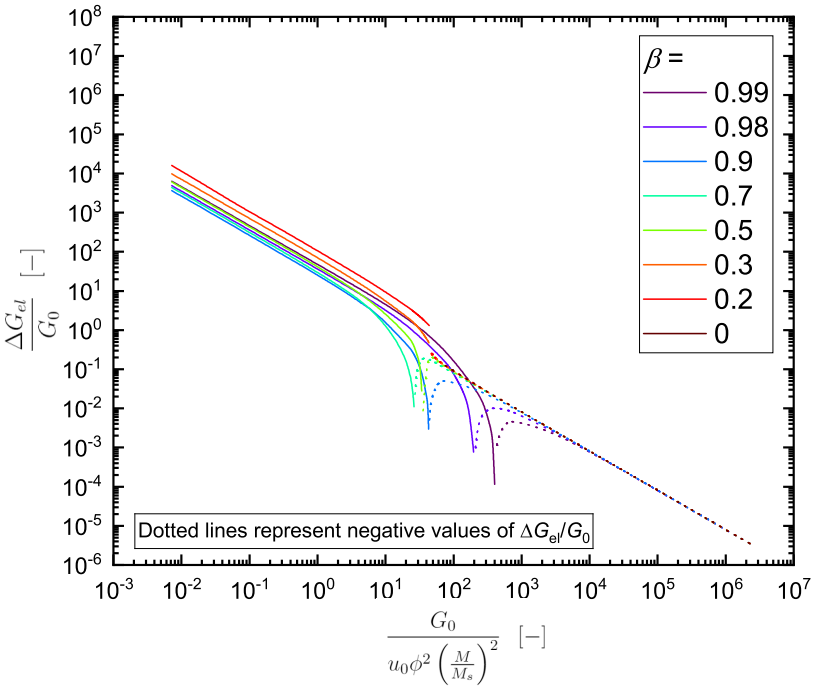

Figure 3.25: A log-log representation of the elastic variable shear stiffness with respect to G_0 and β. A larger point density should be used to fill in the gap between the solid lines and dotted lines. We are considering an isotropic distribution of particles $\alpha = 1$ and predictions are universal and independent of ϕ, M_s, μ_{ini}, and B. This figure is created by finding the equilibrium strain using equation 3.24 and referencing equations 3.22 and 3.30 to find the variable shear stiffness.

transition point between the 'stiff' and 'semi-soft' MRE as

$$\frac{u_o\phi^2\left(\frac{M}{M_s}\right)^2}{G_0} = f(\varepsilon_{eq}, \beta). \tag{3.40}$$

However, the equilibrium strain ε_{eq} has been shown to be dependent on only $\frac{u_o\phi^2\left(\frac{M}{M_s}\right)^2}{G_0}$ and β as shown in equation 3.25. Therefore, the critical transition point between the 'stiff' and 'semi-soft' MRE can be defined in a universal language as

$$\frac{u_o\phi^2\left(\frac{M}{M_s}\right)^2}{G_0} = f(\beta). \tag{3.41}$$

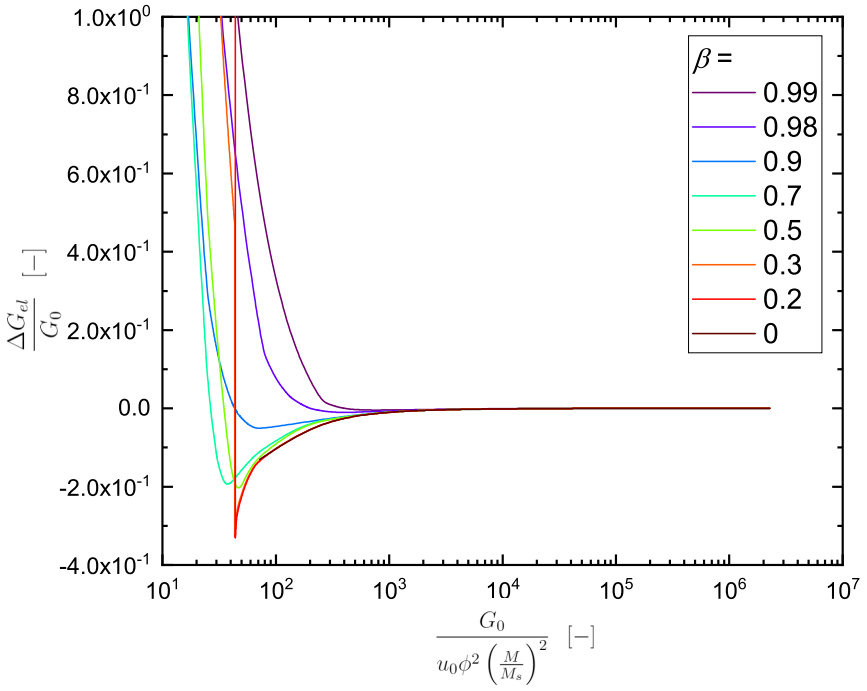

Figure 3.26: The elastic variable shear stiffness with respect to G_0 and β. We are considering an isotropic distribution of particles $\alpha = 1$ and predictions are universal and independent of ϕ, M_s, μ_{ini}, and B. This figure is created by finding the equilibrium strain using equation 3.24 and referencing equations 3.22 and 3.30 to find the variable shear stiffness.

The final solution to the critical transition points between the 3 regimes of a 'soft', 'semi-soft', and 'stiff' MRE are defined as a function of β as opposed to writing out the entire function because there is a summation in the magnetic contribution equations that requires a numerical solver (we developed code in python for this work). This section lays out the steps that need to be taken to solve for the universal critical points.

3.6.6 Limits

The predictions that we made are purely based on the free energies of the MRE and we do not consider limits on a strain to break or fracture stress. Therefore, these results show that a maximum total variable shear stiffness can be achieved with softer and more linear MRE's (decreasing G_0 and β). However, Figures 3.27 and 3.28 show a dramatic increase in equilibrium stress

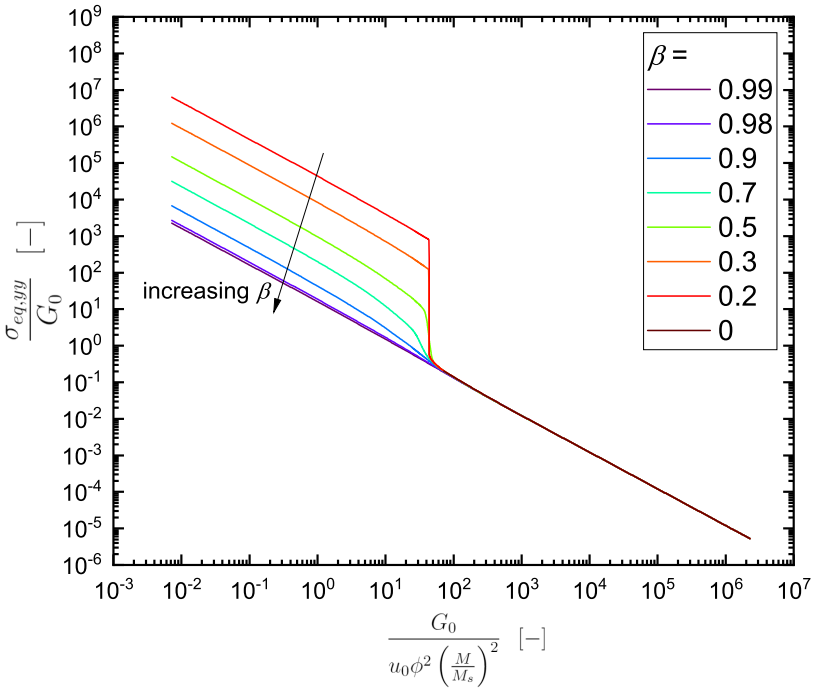

Figure 3.27: The equilibrium stress with respect to G_0 and β. We are considering an isotropic distribution of particles $\alpha = 1$ and predictions are universal and independent of ϕ, M_s, μ_{ini}, and B. This figure is created by finding the equilibrium strain using equation 3.24 and referencing equation 3.21 to find the equilibrium stress.

and equilibrium strain for 'soft' MRE's and this could potentially be beyond the failure strain and stress. In this case, a 'semi-soft' MRE would provide the largest total variable shear stiffness with a softer and extremely nonlinear MRE (decreasing G_0 and increasing β).

3.7 Conclusions

Unlike research that focuses on the magnetic contribution to the MRE performance, we show that hyperelastic material with strong nonlinearity has a nontrivial influence on MRE performance. Surprisingly, we show that nonlinearity hinders the performance of 'soft' MRE's, and only enhances the performance within a narrow range of (dimensionless) material stiffness.

In the case of hindered performance ('soft' MRE's), this is because the non-

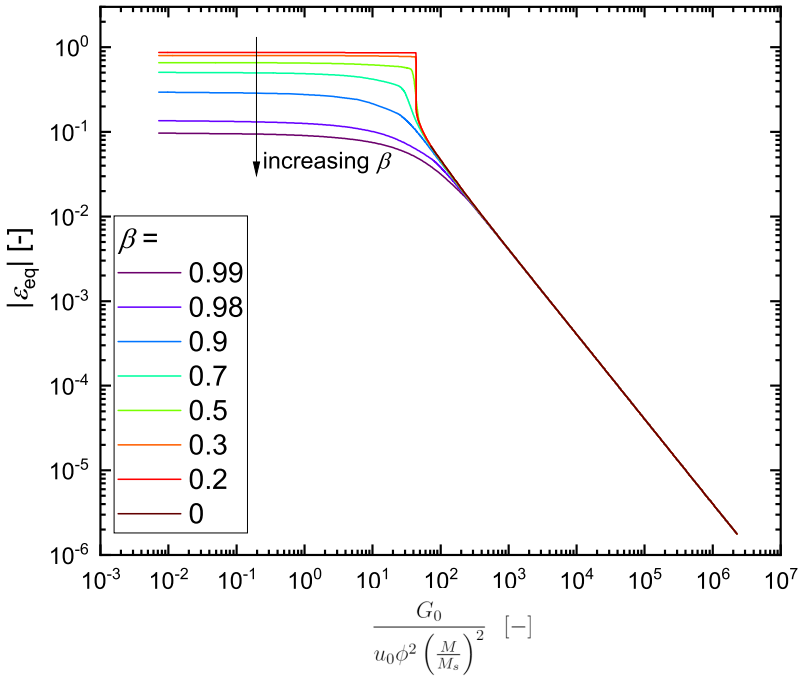

Figure 3.28: The equilibrium strain with respect to G_0 and β. We are considering an isotropic distribution of particles $\alpha = 1$ and predictions are universal and independent of ϕ, M_s, μ_{ini}, and B. This figure is created by finding the equilibrium strain using equation 3.24.

linearity inhibits very large compression and therefore inhibits what might otherwise be a large increase in magnetic elastic modulus due to small particle distances.

In the case of enhanced performance ('semi-soft' MRE's), the nonlinearity must be sufficiently strong to increase G_{el} faster than G_m as a function of compressive strain. This can only occur after a sufficiently large compressive strain, since at small compressive strains there is always compression-softening of the apparent shear modulus.

We found that the MRE demonstrated three different performances for variable shear stiffness depending on the ratio of the elastic modulus to magnetic modulus. The 'stiff' MRE showed a variable shear stiffness response that was independent of the nonlinearity β. Therefore, the variable shear stiffness results in this regime were only dependent on a linear elastic response due to the extremely small equilibrium strain. The 'soft' MRE showed a dependence on the nonlinearity β, unlike the 'stiff' MRE. The more nonlinear

MRE's had a smaller equilibrium strain ε_{eq}. Thus, the magnetic and elastic variable shear stiffness was larger for smaller nonlinearity's β (larger equilibrium strains ε_{eq}), with the exception of the elastic variable shear stiffness of MRE's with extremely large nonlinearity's ($\beta \to 1$). For the 'semi-soft' MRE's, the elastic contribution showed a nonlinear variable shear stiffness behavior. The elastic contribution was strongest for extremely large nonlinearity's approaching unity. This is due to the softening effect that occurs from the superposition of compression and shear due to our nonlinear elastic model. All MRE's increase variable shear stiffness with a decrease in shear modulus G_0, due to the larger equilibrium strain ε_{eq} when the magnetic stress is equivalent to the elastic stress. We discuss potential limits of the model predictions with respect to a strain to break and fracture stress.

As a final embodiment, we show the model predictions as a surface plot that could be used as a 'design of' tool for designing tuneable bottlebrush PDMS using the design framework proposed by *Mohammad Vatankhah-Varnosfaderani, Sergei S. Sheiko, et al.* [91].

Future work could include incorporating other nonlinear constitutive models to describe the elastic behavior of MRE's. The elastic and magnetic contributions to the variable shear stiffness could also be studied on anisotropic MRE's and MRE's with different particle distributions. Experiments could be conducted to validate our results, improve our model, and understand where our predictions may deviate from experimental results.

To relate this theoretical model to experimental work with fibrin, some assumptions could be relaxed such as (i) incompressibility and (ii) square lattice particle distribution [57]. (i) We consider an incompressible MRE in this work and would consider a confined (set gap on the rheometer) MRE to relate our predictions to experimental results. If a material is truly incompressible and confined in one plane, then it is confined in all planes. Since the nonlinear MRE model in this work directly relates internal strains to macroscopic strains assuming affine deformation, this model would assume no particle rearrangement and no internal or external strain. Therefore, the current state of this model cannot predict internal strains for incompressible confined materials and could be improved to more closely relate to experimental work with fibrin [57]. Furthermore, if a compressible material is considered that is confined in one plane (similar to the confinement on a rheometer), the particles along the magnetic field lines would naturally be

attracted to each other and other particles would repel in a perfect square lattice when a magnetic field is induced. However, at the macroscopic level this would cause the material to expand and the Poisson's ratio would be larger than 0.5, which is not achievable. (ii) This model assumes a very simple square lattice distribution of particles. However, the actual distribution of particles is much more complicated and can cause internal compressive and extensive strains. This model should be improved to capture this more realistic behavior to compare to experimental results with fibrin [57]. If these assumptions are considered, we can better model fibrin MRE behavior.

CHAPTER 4

HYPERELASTIC CONSTITUTIVE EQUATIONS STUDIED UNDER THE SUPERPOSITION OF UNIAXIAL COMPRESSION AND SIMPLE SHEAR

4.1 Introduction

Soft solids commonly used in soft machine design, such as silicone rubbers, demonstrate a hyperelastic behavior when subjected to large strains. There are many hyperelastic models that predict the behavior of these finite elastic materials, each having their own benefits. Some of these popular hyperelastic models are the Neo-Hookean, Mooney-Rivlin, Fung, Gent, and Ogden constitutive equations [45, 46]. We study the performance of these constitutive models under the superposition of uniaxial compression and simple shear and demonstrate the effect of the nonlinear material constant on the predicted performance. To the best of our knowledge, a comparison of these constitutive models under this deformation has not been studied before and it is important to understand the predictive performance of these models to make an appropriate model selection for design.

This type of deformation has been previously discussed in magnetorheological elastomers in Chapter 3 where an induced magnetic field caused uniaxial deformation and an imposed simple shear deformation was applied to the material. This type of deformation is also relevant to much experimental rheometry work that studies the effect of pre-strain on elastomeric materials [46, 106, 107].

We find that all models predict an initial compression-softening of apparent shear modulus ($|\varepsilon_{yy}| \uparrow, G'_{0,yx} \downarrow$). Additionally, the Fung, Gent, and nonlinear chain network models reach a finite elastic strain limit in compression where compression-stiffening of apparent shear modulus is observed. This initial compression-softening of apparent shear modulus has been observed in experimental rheometry on semiflexible polymers and biopolymer networks, such as fibrin and collagen [106, 107].

However, experimental work on other hyperelastic materials, such as tissues, demonstrates a continual compression-stiffening of apparent shear modulus that common constitutive models cannot predict ($|\varepsilon_{yy}| \uparrow, G'_{0,yx} \uparrow$) [46]. Previous work attempted to use these popular constitutive models to describe the compression-stiffening of apparent shear modulus of brain and fat tissue, however, their methods for solving for the apparent shear modulus do not correspond to the shear modulus that can be measured on a rheometer since they consider an apparent shear modulus that is derived from a traction stress [46]. In our work, we find the apparent shear modulus by simply taking the derivative of the shear stress with respect to shear strain $G'_{yx}(\lambda, \gamma) = \frac{\partial \sigma_{yx}}{\partial \gamma}$ which should correlate the rheometer measurements.

Therefore, we conclude that all hyperelastic constitutive models that were studied can only predict a compression-softening of apparent shear modulus, relevant to semiflexible polymers and biopolymer networks [106, 107]. We relate the compression-softening of apparent shear modulus seen in these constitutive models to the performance of single chain models to describe the underlying reason for compression-softening. We also conclude that to the best of our knowledge, there is no hyperelastic constitutive model that can properly predict the compression-stiffening of apparent shear modulus seen in tissues [46], even though these are 'good' models for other types of deformation such as uniaxial and simple shear independently. There is a need for a new constitutive model that can predict the performance of these hyperelastic tissues under compression and imposed simple shear.

4.2 Methods

4.2.1 Hyperelastic models

We study hyperelastic models assuming homogeneous, isotropic, and incompressible conditions. The models that we study in this work are the Neo-Hookean, Mooney-Rivlin, Fung, Gent, nonlinear chain network (nonlinear elastic model from chapter 3), and Ogden models shown in Table 4.1.

The Neo-Hookean model is a second order approximation of strain energy density that describes entropic elasticity of polymer chains, and the Mooney-Rivlin model is a third order approximation [46]. The Mooney-

Table 4.1: Common constitutive equations for hyperelastic incompressible materials. All models only contain a maximum of 2 material property constants with the exception of the Ogden model. For the Ogden model, $\lambda_1, \lambda_2, \lambda_3$ are the principle stretches and the number of material property constants depends on the degree of summation.

Hyperelastic constitutive equations [45, 46, 47]	
Name	**Strain energy density function**
Neo-Hookean	$U = \frac{G_0}{2}(I_1 - 3)$ G_0 is a material property
Mooney-Rivlin	$U = \frac{\mu_1}{2}(I_1 - 3) + \frac{\mu_2}{2}(I_2 - 3)$, where $G_0 = \mu_1 + \mu_2$ μ_1, μ_2 are material properties
Fung	$U = \frac{G_0}{2\alpha}(e^{\alpha(I_1-3)} - 1)$ G_0, α are material properties
Gent	$U = -\frac{G_0}{2\beta}\ln(1 - \beta(I_1 - 3))$ G_0, β are material properties
Nonlinear chain network	$U = 3G_0\left[1 + \frac{2}{(1-\beta)^2}\right]^{-1}\left[\frac{I_1}{6} + \beta^{-1}\left(1 - \frac{\beta I_1}{3}\right)^{-1}\right]$ G_0, β are material properties
Ogden	$U = \sum_{i=1}^{N}\frac{2\mu_i}{\alpha_i^2}(\lambda_1^{\alpha_i} + \lambda_2^{\alpha_i} + \lambda_3^{\alpha_i} - 3)$, where $G_0 = \sum_{i=1}^{N}\mu_i$ μ, α are material properties
Arruda-Boyce	$U = \mu\left[\frac{1}{2}(I_1 - 3) + \frac{1}{20\beta^2}(I_1^2 - 9) + \frac{11}{1050\beta^4}(I_1^3 - 27) + ...\right]$ μ, β are material properties

Rivlin model is more complex than the Neo-Hookean model, but it more accurately predicts the deformation of elastomers at larger strains. The Ogden and Arruda-Boyce models are also rubber elasticity models that approximate the strain energy density and include a summation of unlimited terms [45]. Therefore, these models may be more accurate than the Neo-Hookean and Mooney-Rivlin models at larger strains, but they are much more complicated. The Fung, Gent, and nonlinear chain network models best capture

extremely nonlinear materials under uniaxial loading [108, 109]. They are commonly used to predict the nonlinear behavior of biological materials like tissue, skin, fibrin, and other materials with a soft elastic matrix and stiff fibers [108, 110]. Each of these nonlinear models is chosen to predict material performance based on their advantages and disadvantages. However, these advantages and disadvantages are unclear under the superposition of uniaxial compression and simple shear which has not been rigorously studied before.

4.2.2 Macroscopic deformation

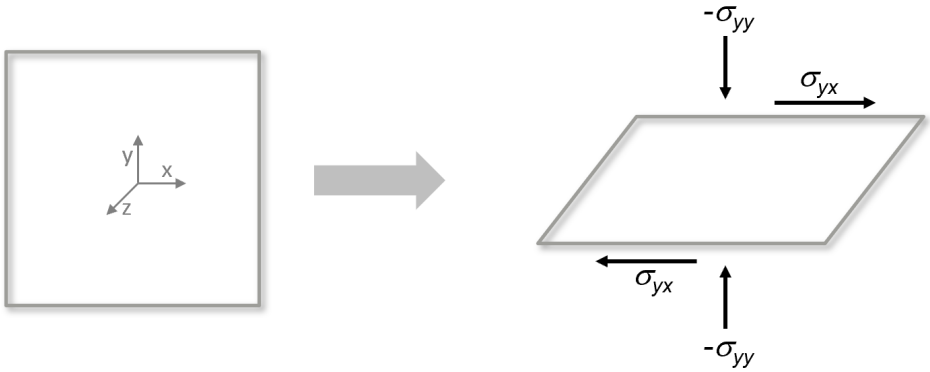

Figure 4.1: Deformation under the superposition of compression and simple shear.

The deformation can be seen in Figure 4.1, where the compressive force is applied normal to the shear force. Assuming an unconfined incompressible material, the displacement equations for the superposition of uniaxial deformation and simple shear are [46, 11]

$$\begin{aligned} x &= x_o\lambda^{-1/2} + y_o\lambda\gamma \\ y &= y_o\lambda \\ z &= z_o\lambda^{-1/2}. \end{aligned} \tag{4.1}$$

In equation 4.1, x_o, y_o, and z_o are the initial positions with respect to each coordinate axis, and x, y, and z are the positions with respect to each coordinate axis after deformation. Also, γ is the imposed shear strain and λ is the uniaxial stretch ratio. The stretch ratio λ is related to the uniaxial engineering strain ε as: $\lambda = 1 + \varepsilon$. The Finger tensor and the inverse Finger

tensor are calculated from the deformation tensor,

$$\underline{\underline{F}} = \begin{bmatrix} \frac{\partial x}{\partial x_o} & \frac{\partial x}{\partial y_o} & \frac{\partial x}{\partial z_o} \\ \frac{\partial y}{\partial x_o} & \frac{\partial y}{\partial y_o} & \frac{\partial y}{\partial z_o} \\ \frac{\partial z}{\partial x_o} & \frac{\partial z}{\partial y_o} & \frac{\partial z}{\partial z_o} \end{bmatrix} \qquad \underline{\underline{F}} = \begin{bmatrix} \lambda^{-\frac{1}{2}} & \gamma\lambda & 0 \\ 0 & \lambda & 0 \\ 0 & 0 & \lambda^{-\frac{1}{2}} \end{bmatrix} \tag{4.2}$$

$$\underline{\underline{B}} = \underline{\underline{F}} \cdot \underline{\underline{F}}^T = \begin{bmatrix} \lambda^{-1} + \gamma^2\lambda^2 & \gamma\lambda^2 & 0 \\ \gamma\lambda^2 & \lambda^2 & 0 \\ 0 & 0 & \lambda^{-1} \end{bmatrix} \tag{4.3}$$

$$\underline{\underline{B}}^{-1} = \begin{bmatrix} \lambda & -\gamma\lambda & 0 \\ -\gamma\lambda & \gamma^2\lambda + \lambda^{-2} & 0 \\ 0 & 0 & \lambda \end{bmatrix}. \tag{4.4}$$

The first invariant I_1 and second invariant I_2 of the Finger tensor for the superposition of uniaxial and simple shear strain are

$$\begin{aligned} I_1 &= tr(\underline{\underline{B}}) = \lambda^2 + 2\lambda^{-1} + \gamma^2\lambda^2 \\ I_2 &= \frac{1}{2}\left(tr(\underline{\underline{B}})^2 - tr(\underline{\underline{B}}^2)\right) = \lambda + \lambda^{-2} + \lambda\gamma^2. \end{aligned} \tag{4.5}$$

Now that the deformation of the material under uniaxial extension / compression and simple shear deformation is understood, the shear stress and apparent shear modulus can be derived from the material strain energy density.

4.2.3 Shear stress and apparent shear modulus calculation

The Cauchy true stress is derived from the strain energy density function U defined for each constitutive model in Table 4.1. The true stress can be written in the Rivlin-Ericksen representation as [46]

$$\underline{\underline{\sigma}} = -p\underline{\underline{I}} + \beta_1\underline{\underline{B}} + \beta_{-1}\underline{\underline{B}}^{-1}, \tag{4.6}$$

where p is the hydrostatic pressure, $\underline{\underline{I}}$ is the identity tensor, $\underline{\underline{B}}$ is the Finger tensor, and β_1 and β_{-1} are derived from the strain energy density function with respect to the first and second invariants of the Finger tensor $\underline{\underline{B}}$ [46].

The material response coefficients β_1 and β_{-1} are

$$\beta_1 = 2\frac{\partial U}{\partial I_1} \qquad\qquad \beta_{-1} = -2\frac{\partial U}{\partial I_2}, \tag{4.7}$$

where I_1 and I_2 are the first and second invariants of the Finger tensor [46]. The shear stress can be found from equation 4.6 and simplified to

$$\begin{aligned} \sigma_{yx} &= \beta_1 B_{yx} + \beta_{-1} B_{yx}^{-1} \\ \sigma_{yx} &= \beta_1 \gamma\lambda^2 - \beta_{-1}\gamma\lambda \end{aligned} \tag{4.8}$$

under the superposition of uniaxial and simple shear strain since the hydrostatic pressure p is equal to zero in shear and $B_{yx} = \gamma\lambda^2$ from equation 4.3. The material response coefficients β_1 and β_{-1} are dependent on the constitutive model that is selected (Table 4.1).

The apparent shear modulus G'_{yx} is derived from the shear stress σ_{yx},

$$G'_{yx} = \frac{\partial \sigma_{yx}}{\partial \gamma} \tag{4.9}$$

where $G'_{yx} = G'_{yx}(\lambda, \gamma)$ is a function of the state of deformation. We are primarily interested in the apparent linear shear modulus $G'_{yx}(\lambda, \gamma = 0)$ as a function of the uniaxial deformation λ. Our method for solving for the shear stress and apparent shear modulus for all constitutive models that are dependent on the Finger tensor invariants are based on equations 4.6-4.9 and specific to a superposition of compression and simple shear deformation.

The Ogden model differs from the other constitutive models that are discussed because it is dependent on principle stretches instead of invariants of the Finger tensor. Therefore, we use a different method to find the shear stress,

$$\sigma_{ij} = \frac{\lambda_1}{\lambda_1\lambda_2\lambda_3}\frac{\partial U}{\partial \lambda_1} b_{1,i} b_{1,j} + \frac{\lambda_2}{\lambda_1\lambda_2\lambda_3}\frac{\partial U}{\partial \lambda_2} b_{2,i} b_{2,j} + \frac{\lambda_3}{\lambda_1\lambda_2\lambda_3}\frac{\partial U}{\partial \lambda_3} b_{3,i} b_{3,j} \tag{4.10}$$

where $\lambda_1, \lambda_2, \lambda_3$ are the principle stretches, $\lambda_1^2, \lambda_2^2, \lambda_3^2$ are the eigenvalues of the Finger tensor $\underline{\underline{B}}$, and b_1, b_2, b_3 are the eigenvectors of the Finger tensor $\underline{\underline{B}}$. The eigenvalues and eigenvectors for the specific deformation of the superposition

of comrpession and simple shear are

$$\begin{aligned}
\lambda_1^2 &= \lambda^{-1} \\
\lambda_2^2 &= \frac{\gamma^2\lambda^2 + \lambda^2 + \lambda^{-1} + \sqrt{(-\gamma^2\lambda^2 - \lambda^2 - \lambda^{-1})^2 - 4\lambda}}{2} \\
\lambda_3^2 &= \frac{\gamma^2\lambda^2 + \lambda^2 + \lambda^{-1} - \sqrt{(-\gamma^2\lambda^2 - \lambda^2 - \lambda^{-1})^2 - 4\lambda}}{2} \\
\underline{b_1} &= \begin{bmatrix} 0 \\ 0 \\ 1 \end{bmatrix} \\
\underline{b_2} &= \begin{bmatrix} 1 \\ -\gamma^{-1}\lambda^{-3} - \gamma + \gamma^{-1}\lambda^{-2}\lambda_2^2 \\ 0 \end{bmatrix} \\
\underline{b_3} &= \begin{bmatrix} 1 \\ -\gamma^{-1}\lambda^{-3} - \gamma + \gamma^{-1}\lambda^{-2}\lambda_3^2 \\ 0 \end{bmatrix}.
\end{aligned} \tag{4.11}$$

The method for finding the apparent shear modulus G'_{yx} from the shear stress σ_{yx} is the same for all constitutive models so we can reference equation 4.9. This summarizes the methods used to find the shear modulus based on the selected constitutive model under the deformation of the superposition of compression and simple shear.

4.3 Results

4.3.1 Neo-Hookean

The Neo-Hookean strain energy density function is

$$U = \frac{G_0}{2}(I_1 - 3). \tag{4.12}$$

From equation 4.7 we find that the material response coefficients for the Neo-Hookean model are

$$\beta_1 = G_0 \qquad\qquad \beta_{-1} = 0. \tag{4.13}$$

From equation 4.8 the shear stress for the Neo-Hookean model is solved,

$$\sigma_{yx} = G_0 \gamma \lambda^2. \tag{4.14}$$

Then the apparent shear modulus found from equation 4.9 for the Neo-Hookean model is

$$G'_{yx} = G_0 \lambda^2. \tag{4.15}$$

When $\lambda = 1$, the apparent shear modulus is equivalent to the shear modulus $G'_{yx} = G_0$. This is the same result as in simple shear deformation. The apparent shear modulus is also independent of shear strain γ, therefore, the Neo-Hookean model predicts a linear response in shear and $G'_{0,yx} = G_0 \lambda^2$. However, this model predicts a nonlinear response in compression. As the material is compressed ($\lambda < 1$), the apparent shear modulus decreases and a nonlinear softening behavior is observed. As the material is extended ($\lambda > 1$), the apparent shear modulus increases and a nonlinear stiffening behavior is observed. This behavior can be seen in Figures 4.2-4.4.

4.3.2 Mooney-Rivlin

The Mooney-Rivlin strain energy density function is

$$U = \frac{\mu_1}{2}(I_1 - 3) + \frac{\mu_2}{2}(I_2 - 3). \tag{4.16}$$

From equation 4.7 we find that the material response coefficients for the Mooney-Rivlin model are

$$\beta_1 = \mu_1 \qquad\qquad \beta_{-1} = -\mu_2. \tag{4.17}$$

From equation 4.8 the shear stress for the Mooney-Rivlin model is solved,

$$\begin{aligned} \sigma_{yx} &= \mu_1 \gamma \lambda^2 + \mu_2 \gamma \lambda \\ \sigma_{yx} &= \gamma \lambda^2 (\mu_1 + \mu_2 \lambda^{-1}). \end{aligned} \tag{4.18}$$

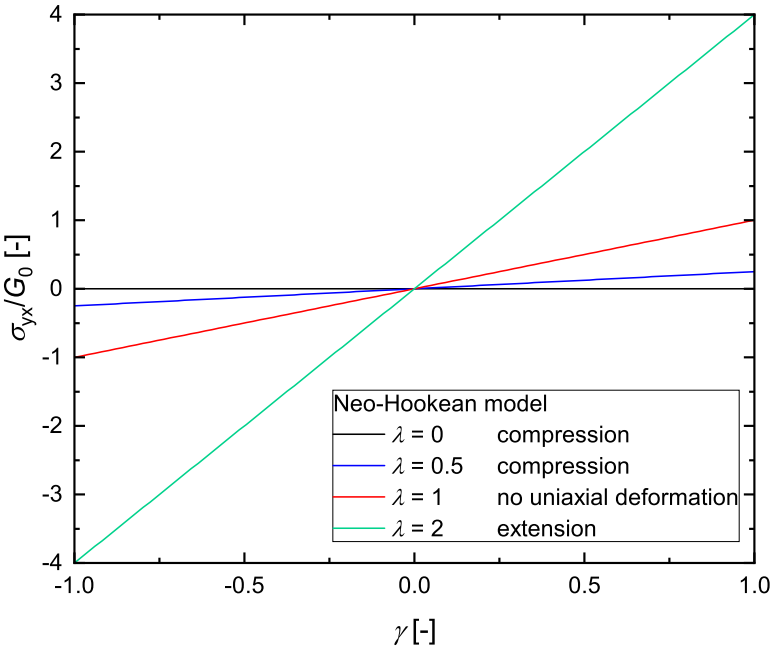

Figure 4.2: The Neo-Hookean shear stress response normalized by the shear modulus of a material under uniaxial pre-strain and applied simple shear deformation. This figure is created from equation 4.14.

Then the apparent shear modulus found from equation 4.9 for the Mooney-Rivlin model is

$$G'_{yx} = \lambda^2(\mu_1 + \mu_2\lambda^{-1}). \tag{4.19}$$

When $\lambda = 1$, the apparent shear modulus is equal to the summation of the material response coefficients $G'_{yx} = \mu_1 + \mu_2$. Therefore, $\mu_1 + \mu_2 = G_0$ in the limit of small strains and without extension or compression. Similar to the Neo-Hookean model, we also see that the Mooney-Rivlin model predicts a linear response in shear. However, the apparent shear modulus changes in compression and extension, with an extra term included compared to the Neo-Hookean model. This model also predicts a softening behavior in compression and a stiffening behavior in extension. This behavior can be seen in Figures 4.5-4.7.

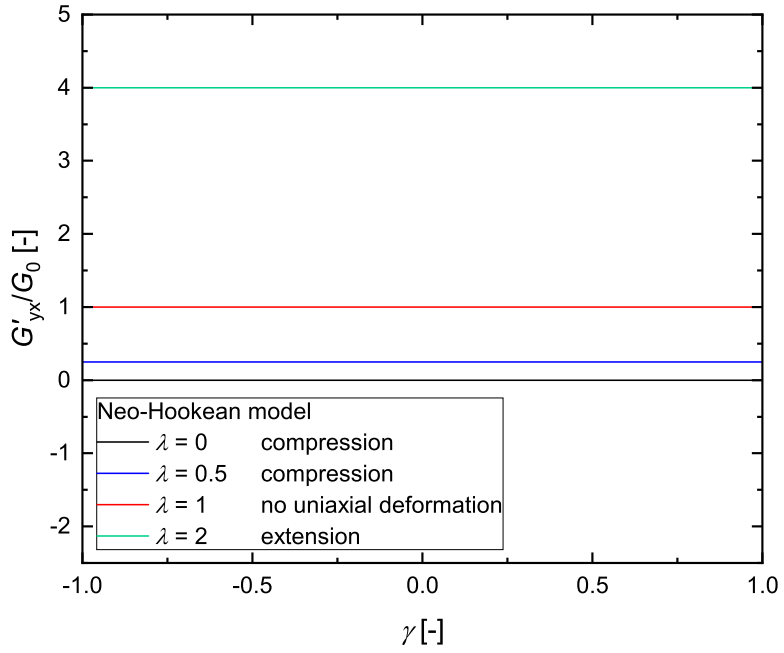

Figure 4.3: The Neo-Hookean apparent shear modulus normalized by the shear modulus of a material under uniaxial pre-strain and applied simple shear deformation. This figure is created from equation 4.15.

4.3.3 Fung

The Fung strain energy density function is

$$U = \frac{G_0}{2\alpha}(e^{\alpha(I_1-3)} - 1). \tag{4.20}$$

From equation 4.7 we find that the material response coefficients for the Fung model are

$$\beta_1 = G_0 e^{\alpha(I_1-3)} \qquad \beta_{-1} = 0. \tag{4.21}$$

From equation 4.8 the shear stress for the Fung model is solved,

$$\begin{aligned} \sigma_{yx} &= G_0\gamma\lambda^2 e^{\alpha(I_1-3)} \\ \sigma_{yx} &= G_0\gamma\lambda^2 e^{\alpha(\lambda^2+2\lambda^{-1}+\lambda^2\gamma^2-3)}. \end{aligned} \tag{4.22}$$

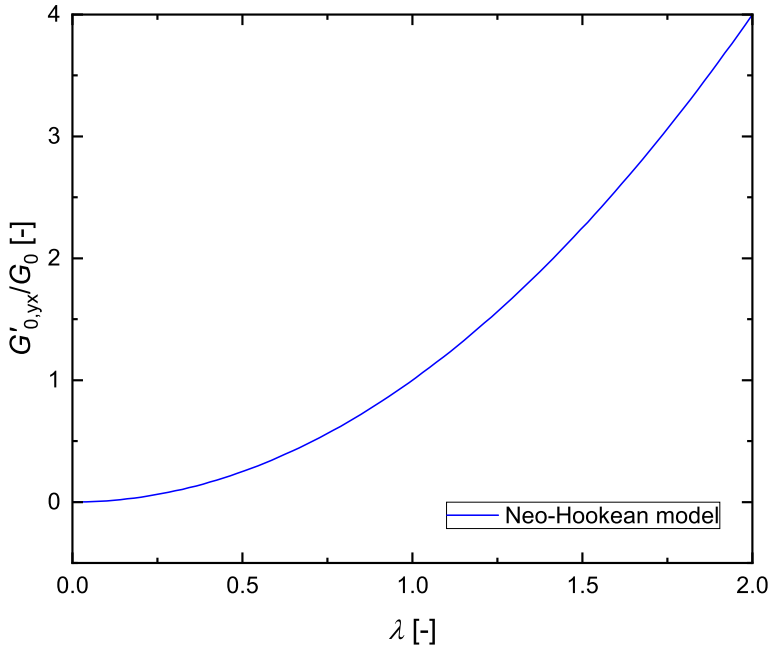

Figure 4.4: The Neo-Hookean apparent tangent shear modulus normalized by the shear modulus of a material under uniaxial pre-strain and applied simple shear deformation. This figure is created from equation 4.15 when $\gamma = 0$.

Then the apparent shear modulus found from equation 4.9 for the Fung model is

$$G'_{yx} = G_0\lambda^2 e^{\alpha(\lambda^2+2\lambda^{-1}+\lambda^2\gamma^2-3)}\left(2\lambda^2\gamma^2\alpha+1\right). \tag{4.23}$$

While the Neo-Hookean and Mooney-Rivlin models predict a constant G'_{yx} in shear, the Fung model predicts a non-constant G'_{yx} as a function of γ. If we consider the case where $\gamma = 0$, then the shear modulus is dependent only on compression $G'_{0,yx} = G_0\lambda^2 e^{\alpha(\lambda^2+2\lambda^{-1}-3)}$. Therefore, we see that in a small shear strain limit, the apparent shear modulus still has a dependence on the uniaxial stretch ratio and softens in compression and stiffens in extension. If we consider the case when $\lambda = 1$, then $G'_{yx} = G_0 e^{\alpha\gamma^2}(2\alpha\gamma^2+1)$. This is the nonlinear apparent shear modulus in simple shear. The response to the superposition of compression and simple shear can be seen in Figures 4.8-4.10. Figure 4.10 shows the dependence on the nonlinear parameter α where a

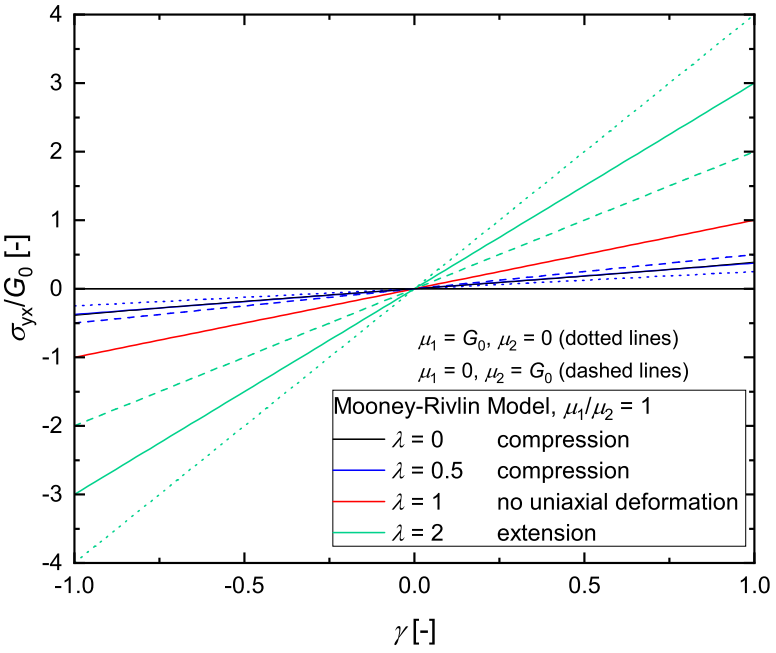

Figure 4.5: The Mooney-Rivlin shear stress response normalized by the shear modulus of a material under uniaxial pre-strain and applied simple shear deformation. This figure is created from equation 4.18.

larger nonlinear term shows compression-stiffening of apparent shear modulus at smaller uniaxial deformations.

4.3.4 Gent

The Gent strain energy density function is

$$U = -\frac{G_0}{2\beta}\ln(1-\beta(I_1-3)). \tag{4.24}$$

From equation 4.7 we find that the material response coefficients for the Gent model are

$$\beta_1 = \frac{G_0}{1-\beta(I_1-3)} \qquad \beta_{-1} = 0. \tag{4.25}$$

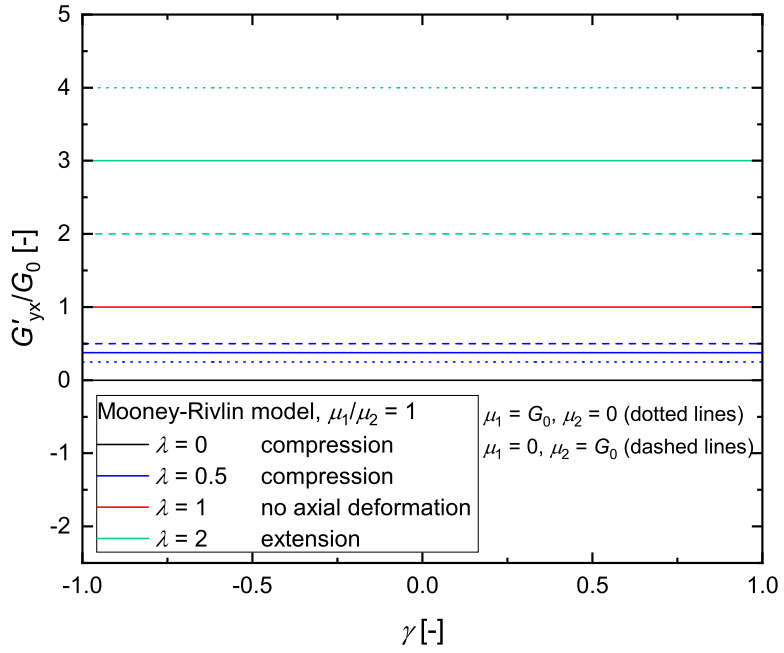

Figure 4.6: The Mooney-Rivlin apparent shear modulus normalized by the shear modulus of a material under uniaxial pre-strain and applied simple shear deformation. This figure is created from equation 4.19.

From equation 4.8 the shear stress for the Gent model is solved,

$$\begin{aligned} \sigma_{yx} &= \frac{G_0\gamma\lambda^2}{1-\beta(I_1-3)} \\ \sigma_{yx} &= \frac{G_0\gamma\lambda^2}{1-\beta(\lambda^2+2\lambda^{-1}+\gamma^2\lambda^2-3)}. \end{aligned} \tag{4.26}$$

Then the apparent shear modulus found from equation 4.9 for the Gent model is

$$G'_{yx} = \frac{G_0\lambda^2}{1-\beta(\lambda^2+2\lambda^{-1}+\gamma^2\lambda^2-3)}\left[1+\frac{2\lambda^2\beta\gamma^2}{(1-\beta(\lambda^2+2\lambda^{-1}+\lambda^2\gamma^2-3))^2}\right]. \tag{4.27}$$

The Gent model response is similar to the Fung model, as they are both models that typically capture extremely nonlinear behavior of fibrous biological materials. If we consider the case where $\gamma = 0$, then $G'_{0,yx} = \frac{G_0\lambda^2}{1-\beta(\lambda^2+2\lambda^{-1}-3)}$ and the apparent shear modulus still has a dependence on

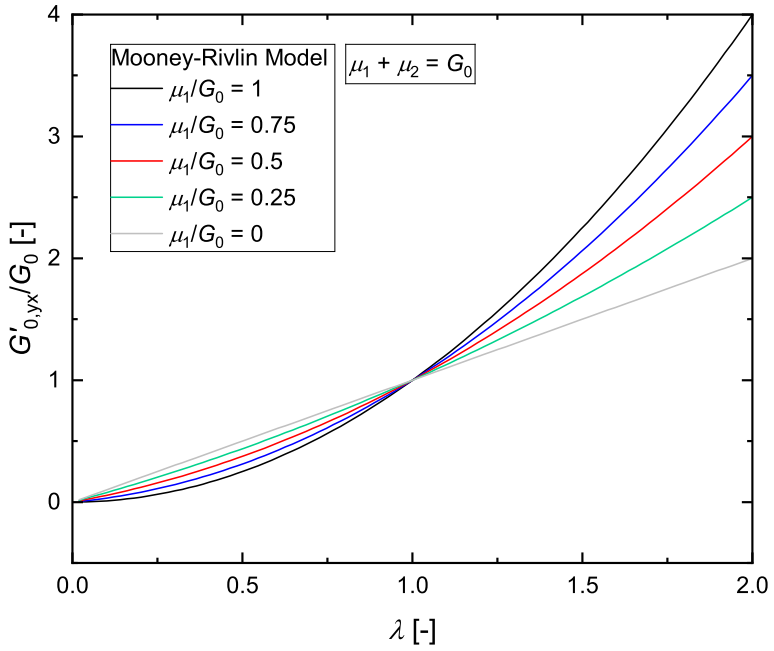

Figure 4.7: The Mooney-Rivlin apparent tangent shear modulus normalized by the shear modulus of a material under uniaxial pre-strain and applied simple shear deformation. This figure is created from equation 4.19 when $\gamma = 0$.

λ^2 at small shear strains, which causes a softening behavior in compression and a stiffening behavior in extension. However, there is a singularity when $\beta(\lambda^2 + 2\lambda^{-1} - 3) = 1$ and this singularity typically captures a dramatic stiffening behavior due to finite extensibility in fibrous biological materials. If we consider $\lambda = 1$, then $G'_{yx} = \frac{G_0}{1-\beta\gamma^2}[1 + \frac{2\beta\gamma^2}{(1-\beta\gamma^2)^2}]$ and the apparent shear modulus for simple shear deformation is recovered. The apparent shear modulus behavior for the Gent model can be seen in Figures 4.11-4.13. Figure 4.13 shows the dependence on the nonlinear parameter β where a larger nonlinear term shows compression-stiffening of apparent shear modulus at smaller uniaxial and shear deformations.

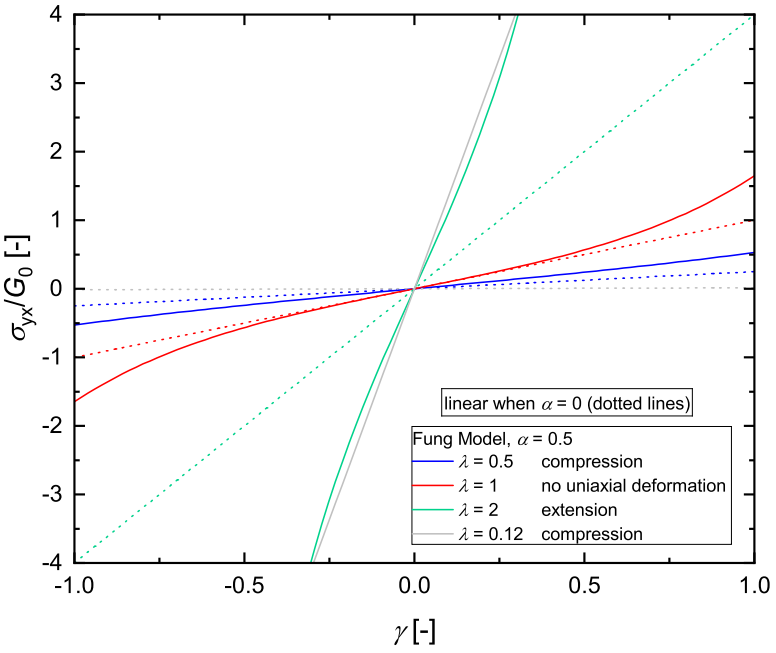

Figure 4.8: The Fung shear stress response normalized by the shear modulus of a material under uniaxial pre-strain and applied simple shear deformation. This figure is created from equation 4.22.

4.3.5 Nonlinear chain network

The strain energy density function described in a paper by *Andrey V. Dobrynin* and *Jan-Michael Y. Carrillo* [12] is

$$U = 3G_0 \left[1 + \frac{2}{(1-\beta)^2}\right]^{-1} \left[\frac{I_1}{6} + \beta^{-1}\left(1 - \frac{\beta I_1}{3}\right)^{-1}\right]. \tag{4.28}$$

From equation 4.7 we find that the material response coefficients for the nonlinear chain network model are

$$\beta_1 = G_0 \left[1 + \frac{2}{(1-\beta)^2}\right]^{-1} \left[1 + \frac{18}{(\beta I_1 - 3)^2}\right] \qquad \beta_{-1} = 0. \tag{4.29}$$

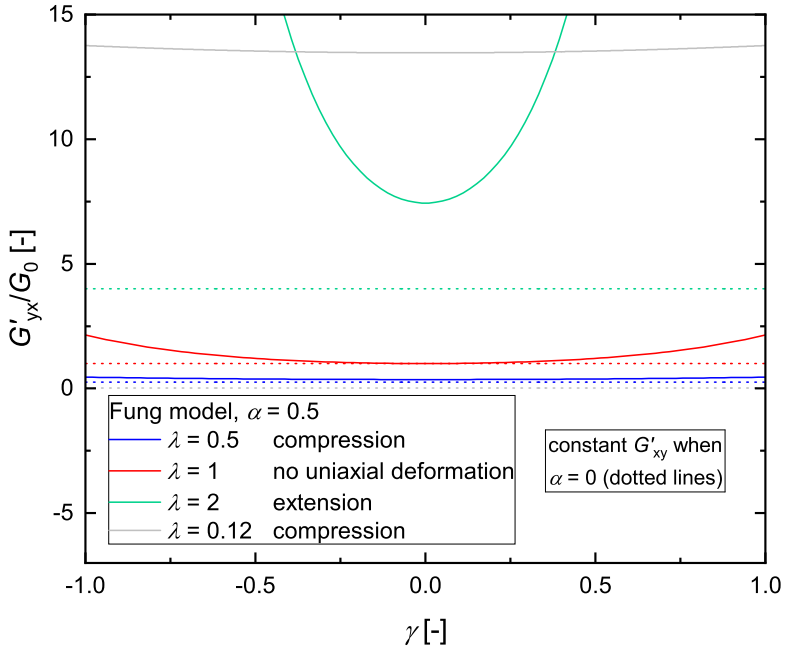

Figure 4.9: The Fung apparent shear modulus normalized by the shear modulus of a material under uniaxial pre-strain and applied simple shear deformation. This figure is created from equation 4.23.

From equation 4.8 the shear stress for the nonlinear chain network model is solved,

$$\begin{aligned}\sigma_{yx} &= G_0\gamma\lambda^2\left[1+\frac{2}{(1-\beta)^2}\right]^{-1}\left[1+\frac{18}{(\beta I_1-3)^2}\right]\\ \sigma_{yx} &= G_0\gamma\lambda^2\left[1+\frac{2}{(1-\beta)^2}\right]^{-1}\left[1+\frac{18}{(\beta(\lambda^2+2\lambda^{-1}+\lambda^2\gamma^2)-3)^2}\right].\end{aligned} \tag{4.30}$$

Then the apparent shear modulus found from equation 4.9 for the nonlinear chain network model is

$$G'_{yx} = G_0\lambda^2\left[1+\frac{2}{(1-\beta)^2}\right]^{-1}\left[1+2\left(1-\frac{\beta I_1}{3}\right)^{-2}+\frac{8}{3}\lambda^2\gamma^2\beta\left(1-\frac{\beta I_1}{3}\right)^{-3}\right], \tag{4.31}$$

where $I_1 = \lambda^2 + 2\lambda^{-1} + \lambda^2\gamma^2$.

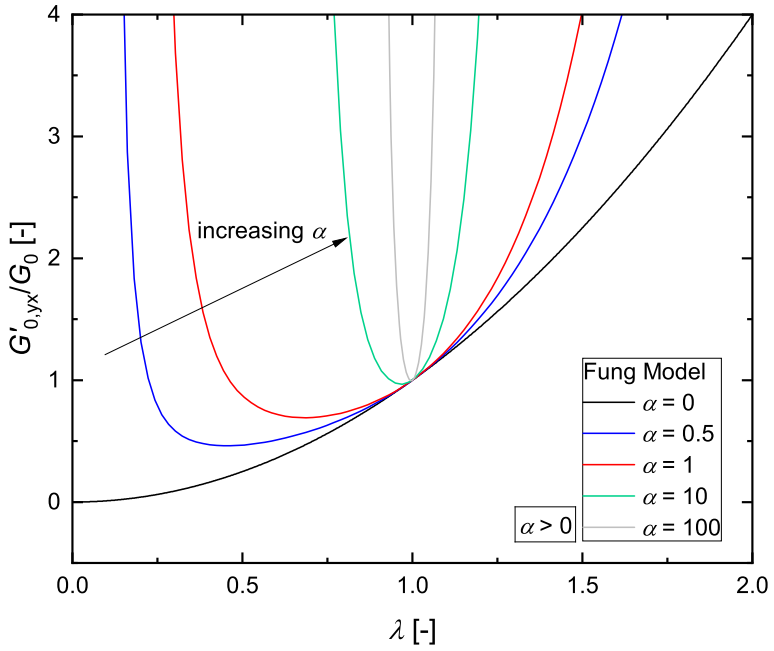

Figure 4.10: The Fung apparent tangent shear modulus normalized by the shear modulus of a material under uniaxial pre-strain and applied simple shear deformation. This figure is created from equation 4.23 when $\gamma = 0$.

The model used by Dobrynin also captures extremely nonlinear behavior from fibrous materials, similar to the Fung and Gent models. This nonlinear behavior is captured from the singularity at $\beta = 1$ and $\frac{\beta I_1}{3} = 1$. A significant dependence of the apparent shear modulus on λ^2 can also be seen in equation 4.31. If we consider the case where $\gamma = 0$, then the shear modulus is recovered as a function of λ: $G'_{0,yx} = G_0\lambda^2\left[1+\frac{2}{(1-\beta)^2}\right]^{-1}\left[1+2\left(1-\frac{\beta(\lambda^2+2\lambda^{-1})}{3}\right)^{-2}\right]$. This model also describes a softening apparent shear modulus in compression and stiffening in extension. The model predictions can be seen in Figures 4.14-4.16. Figure 4.16 shows the dependence on the nonlinear parameter β where a larger nonlinear term shows compression-stiffening of apparent shear modulus at smaller uniaxial and shear deformations.

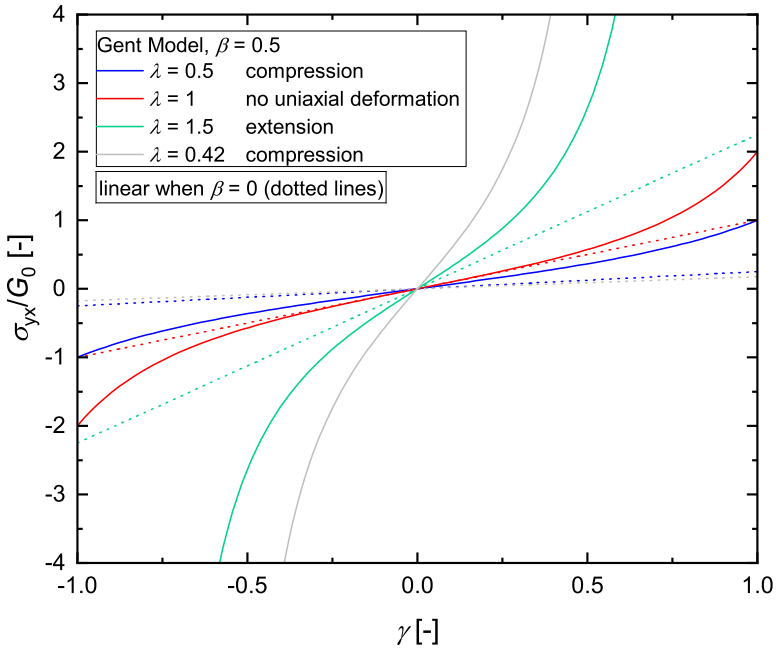

Figure 4.11: The Gent shear stress response normalized by the shear modulus of a material under uniaxial pre-strain and applied simple shear deformation. This figure is created from equation 4.26.

4.3.6 Ogden

The Ogden strain energy density function is

$$U = \sum_{i=1}^{N} \frac{2\mu_i}{\alpha_i^2}(\lambda_1^{\alpha_i} + \lambda_2^{\alpha_i} + \lambda_3^{\alpha_i} - 3). \tag{4.32}$$

The shear stress found from equation 4.10 can be simplified to

$$\sigma_{yx} = \lambda_2 \frac{\partial U}{\partial \lambda_2} b_{2,x} b_{2,y} + \lambda_3 \frac{\partial U}{\partial \lambda_3} b_{3,x} b_{3,y} \tag{4.33}$$

for the superposition of compression and simple shear deformation since $\lambda_1\lambda_2\lambda_3 = 1$ and $b_{1,x}b_{1,y} = 0$. The parameters $\lambda_2, \lambda_3, b_{2,x}, b_{2,y}, b_{3,x}, b_{3,y}$ can be found in equation 4.11 in terms of γ and λ. We also find that $\frac{\partial U}{\partial \lambda_2} = \sum_{i=1}^{N} \frac{2\mu_i}{\alpha_i} \lambda_2^{\alpha_i - 1}$ and $\frac{\partial U}{\partial \lambda_3} = \sum_{i=1}^{N} \frac{2\mu_i}{\alpha_i} \lambda_3^{\alpha_i - 1}$. Therefore, we have each term in the shear stress equation in terms of λ and γ. Now we can solve for the apparent shear modulus for the Ogden model using the method described in equation

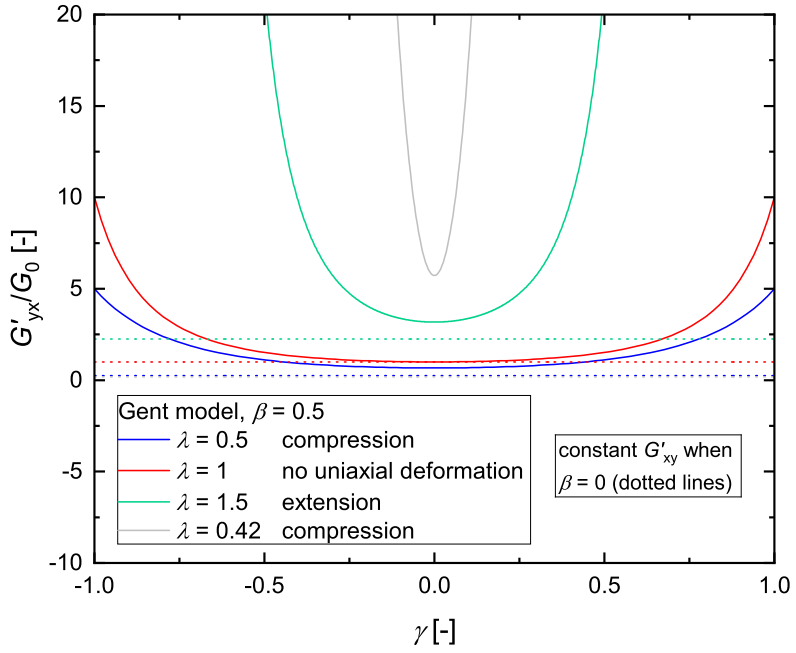

Figure 4.12: The Gent apparent shear modulus normalized by the shear modulus of a material under uniaxial pre-strain and applied simple shear deformation. This figure is created from equation 4.27.

4.9. We do not show the full equation here because it is too lengthy to write out in full.

The Ogden model results differ from the other analyzed constitutive models because it cannot predict shear strain and shear modulus under the superposition of uniaxial deformation and simple shear for small shear strains. For our results, we use model fit parameters that were previously used to fit the response of brain tissue under a combination of uniaxial deformation and simple shear [46]. As shown in Figure 4.17, there is a singularity when $\gamma = 0$ if any uniaxial deformation is imposed. Therefore, this model may not be well suited for this type of deformation. At larger shear strains, we also see that the apparent shear modulus decreases in compression as shown in Figure4.18.

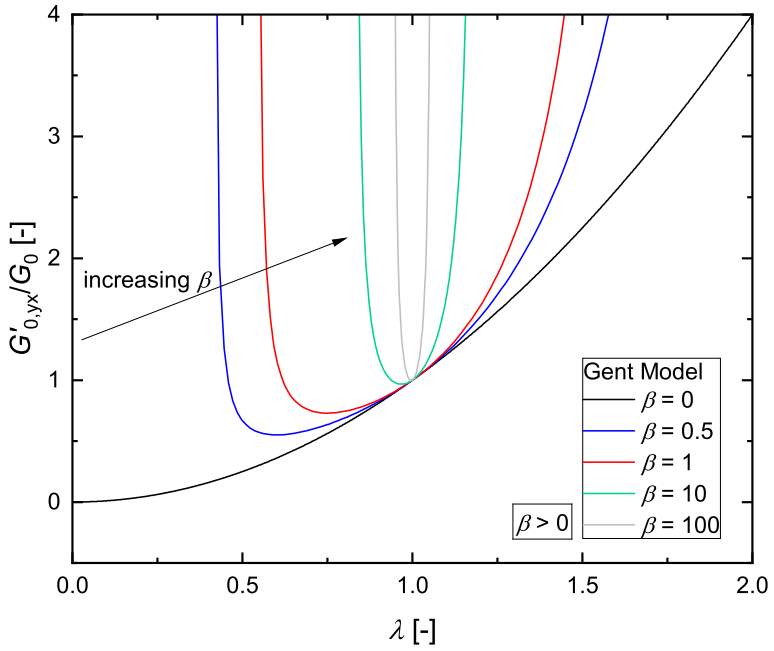

Figure 4.13: The Gent apparent tangent shear modulus normalized by the shear modulus of a material under uniaxial pre-strain and applied simple shear deformation. This figure is created from equation 4.27 when $\gamma = 0$.

4.4 Discussion

4.4.1 Model comparison

Our results show that for all constitutive models that were reviewed, uniaxial compression softens the apparent shear modulus G'_{yx}. To the best of our knowledge, this is a conclusion that has previously not been reported. This is significant since many elastomeric materials, such as biological tissues, show a stiffening effect under the superposition of compression and simple shear [46], however there is no existing model that can predict this behavior. The Fung, Gent, and nonlinear chain network models eventually show stiffening, but not until a critical strain is approached, as shown in Figure 4.19. This critical strain can be controlled by the nonlinear material constants α and β. The Neo-Hookean and Mooney-Rivlin models are not capable of predicting any stiffening behavior under compression (or simple shear) as shown in Figure 4.19 and Table 4.3. The apparent shear modulus equations for each

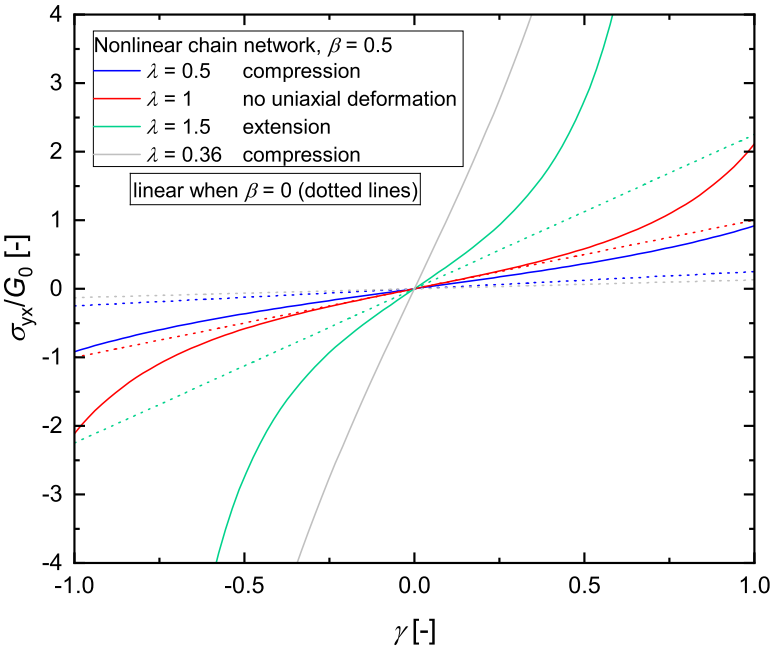

Figure 4.14: The nonlinear chain network shear stress response normalized by the shear modulus of a material under uniaxial pre-strain and applied simple shear deformation. This figure is created from equation 4.30.

nonlinear constitutive equation can be seen in Table 4.2.

4.4.2 Molecular theory of rubber elasticity

We investigate the molecular theory of rubber elasticity to find an underlying explanation for this compression softening behavior that is predicted by the researched constitutive models.

4.4.3 Gaussian spring model

We consider an elastic matrix as a continuum of many polymer chains. The force on a single polymer chain that is deformed, assuming a linear relationship between force and extension described by a Gaussian chain, is [111]

$$\underline{f} = 2k_bT\beta^2\underline{R} \tag{4.34}$$

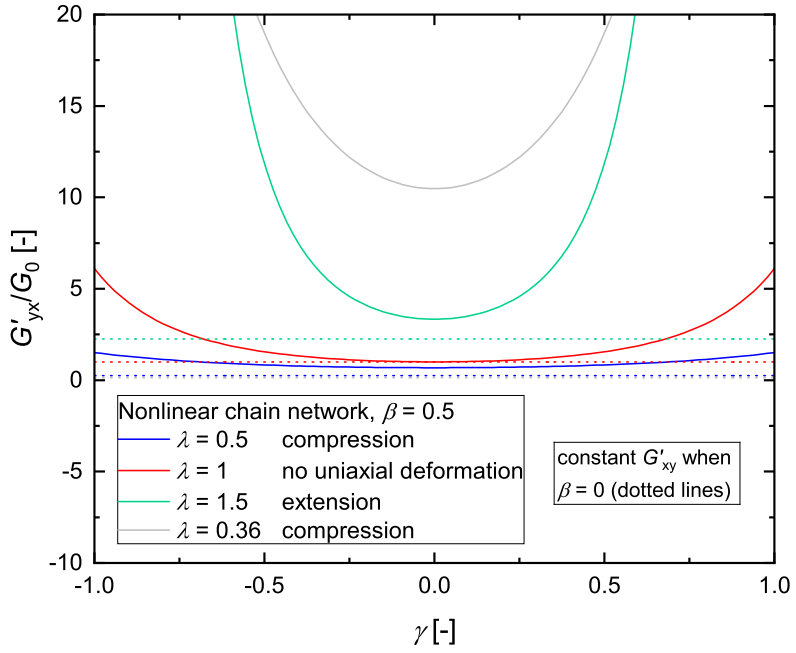

Figure 4.15: The nonlinear chain network apparent shear modulus normalized by the shear modulus of a material under uniaxial pre-strain and applied simple shear deformation. This figure is created from equation 4.31.

where k_b is the Boltzmann constant, T is the temperature, $\underline{R}$ describes the dimensions of the polymer chain after deformation, and $\beta^2 = 3/(2N_k b_k^2)$ where N_k is the number of random walk steps and b_k is the Kuhn length. The force on a single polymer chain in the shearing direction is a function of both the uniaxial deformation and the shear deformation since $R_x = \lambda^{-1/2} R'_x + \lambda\gamma R'_y$,

$$f_x \sim R_x = \lambda^{-1/2} R'_x + \lambda\gamma R'_y. \tag{4.35}$$

The force as a function of the extension ratio can be seen in Figure 4.20.

The stress can be found by the rationale $\sigma \sim \frac{f}{A} \sim \frac{f}{chain} \frac{\#chain}{A}$. The total stress equation is

$$\underline{\underline{T}} = \nu < \underline{R}\,\underline{f} > \tag{4.36}$$

where ν is the number of elastically active chains per volume. Assuming that

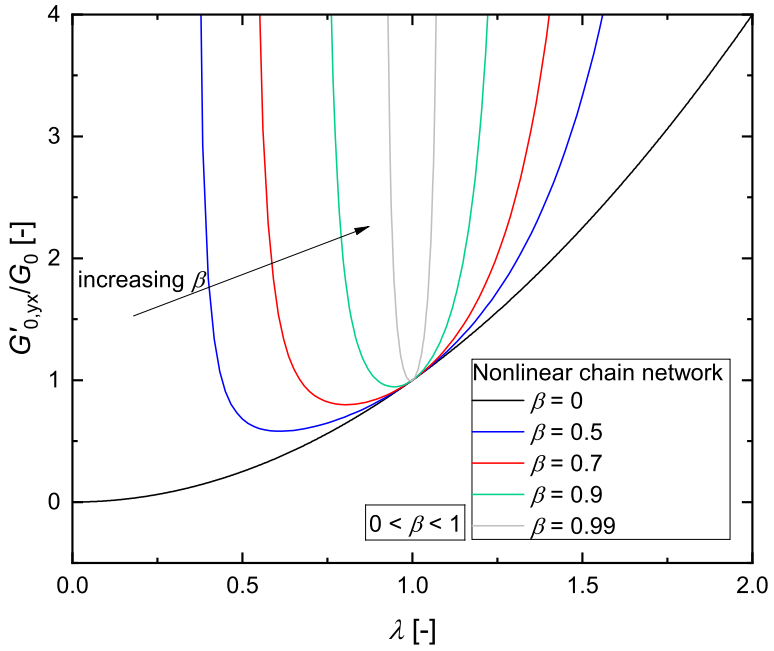

Figure 4.16: The nonlinear chain network apparent tangent shear modulus normalized by the shear modulus of a material under uniaxial pre-strain and applied simple shear deformation. This figure is created from equation 4.31 when $\gamma = 0$.

force is linear, the stress tensor is

$$\underline{\underline{T}} = 2\nu k_b T \beta^2 < \underline{R}\,\underline{R} > \tag{4.37}$$

by combining equations 4.34 and 4.36. To solve for the deformed vector $\underline{R}$ of the polymer chains, we assume affine deformation

$$\underline{R} = \underline{\underline{F}} \cdot \underline{R'}, \tag{4.38}$$

where $\underline{R'}$ is the initial vector of the polymer chain and $\underline{\underline{F}}$ is the deformation tensor shown in equation 4.2. We find that $< \underline{R}\,\underline{R} >=< \underline{\underline{F}} \cdot \underline{R'}\,\underline{R'} \cdot \underline{\underline{F}}^T >= \underline{\underline{F}} \cdot \underline{\underline{F}}^T = \underline{\underline{B}}$. Therefore, the microscopic deformation of the polymer chains is related to the macroscopic deformation by $< \underline{RR} > \sim \underline{\underline{B}}$. By substituting this relation into equation 4.37, we find that $\underline{\underline{T}} \sim \underline{\underline{B}}$. Then, specifically for

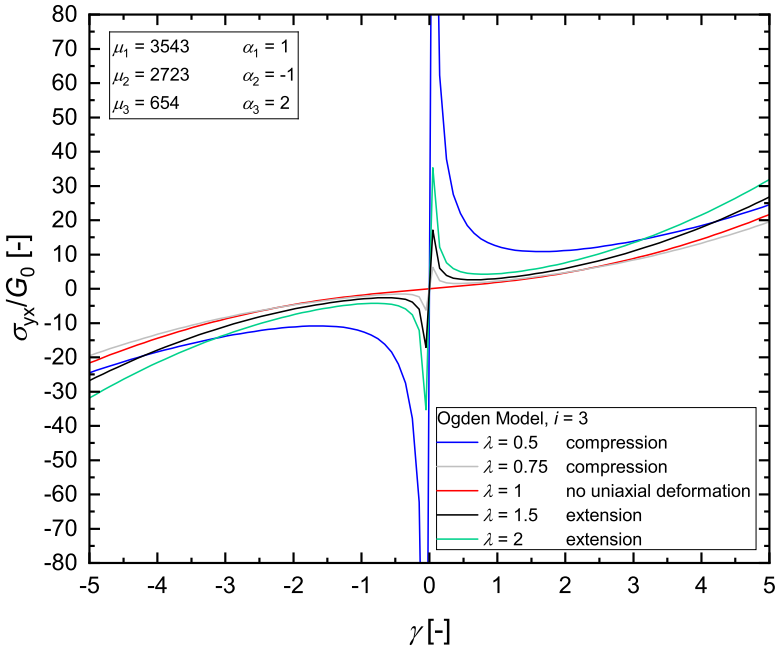

Figure 4.17: The Ogden shear stress response normalized by the shear modulus of a material under uniaxial pre-strain and applied simple shear deformation. This figure is created from equation 4.33.

the superposition of uniaxial deformation and simple shear,

$$T_{yx} = \sigma_{yx} \sim \gamma\lambda^2 \tag{4.39}$$

where λ^2 contributes to the softening behavior in compression and stiffening in extension. Therefore, the molecular theory of rubber elasticity predicts a softening behavior that scales like the Neo-Hookean model assuming a linear force extension ratio. For a constitutive model to predict a stiffening behavior, the linear force extension ratio assumption cannot be made.

4.4.4 Warner spring model

We already discussed the molecular theory of rubber elasticity assuming a linear Gaussian spring model. We found that $\underline{f} \sim \underline{R}$ and we are specifically interested in the force in the direction of shear f_x to understand the softening behavior in G'_{yx} under a combination of uniaxial deformation and simple

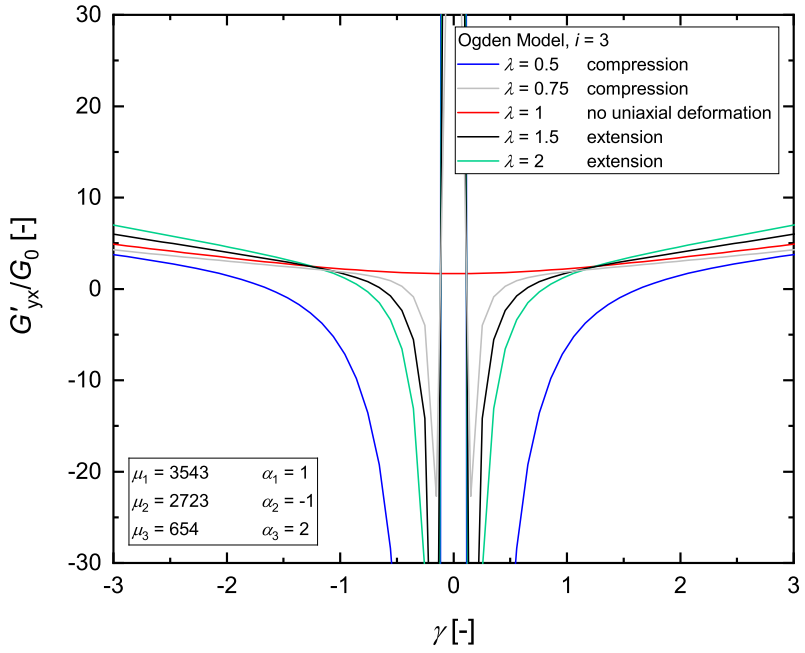

Figure 4.18: The Ogden apparent shear modulus normalized by the shear modulus of a material under uniaxial pre-strain and applied simple shear deformation. This figure is created in Origin by taking the derivative of equation 4.33 with respect to γ.

shear.

If we consider a finitely extensible nonlinear elastic (FENE) spring proposed by Warner, the force on a single polymer chain is [112, 113]

$$\underline{f} = \frac{H\underline{R}}{1 - \left(\frac{|\underline{R}|}{|\underline{R}_{max}|}\right)^2}, \tag{4.40}$$

where $H = 2k_bT\beta^2$ is the spring constant. Then the force in the direction of shear strain is nonlinearly proportional to the extension,

$$f_x \sim \frac{R_x}{1 - \left(\frac{|\underline{R}|}{|\underline{R}_{max}|}\right)^2}. \tag{4.41}$$

We can relate the force to the specific deformation of the superposition of compression and simple shear by referencing equation 4.35. Then the force is shown in equation 4.42 and has a dependence on both the uniaxial de-

Table 4.2: Apparent shear modulus equations (derived from equation 4.9) for common constitutive models for hyperelastic incompressible materials. All models only contain a maximum of 2 material property constants.

Name	**Equation**
Neo-Hookean	$G'_{yx} = G_0\lambda^2$
Mooney-Rivlin	$G'_{yx} = \lambda^2(\mu_1 + \mu_2\lambda^{-1})$
Fung	$G'_{yx} = G_0\lambda^2 e^{\alpha(\lambda^2+2\lambda^{-1}+\lambda^2\gamma^2-3)}\left(2\lambda^2\gamma^2\alpha+1\right)$
Gent	$G'_{yx} = \frac{G_0\lambda^2}{1-\beta(\lambda^2+2\lambda^{-1}+\gamma^2\lambda^2-3)}\left[1+\frac{2\lambda^2\beta\gamma^2}{(1-\beta(\lambda^2+2\lambda^{-1}+\lambda^2\gamma^2-3))^2}\right]$
Nonlinear chain network	$G'_{yx} = G_0\lambda^2\left[1+\frac{2}{(1-\beta)^2}\right]^{-1}$ $\cdot\left[1+2\left(1-\frac{\beta I_1}{3}\right)^{-2}+\frac{8}{3}\lambda^2\gamma^2\beta\left(1-\frac{\beta I_1}{3}\right)^{-3}\right]$

Table 4.3: Apparent shear modulus behavior for common constitutive models for hyperelastic incompressible materials.

Name	**Softening**	**Eventual Stiffening**
Neo-Hookean	Yes	No
Mooney-Rivlin	Yes	No
Fung	Yes	Yes
Gent	Yes	Yes
Nonlinear chain network	Yes	Yes

formation and shear deformation, similar to the Gaussian spring model that showed a softening behavior in G'_{yx} in compression. However, this model also shows a sudden stiffening behavior since the force f_x is dependent on

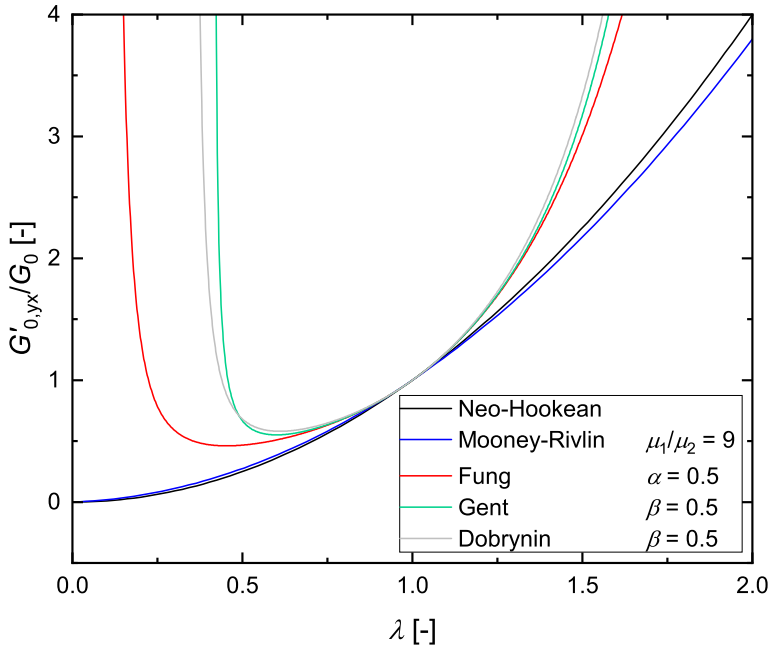

Figure 4.19: The apparent tangent shear modulus normalized by the shear modulus of a material under uniaxial pre-strain and applied simple shear deformation for all constitutive models. $G'_{0,yx}$ is equal to G'_{yx} for all models when $\gamma = 0$.

the extension ratio $\frac{|\underline{R}|}{|\underline{R}_{max}|}$,

$$f_x \sim \frac{\lambda^{-1/2} R'_x + \lambda\gamma R'_y}{1 - \left(\frac{|\underline{R}|}{|\underline{R}_{max}|}\right)^2}. \tag{4.42}$$

The force as a function of the extension ratio can be seen in Figure 4.20, where the extension ratio $\frac{|\underline{R}|}{|\underline{R}_{max}|}$ is equivalent to the nonlinearity β in the nonlinear chain network model.

4.4.5 Wormlike chain model

A popular single chain model is the worm-like chain model (WLC) [114],

$$\underline{f} = \left(\frac{|\underline{R}|}{|\underline{R_{max}}|} + \frac{1}{4\left(1 - \frac{|\underline{R}|}{|\underline{R_{max}}|}\right)^2} - \frac{1}{4} \right) \frac{k_b T}{A}. \tag{4.43}$$

The force is dependent on the uniaxial stretch λ and shear strain γ similar to the Warner spring model. Therefore, this single chain model can predict an initial compression-softening of apparent shear modulus and a sudden compression-stiffening of apparent shear modulus at a critical strain. The Gent constitutive model is also based off of a WLC model. The force as a function of the extension ratio can be seen in Figure 4.20.

4.4.6 Freely jointed chain model

The freely jointed chain model (FJC) is a common single chain model used to describe nonlinear elastic behavior and capture the finite extensibility of polymer chains. The nonlinear chain network constitutive model is derived from the freely jointed chain model [105]. The force equation for the FJC model is [115]

$$\frac{|\underline{R}|}{|\underline{R_{max}}|} = L\xi\left(\frac{3f}{2\beta^2|\underline{R_{max}}|k_b T}\right), \tag{4.44}$$

where $\xi(...)$ is the Langevin function [116]. The force as a function of the extension ratio can be seen in Figure 4.20.

4.4.7 Force vs. extension ratio

In Figure 4.20, we show that the force on a single polymer chain is linearly proportional to the extension ratio assuming the Gaussian spring model. This corresponds to the compression-softening of apparent shear modulus for the Neo-Hookean model. However, the force sharply increases at larger extension ratios assuming the Wagner spring model, wormlike chain model, and freely jointed chain model, corresponding to the sharp compression-stiffening of apparent shear modulus for the Gent and nonlinear chain network models.

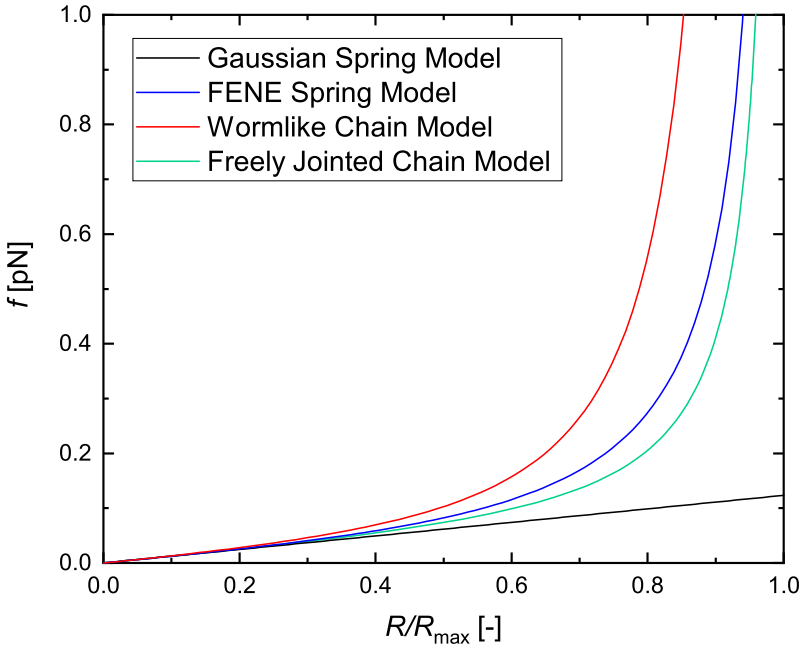

Figure 4.20: The force on a single chain with respect to the extension ratio of a single chain. The Gaussian spring model predicts a linear relationship. The FENE, WLC, and FJC models predict a nonlinear relationship where the force dramatically increases with an increasing extension ratio. This figure is created by referencing equations 4.34, 4.40, 4.43, and 4.44.

As discussed in this section, the force and extension ratio are dependent on both λ and γ. Additionally, the extension ratio is dependent on the initial extension ratio before any macroscopic deformation, which relates to the nonlinearity term in the Gent and nonlinear chain network models.

Therefore, Figure 4.20 can be used as a design tool for designing nonlinear elastic materials where a large extension ratio is desired for a rapid increase in force and a dramatic stiffening behavior. This dramatic stiffening behavior has been shown in work with fibrin and collagen [106, 107, 117].

4.5 Conclusions

In this work, we investigated the predictive performance G'_{yx} of many common hyperelastic constitutive models under the specific deformation of a

superposition of uniaxial and simple shear strains. This type of deformation is common in unconstrained magnetorheological materials as discussed in Chapter 3.

We showed that all constitutive models that were investigated showed an initial compression-softening of apparent shear modulus G'_{yx}. The Fung, Gent, and nonlinear chain network models showed a sudden stiffening behavior in compression only after a critical strain limit was reached. The Ogden model seemed to be incompatible with this type of deformation. All hyperelastic models, to the best of our knowledge, predict an initial compression-softening behavior, which has never been reported before. However, this initial softening behavior is not apparent from experimental work for biological tissues [46]. Therefore, there is a need for new hyperelastic models that can predict the stiffening observed in these studies.

The effect of the material constant parameters on the predictive performance was discussed. The most notable comment on the material constant parameters would be that a larger nonlinear parameter decreased the degree of softening and the stiffening behavior could be approached with a smaller compressive and shear deformation.

The predictive performance of the hyperelastic constitutive models was further explained by relating these macroscopic models to corresponding single chain models and the molecular theory of rubber elasticity. We are able to draw conclusions on design of the microstructure and the effect that the extension ratio (nonlinearity) can have on the stiffening behavior which is apparent in experiments with Fibrin [106, 107, 117].

As discussed, these constitutive models predict an initial softening of G'_{yx} under compression and this behavior is seen in experimental work for semi-flexible polymers and biopolymer networks. This finding leaves a lingering question: Is it possible to make a functional ultra-soft material by applying a uniaxial compressive load at a micro- or molecular scale? We previously showed in Chapter 3 that magnetorheological elastomers can compress when a magnetic field is induced. However, this typically leads to a stiffening of G'_{yx} due to magnetic dipole-dipole interactions. The design space for functional materials needs to be explored in more depth to potentially design these ultra-soft materials.

CHAPTER 5

CONCLUSIONS AND FUTURE WORK

This thesis explored existing design tools (Chapter 1), identified limitations (Chapter 1), and presented new design tools (Chapter 2) for rheologically-complex soft solids with a focus on material selection charts and constitutive equations. We studied mathematical models to support the 'design of' nonlinear elastic functional solids for soft machines (Chapter 3). We studied the behavior of magnetorheological elastomers (MRE's), and specifically the effect that nonlinearity and softness have on the variable shear stiffness response of MRE's. We studied constitutive models under an initial uniaxial stretch (pre-strain) and imposed simple shear to understand the effect on shear stiffness (Chapter 4). Surprisingly, we found that many of the constitutive models that were studied soften in compression and some eventually stiffen in compression when a finite elastic strain is achieved. Overall, throughout this thesis we made a contribution to knowledge through studies that support the 'design with' nonlinear elastic solids and the 'design of' nonlinear elastic solids specific to soft machine and soft material design.

There is much future work that could be done based on this research contribution. This includes creating additional design tools to support the 'design with' materials for soft machine design. Based on the literature review, there is a limited number of existing material selection charts ideal for soft machine design and an effort could be put forth in future work to populate a design toolbox for soft machine design.

Future work could be done with MRE variable shear stiffness predictions by comparing uniaxial compression predictions to extension predictions by changing the distribution of magnetic particles in the MRE. Also, the effect of the choice of nonlinear elastic model on the MRE predictions could be studied. For instance, how do the Neo-Hookean model MRE predictions compare to the Fung model MRE predictions? Also, future work could be done to describe the MRE predictions in a universal language considering

the nonlinear parameter b. The nonlinear MRE model assumptions could also be relaxed to more closely relate to experimental work (see conclusions in Chapter 3) [57].

The MRE model predictions that were discussed in Chapter 3 could be further supported by experiments. Various pre-strains could be applied to a nonlinear elastic sample on a rheometer before applying a simple shear strain to experimentally research the effect of pre-strain on shear stiffness. A bio-polymer network (like fibrin) is expected to show compression-softening of apparent shear modulus initially before showing compression-stiffening of apparent shear modulus at a critical strain.

Additionally, MRE predictions could be made for a confined MRE. This model is more complicated because the internal strains cannot be directly related to the external strains $\varepsilon = 0$. Experiments could also be made on a rheometer using a fixed gap to support the model predictions of a confined MRE.

REFERENCES

[1] A. Seibel and L. Schiller, "Systematic engineering design helps creating new soft machines," *Robotics and Biomimetics*, vol. 5, Oct 2018. [Online]. Available: https://doi.org/10.1186/s40638-018-0088-4

[2] J. E. Shigley, *Mechanical Engineering Design*. McGraw-Hill College, 1993.

[3] M. Kovač, "The bioinspiration design paradigm: A perspective for soft robotics," *Soft Robotics*, vol. 1, pp. 28–37, Mar 2014. [Online]. Available: http://doi.org/10.1089/soro.2013.0004

[4] Z. Zhakypov and J. Paik, "Design methodology for constructing multimaterial origami robots and machines," *IEEE Transactions on Robotics*, vol. 34, pp. 151–165, Jan 2018. [Online]. Available: https://doi.org/10.1109/TRO.2017.2775655

[5] Z. S. Jianyu Li and J. J. Vlassak, "Stiff, strong, and tough hydrogels with good chemical stability," *Journal of Materials Chemistry B*, vol. 2, pp. 6708–6713, Aug 2014. [Online]. Available: https://doi.org/10.1039/C4TB01194E

[6] Y. C. C. M. F. I. E. A. Liyu Wang, Yang Yang and Q. Pei, "Controllable and reversible tuning of material rigidity for robot applications," *Materials Today*, vol. 21, pp. 563–576, June 2018. [Online]. Available: https://doi.org/10.1016/j.mattod.2017.10.010

[7] P. L. Stephen Coyle, Carmel Majidi and K. J. Hsia, "Bio-inspired soft robotics: Material selection, actuation, and design," *Extreme Mechanics Letters*, vol. 22, pp. 51–59, July 2018. [Online]. Available: https://doi.org/10.1016/j.eml.2018.05.003

[8] R. L. Truby and J. A. Lewis, "Printing soft matter in three dimensions," *Nature*, vol. 540, pp. 371–378, Dec 2016. [Online]. Available: https://doi.org/10.1038/nature21003

[9] D. J. F. B. M. G. M. W. J. A. L. Michael Wehner, Ryan L. Truby and R. J. Wood, "An integrated design and fabrication strategy for entirely soft, autonomous robots," *Nature*, vol. 536, pp. 451–455, Aug 2016. [Online]. Available: https://doi.org/10.1038/nature19100

[10] O. C.-D. L. Torre, "Elastic stiffening in pva-borax studied with experimental medium amplitude oscillatory shear," *UIUC Thesis*, Aug 2017. [Online]. Available: https://doi.org/10.1007/s10853-012-6855-7

[11] M. S. Dmytro Ivaneyko, Vladimir P. Toshchevikov and G. Heinrich, "Magneto-sensitive elastomers in a homogeneous magnetic field: A regular rectangular lattice model," *Macromolecular Theory and Simulations*, vol. 20, pp. 411–424, Jun 2011. [Online]. Available: https://doi.org/10.1002/mats.201100018

[12] A. V. Dobrynin and J.-M. Y. Carrillo, "Universality in non-linear elasticity of biological and polymeric networks and gels," *Macromolecules*, vol. 44, pp. 140–146, 2011. [Online]. Available: https://doi.org/10.1021/ma102154u

[13] M. F. Ashby, *Materials Selection in Mechanical Design.* Butterworth-Heinemann, 2010.

[14] R. C. D. K. W. M. W. I. D. Trivedi, Deepak, "Soft robotics: Biological inspiration, state of the art, and future research," *Applied Bionics and Biomechanics*, vol. 5, pp. 99–117, 2008. [Online]. Available: DOI: 10.1080/11762320802557865

[15] J. Paik, "Soft robot design methodology for 'push-button' manufacturing," *Nature Reviews Materials*, vol. 3, p. 81–83, May 2018. [Online]. Available: https://doi.org/10.1038/s41578-018-0014-y

[16] R. F. S. Shuo Li, Hedan Bai and H. Zhao, "Bio-inspired design and additive manufacturing of soft materials, machines, robots, and haptic interfaces," *Angewandte Chemie International Edition*, vol. 58, Feb 2019. [Online]. Available: https://doi.org/10.1002/anie.201813402

[17] C. Majidi, "Soft-matter engineering for soft robotics," *Advanced Materials Technologies*, Dec 2018. [Online]. Available: https://doi.org/10.1002/admt.201800477

[18] S. B. K. D. T. A. M. D. Steck, J. Qu and J. Kameoka, "Mechanical responses of ecoflex silicone rubber: Compressible and incompressible behaviors," *Applied Polymer Science*, Aug 2018. [Online]. Available: https://doi.org/10.1002/app.47025

[19] T. J. O. M. D. M. James S. Peerless, Nina J. B. Milliken and Y. G. Yingling, "Soft matter informatics: Current progress and challenges," *Advanced Theory and Simulations*, vol. 2, Nov 2018. [Online]. Available: https://doi.org/10.1002/adts.201800129

[20] A. Z. Nelson, K. S. Schweizer, B. M. Rauzan, R. G. Nuzzo, J. Vermant, and R. H. Ewoldt, "Designing and transforming yield-stress fluids," *Current Opinion in Solid State and Materials Science*, vol. 23, no. 5, p. 100758, 2019. [Online]. Available: http://www.sciencedirect.com/science/article/pii/S1359028619300762

[21] R. H. Ewoldt, "Extremely soft: Design with rheologically complex fluids," *Soft Robotics*, vol. 1, no. 1, pp. 12–20, 2014. [Online]. Available: https://doi.org/10.1089/soro.2013.1508

[22] N. A. B. J. T. A. R. H. E. R. E. Corman, Lakshmi Rao, "Setting material function design targets for linear viscoelastic materials and structures," *Journal of Mechanical Design*, vol. 138, no. 5, p. 051402, 2016. [Online]. Available: https://doi.org/10.1115/1.4032698

[23] S. P. L. L. S. C. T. L. Guoying Gu, Haipeng Xu and X. Guo, "Integrated soft ionotronic skin with stretchable and transparent hydrogel–elastomer ionic sensors for hand-motion monitoring," *Soft Robotics*, vol. 6, June 2019. [Online]. Available: https://doi.org/10.1089/soro.2018.0116

[24] W. C. S. A. M. A. A. S. A. D. M. X. C. M. W. G. M. W. R. F. Shepherd, F. Ilievski, "Multigait soft robot," *Proceedings of the National Academy of Sciences*, Dec 2011. [Online]. Available: https://doi.org/10.1073/pnas.1116564108

[25] S.-E. C. H. L. J. K. Jiyun Kim, Su Eun Chung and S. Kwon, "Programming magnetic anisotropy in polymeric microactuators," *Nature Materials*, vol. 10, pp. 747–752, Aug 2011. [Online]. Available: https://doi.org/10.1038/nmat3090

[26] X. D. H. M. O. E. W. H. Guo Zhan Lum, Zhou Ye and M. Sitti, "Shape-programmable magnetic soft matter," *Proceedings of the National Academy of Sciences*, Oct 2016. [Online]. Available: https://doi.org/10.1073/pnas.1608193113

[27] S. G. M. S. S. Tasoglu, E. Diller and U. Demirci, "Untethered micro-robotic coding of three-dimensional material composition," *Nature Communications*, vol. 5, Jan 2014. [Online]. Available: https://doi.org/10.1038/ncomms4124

[28] G. Y. Zhou, "Shear properties of a magnetorheological elastomer," *Smart Materials and Structures*, vol. 12, pp. 139–146, Jan 2003. [Online]. Available: 10.1088/0964-1726/12/1/316

[29] C. M. M. T. N. X. F. . X. Z. Hyunwoo Yuk, Shaoting Lin, "Hydraulic hydrogel actuators and robots optically and sonically camouflaged in water," *Nature Communications*, vol. 8, Feb 2017. [Online]. Available: https://doi.org/10.1038/ncomms14230

[30] "Soft robotics toolkit." [Online]. Available: https://softroboticstoolkit.com/home

[31] *Soft Robotics*. [Online]. Available: https://home.liebertpub.com/publications/soft-robotics/616/overview

[32] *Bioinspiration Biomimetics*. [Online]. Available: https://iopscience.iop.org/journal/1748-3190

[33] *IEEE: Institute of Electrical and Electronics Engineers*. [Online]. Available: https://www.ieee.org/

[34] *Nature*. [Online]. Available: https://www.nature.com/

[35] J. B. William Murphy and G. Hastings, Eds., *Handbook of Biomaterial Properties*. Springer, 2016.

[36] *Materials Data Book*. Cambridge University Engineering Department, 2003.

[37] "Polymer database (polyinfo)." [Online]. Available: https://polymer.nims.go.jp/index-en.html

[38] "Crow polymer database." [Online]. Available: http://www.polymerdatabase.com/

[39] "Matweb material property data." [Online]. Available: http://www.matweb.com/

[40] "Citrine informatics." [Online]. Available: https://citrine.io/research/open-citrination-platform/

[41] "Material properties database." [Online]. Available: https://www.makeitfrom.com/

[42] "Granta design." [Online]. Available: https://grantadesign.com/

[43] A. S. P.S. Ramalhete and C. Aguiar, "Digital tools for material selection in product design," *Materials and Design*, vol. 31, pp. 2275–2287, May 2010. [Online]. Available: https://doi.org/10.1016/j.matdes.2009.12.013

[44] E. C. Nikolas Kastor, Vishesh Vikas and R. D. White, "A definition of soft materials for use in the design of robots," *Soft Robotics*, vol. 4, pp. 181–182, Sep 2017. [Online]. Available: http://doi.org/10.1089/soro.2017.29012.nka

[45] A. F. Bower, *Applied Mechanics of Solids*. CRC Press, 2012.

[46] P. A. J. L. Angela Mihai, LiKang Chin and A. Goriely, "A comparison of hyperelastic constitutive models applicable to brain and fat tissues," *Journal of the Royal Society Interface*, Sep 2015. [Online]. Available: https://doi.org/10.1098/rsif.2015.0486

[47] Y. cheng Fung, *Biomechanics: mechanical properties of living tissues.* Springer Science Business Media, 2013.

[48] R. K. K. Andrew D. Marchese and D. Rus, "A recipe for soft fluidic elastomer robots," *Soft Robotics*, vol. 2, Mar 2015. [Online]. Available: https://doi.org/10.1089/soro.2014.0022

[49] J. W. B. J. R. R. A. C. A. K. J. D. B. M. F. D. Alexander D. Valentine, Travis A. Busbee and J. A. Lewis, "Hybrid 3d printing of soft electronics," *Advanced Materials*, Sep 2017. [Online]. Available: https://doi.org/10.1002/adma.201703817

[50] L. Böcker, P. A. Rühs, L. Böni, P. Fischer, and S. Kuster, "Fiber-enforced hydrogels: Hagfish slime stabilized with biopolymers including -carrageenan," *ACS Biomaterials Science & Engineering*, vol. 2, no. 1, pp. 90–95, 2016. [Online]. Available: https://doi.org/10.1021/acsbiomaterials.5b00404

[51] R. H. Ewoldt, T. M. Winegard, and D. S. Fudge, "Non-linear viscoelasticity of hagfish slime," *International Journal of Non-Linear Mechanics*, vol. 46, no. 4, pp. 627 – 636, 2011, special issue on non-linear mechanics of biological structures. [Online]. Available: http://www.sciencedirect.com/science/article/pii/S0020746210001629

[52] G. Chaudhary, D. S. Fudge, B. Macias-Rodriguez, and R. H. Ewoldt, "Concentration-independent mechanics and structure of hagfish slime," *Acta Biomaterialia*, vol. 79, pp. 123 – 134, 2018. [Online]. Available: http://www.sciencedirect.com/science/article/pii/S1742706118304896

[53] T. J. M. C. F. K. S. S. F. C. T. v. d. H. S. J. P. A. F. C. G. P. A. W. H. S. H. J. S. Ivo Schoemaker, Pepijn P. W. Hoefnagel, "Elasticity, viscosity, and deformation of orbital fat," *Investigative Ophthalmology Visual Science*, vol. 47, pp. 4819–4826, 2006.

[54] W. Grellmann, A. Berghaus, E.-J. Haberland, Y. Jamali, K. Holweg, K. Reincke, and C. Bierögel, "Determination of strength and deformation behavior of human cartilage for the definition of significant parameters," *Journal of Biomedical Materials Research Part A*, vol. 78A, no. 1, pp. 168–174, 2006. [Online]. Available: https://onlinelibrary.wiley.com/doi/abs/10.1002/jbm.a.30625

[55] B. BHUSHAN, W. TANG, and S. GE, "Nanomechanical characterization of skin and skin cream," *Journal of Microscopy*, vol. 240, no. 2, pp. 135–144, 2010. [Online]. Available: https://onlinelibrary.wiley.com/doi/abs/10.1111/j.1365-2818.2010.03407.x

[56] M. Pawlaczyk, M. Lelonkiewicz, and M. Wieczorowski, "Review papers¡br¿age-dependent biomechanical properties of the skin," *Advances in Dermatology and Allergology/Postepy Dermatologii i Alergologii*, vol. 30, no. 5, pp. 302–306, 2013. [Online]. Available: http://dx.doi.org/10.5114/pdia.2013.38359

[57] G. Chaudhary, "Mechanics of biopolymer networks, stimuli responsive particle suspensions, and their combinations," Ph.D. dissertation, University of Illinois, Urbana, Aug. 2019. [Online]. Available: http://hdl.handle.net/2142/105943

[58] A. N. Bharadwaj, "Asymptotically nonlinear oscillatory shear: theory, modeling, measurements and applications of nonlinear elasticity to stimuli-responsive composites," Ph.D. dissertation, University of Illinois, Urbana, Aug. 2016. [Online]. Available: http://hdl.handle.net/2142/93007

[59] R. I. Litvinov and J. W. Weisel, "Fibrin mechanical properties and their structural origins," *Matrix Biology*, vol. 60-61, pp. 110 – 123, 2017, special issue on Provisional Matrix. [Online]. Available: http://www.sciencedirect.com/science/article/pii/S0945053X16301846

[60] S. Lin-Gibson, S. Bencherif, J. A. Cooper, S. J. Wetzel, J. M. Antonucci, B. M. Vogel, F. Horkay, and N. R. Washburn, "Synthesis and characterization of peg dimethacrylates and their hydrogels," *Biomacromolecules*, vol. 5, no. 4, pp. 1280–1287, 2004, pMID: 15244441. [Online]. Available: https://doi.org/10.1021/bm0498777

[61] K. Sungsanit, N. Kao, and S. Bhattacharya, "Properties of linear poly(lactic acid)/polyethylene glycol blends," *Polymer Engineering & Science*, vol. 52, no. 1, pp. 108–116, 2012. [Online]. Available: https://www.onlinelibrary.wiley.com/doi/abs/10.1002/pen.22052

[62] A. Nakayama, A. Kakugo, J. Gong, Y. Osada, M. Takai, T. Erata, and S. Kawano, "High mechanical strength double-network hydrogel with bacterial cellulose," *Advanced Functional Materials*, vol. 14, no. 11, pp. 1124–1128, 2004. [Online]. Available: https://onlinelibrary.wiley.com/doi/abs/10.1002/adfm.200305197

[63] W. R. K. I. O. C. K. H. O. D. J. M. J. J. V. . Z. S. Jeong-Yun Sun, Xuanhe Zhao, "Highly stretchable and tough hydrogels," *Nature*, vol. 489, pp. 133–136, 2012. [Online]. Available: https://doi.org/10.1038/nature11409

[64] J. Xu, W. H. Schwarz, J. A. Käs, T. P. Stossel, P. A. Janmey, and T. D. Pollard, "Mechanical properties of actin filament networks depend on preparation, polymerization conditions, and storage of actin monomers," *Biophysical Journal*, vol. 74, no. 5, pp. 2731 – 2740, 1998. [Online]. Available: http://www.sciencedirect.com/science/article/pii/S0006349598779792

[65] A. El-Shamy, W. Attia, and K. A. El-Kader], "The optical and mechanical properties of pva-ag nanocomposite films," *Journal of Alloys and Compounds*, vol. 590, pp. 309 – 312, 2014. [Online]. Available: http://www.sciencedirect.com/science/article/pii/S0925838813029459

[66] L. Zhang, J. Zhao, J. Zhu, C. He, and H. Wang, "Anisotropic tough poly(vinyl alcohol) hydrogels," *Soft Matter*, vol. 8, pp. 10 439–10 447, 2012. [Online]. Available: http://dx.doi.org/10.1039/C2SM26102B

[67] A. Dixit, D. S. Bag, and S. Kalra, "Synthesis of strong and stretchable double network (dn) hydrogels of pva-borax and p(am-co-hema) and study of their swelling kinetics and mechanical properties," *Polymer*, vol. 119, pp. 263 – 273, 2017. [Online]. Available: http://www.sciencedirect.com/science/article/pii/S003238611730469X

[68] M. Amjadi, Y. J. Yoon, and I. Park, "Ultra-stretchable and skin-mountable strain sensors using carbon nanotubes–ecoflex nanocomposites," *Nanotechnology*, vol. 26, no. 37, p. 375501, aug 2015. [Online]. Available: https://doi.org/10.1088/0957-4484/26/37/375501

[69] C. Larson, B. Peele, S. Li, S. Robinson, M. Totaro, L. Beccai, B. Mazzolai, and R. Shepherd, "Highly stretchable electroluminescent skin for optical signaling and tactile sensing," *Science*, vol. 351, no. 6277, pp. 1071–1074, 2016. [Online]. Available: https://science.sciencemag.org/content/351/6277/1071

[70] J. C. Case, E. L. White, and R. K. Kramer, "Soft material characterization for robotic applications," *Soft Robotics*, vol. 2, no. 2, pp. 80–87, 2015. [Online]. Available: https://doi.org/10.1089/soro.2015.0002

[71] D. J. Buckwalter, M. Zhang, D. L. Inglefield, R. B. Moore, and T. E. Long, "Synthesis and characterization of siloxane-containing poly(urea oxamide) segmented copolymers," *Polymer*, vol. 54, no. 18, pp. 4849 – 4857, 2013. [Online]. Available: http://www.sciencedirect.com/science/article/pii/S0032386113006502

[72] S. Coyle, C. Majidi, P. LeDuc, and K. J. Hsia, "Bio-inspired soft robotics: Material selection, actuation, and design," *Extreme Mechanics Letters*, vol. 22, pp. 51 – 59, 2018. [Online]. Available: http://www.sciencedirect.com/science/article/pii/S2352431617302316

[73] J. Guan, K. L. Fujimoto, M. S. Sacks, and W. R. Wagner, "Preparation and characterization of highly porous, biodegradable polyurethane scaffolds for soft tissue applications," *Biomaterials*, vol. 26, no. 18, pp. 3961 – 3971, 2005. [Online]. Available: http://www.sciencedirect.com/science/article/pii/S014296120400938X

[74] J. Oberdisse, "Structure and rheological properties of latexsilica nanocomposite films: stressstrain isotherms," *Macromolecules*, vol. 35, no. 25, pp. 9441–9450, 2002. [Online]. Available: https://doi.org/10.1021/ma020635d

[75] I. D. Johnston, D. K. McCluskey, C. K. L. Tan, and M. C. Tracey, "Mechanical characterization of bulk sylgard 184 for microfluidics and microengineering," *Journal of Micromechanics and Microengineering*, vol. 24, no. 3, p. 035017, feb 2014. [Online]. Available: https://doi.org/10.1088/0960-1317/24/3/035017

[76] J. C. Case, E. L. White, and R. K. Kramer, "Soft material characterization for robotic applications," *Soft Robotics*, vol. 2, no. 2, pp. 80–87, 2015. [Online]. Available: https://doi.org/10.1089/soro.2015.0002

[77] Y. Li, J. Li, W. Li, and B. Samali, "Development and characterization of a magnetorheological elastomer based adaptive seismic isolator," *Smart Materials and Structures*, vol. 22, no. 3, p. 035005, jan 2013. [Online]. Available: https://doi.org/10.1088/0964-1726/22/3/035005

[78] J. D. W. Madden, N. A. Vandesteeg, P. A. Anquetil, P. G. A. Madden, A. Takshi, R. Z. Pytel, S. R. Lafontaine, P. A. Wieringa, and I. W. Hunter, "Artificial muscle technology: physical principles and naval prospects," *IEEE Journal of Oceanic Engineering*, vol. 29, no. 3, pp. 706–728, July 2004.

[79] R. D. Kornbluh, H. Prahlad, R. Pelrine, S. Stanford, M. A. Rosenthal, and P. A. von Guggenberg, "Rubber to rigid, clamped to undamped: toward composite materials with wide-range controllable stiffness and damping," in *Smart Structures and Materials 2004: Industrial and Commercial Applications of Smart Structures Technologies*, E. H. Anderson, Ed., vol. 5388, International Society for Optics and Photonics. SPIE, 2004. [Online]. Available: https://doi.org/10.1117/12.548971 pp. 372 – 386.

[80] I. Levental, P. C. Georges, and P. A. Janmey, "Soft biological materials and their impact on cell function," *Soft Matter*, vol. 3, pp. 299–306, 2007. [Online]. Available: http://dx.doi.org/10.1039/B610522J

[81] V. S. R. S. J. C. V. . S. L.-M. P. Costa, J. Silva, "Mechanical, electrical and electro-mechanical properties of thermoplastic elastomer styrene–butadiene–styrene/multiwall carbon nanotubes composites," *Journal of Materials Science*, vol. 48, pp. 1172–1179, Sep 2013. [Online]. Available: https://doi.org/10.1007/s10853-012-6855-7

[82] F. C. M. T. C. L. . P. A. J. Cornelis Storm, Jennifer J. Pastore, "Nonlinear elasticity in biological gels," *Nature*, vol. 435, pp. 191–194, 2005. [Online]. Available: https://doi.org/10.1038/nature03521

[83] C. R. D. . E. A. F. Junhua Zhang, "Characterization of polyacrylamide gels as an elastic model for food gels," *Rheologica Acta*, vol. 44, pp. 622–630, 2005. [Online]. Available: https://doi.org/10.1007/s00397-005-0444-5

[84] L. M. Barrangou, C. R. Daubert, and E. A. Foegeding], "Textural properties of agarose gels. i. rheological and fracture properties," *Food Hydrocolloids*, vol. 20, no. 2, pp. 184 – 195, 2006, 7th International Hydrocolloids Conference. [Online]. Available: http://www.sciencedirect.com/science/article/pii/S0268005X05001116

[85] T. Z. Pavan, E. L. Madsen, G. R. Frank, A. A. O. Carneiro, and T. J. Hall, "Nonlinear elastic behavior of phantom materials for elastography," *Physics in Medicine and Biology*, vol. 55, no. 9, pp. 2679–2692, apr 2010. [Online]. Available: https://doi.org/10.1088/0031-9155/55/9/017

[86] C. P. S. . D. S. Cronin, "Mechanical properties of ballistic gelatin at high deformation rates," vol. 49, p. 829, Jan 2009. [Online]. Available: https://doi.org/10.1007/s11340-008-9207-4

[87] H. Yuan, S. Kononov, F. S. A. Cavalcante, K. R. Lutchen, E. P. Ingenito, and B. Suki, "Effects of collagenase and elastase on the mechanical properties of lung tissue strips," *Journal of Applied Physiology*, vol. 89, no. 1, pp. 3–14, 2000, pMID: 10904029. [Online]. Available: https://doi.org/10.1152/jappl.2000.89.1.3

[88] K. Tan, S. Cheng, L. Jugé, and L. E. Bilston, "Characterising soft tissues under large amplitude oscillatory shear and combined loading," *Journal of Biomechanics*, vol. 46, no. 6, pp. 1060 – 1066, 2013. [Online]. Available: http://www.sciencedirect.com/science/article/pii/S0021929013000717

[89] S. Cheng, E. C. Clarke, and L. E. Bilston, "Rheological properties of the tissues of the central nervous system: A review," *Medical Engineering Physics*, vol. 30, no. 10, pp. 1318 – 1337, 2008, special issue to commemorate the 30th anniversary of Medical Engineering Physics. [Online]. Available: http://www.sciencedirect.com/science/article/pii/S1350453308001057

[90] P. Fernández, L. Heymann, A. Ott, N. Aksel, and P. A. Pullarkat, "Shear rheology of a cell monolayer," *New Journal of Physics*, vol. 9, no. 11, pp. 419–419, nov 2007. [Online]. Available: https://doi.org/10.1088/1367-2630/9/11/419

[91] M. H. E. A. A. P. H. L. K. M. A. V. D. Mohammad Vatankhah-Varnosfaderani, William F. M. Daniel and S. S. Sheiko, "Mimicking biological stress–strain behaviour with synthetic elastomers," *Nature*, vol. 549, pp. 497–501, Sep 2017. [Online]. Available: https://doi.org/10.1038/nature23673

[92] M. A. Cantera, M. Behrooz, R. F. Gibson, and F. Gordaninejad, "Modeling of magneto-mechanical response of magnetorheological elastomers (MRE) and MRE-based systems: a review," *Smart Materials and Structures*, vol. 26, no. 2, Jan 2017. [Online]. Available: https://doi.org/10.1088/1361-665x/aa549c

[93] S. W. Chen, R. Li, Z. Zhang, and X. J. Wang, "Micromechanical analysis on tensile modulus of structured magneto-rheological elastomer," *Smart Materials and Structures*, vol. 25, no. 3, feb 2016. [Online]. Available: https://doi.org/10.1088/0964-1726/25/3/035001

[94] M. T. Lopez-Lopez, D. Y. Borin, and A. Y. Zubarev, "Shear elasticity of isotropic magnetic gels," *Phys. Rev. E*, vol. 96, no. 7, Aug 2017. [Online]. Available: https://link.aps.org/doi/10.1103/PhysRevE.96.022605

[95] L. Chen and S. Jerrams, "A rheological model of the dynamic behavior of magnetorheological elastomers," *Journal of Applied Physics*, vol. 110, no. 1, p. 013513, 2011. [Online]. Available: https://doi.org/10.1063/1.3603052

[96] J. Maas and D. Uhlenbusch, "Experimental and theoretical analysis of the actuation behavior of magnetoactive elastomers," *Smart Materials and Structures*, vol. 25, no. 10, sep 2016. [Online]. Available: https://doi.org/10.1088/0964-1726/25/10/104002

[97] D. Ivaneyko, V. Toshchevikov, D. Borin, M. Saphiannikova, and G. Heinrich, "Mechanical properties of magneto-sensitive elastomers in a homogeneous magnetic field: Theory and experiment," *Macromolecular Symposia*, vol. 338, no. 1, pp. 96–107. [Online]. Available: https://onlinelibrary.wiley.com/doi/abs/10.1002/masy.201450401

[98] Y. Han, W. Hong, and L. E. Faidley, "Field-stiffening effect of magneto-rheological elastomers," *International Journal of Solids and Structures*, vol. 50, no. 14, pp. 2281 – 2288, 2013. [Online]. Available: http://www.sciencedirect.com/science/article/pii/S002076831300139X

[99] K. Danas, S. Kankanala, and N. Triantafyllidis, "Experiments and modeling of iron-particle-filled magnetorheological elastomers," *Journal of the Mechanics and Physics of Solids*, vol. 60, no. 1, pp. 120 – 138, 2012. [Online]. Available: http://www.sciencedirect.com/science/article/pii/S0022509611001736

[100] I. Brigadnov and A. Dorfmann, "Mathematical modeling of magneto-sensitive elastomers," *International Journal of Solids and Structures*, vol. 40, no. 18, pp. 4659 – 4674, 2003. [Online]. Available: http://www.sciencedirect.com/science/article/pii/S0020768303002658

[101] A. M. Biller, O. V. Stolbov, and Y. L. Raikher, "Modeling of particle interactions in magnetorheological elastomers," *Journal of Applied Physics*, vol. 116, no. 11, p. 114904, 2014. [Online]. Available: https://doi.org/10.1063/1.4895980

[102] Y. Shen, M. F. Golnaraghi, and G. R. Heppler, "Experimental research and modeling of magnetorheological elastomers," *Journal of Intelligent Material Systems and Structures*, vol. 15, no. 1, pp. 27–35, 2004. [Online]. Available: https://doi.org/10.1177/1045389X04039264

[103] F.-M. A. J.L.Arias, V.Gallardo, "Preparation and characterization of carbonyl iron/poly(butylcyanoacrylate) core/shell nanoparticles," *Journal of Colloid and Interface Science*, vol. 299, pp. 599–607, Jul 2006. [Online]. Available: https://doi.org/10.1016/j.jcis.2006.03.005

[104] J. D. Jackson, *Classical Electrodynamics*, 3rd ed. New York: John Wiley Sons, Inc., 1998.

[105] J.-M. Y. Carrillo, F. C. MacKintosh, and A. V. Dobrynin, "Nonlinear elasticity: From single chain to networks and gels," *Macromolecules*, vol. 46, no. 9, pp. 3679–3692, 2013. [Online]. Available: https://doi.org/10.1021/ma400478f

[106] M. Vahabi, A. Sharma, A. J. Licup, A. S. G. van Oosten, P. A. Galie, P. A. Janmey, and F. C. MacKintosh, "Elasticity of fibrous networks under uniaxial prestress," *Soft Matter*, vol. 12, pp. 5050–5060, 2016. [Online]. Available: http://dx.doi.org/10.1039/C6SM00606J

[107] A. J. L. A. S. P. A. G. F. C. M. Anne S. G. van Oosten, Mahsa Vahabi and P. A. Janmey, "Uncoupling shear and uniaxial elastic moduli of semiflexible biopolymer networks: compression-softening and stretch-stiffening," *Scientific Reports*, vol. 6, 2016. [Online]. Available: https://doi.org/10.1038/srep19270

[108] P. Tong and Y.-C. Fung, "The stress-strain relationship for the skin," *Journal of Biomechanics*, vol. 9, no. 10, pp. 649 – 657, 1976. [Online]. Available: https://doi.org/10.1016/0021-9290(76)90107-X

[109] C. O. Horgan and G. Saccomandi, "A molecular-statistical basis for the gent constitutive model of rubber elasticity," *Journal of Elasticity*, vol. 68, pp. 167–176, 2002. [Online]. Available: https://doi.org/10.1023/A:1026029111723

[110] S. X. Deng, J. Tomioka, J. C. Debes, and Y. C. Fung, "New experiments on shear modulus of elasticity of arteries," *American Journal of Physiology-Heart and Circulatory Physiology*, vol. 266, no. 1, pp. H1–H10, 1994. [Online]. Available: https://doi.org/10.1152/ajpheart.1994.266.1.H1

[111] R. G. Larson, *The structure and rheology of complex fluids*. OUP USA, 1999.

[112] B. van den Brule, "Browian dynamics simulation of finitely extensible bead-spring chains," *Journal of Non-Newtonian Fluid Mechanics*, vol. 47, pp. 357 – 378, 1993. [Online]. Available: https://doi.org/10.1016/0377-0257(93)80058-J

[113] H. R. Warner, "Kinetic theory and rheology of dilute suspensions of finitely extendible dumbbells," *Industrial & Engineering Chemistry Fundamentals*, vol. 11, no. 3, pp. 379–387, 1972. [Online]. Available: https://doi.org/10.1021/i160043a017

[114] J. F. Marko and E. D. Siggia, "Stretching dna," *Macromolecules*, vol. 28, no. 26, pp. 8759–8770, 1995. [Online]. Available: https://doi.org/10.1021/ma00130a008

[115] G. Glatting, R. Winkler, and P. Reineker, "Partition function and force extension relation for a generalized freely jointed chain," *Macromolecules*, vol. 26, no. 22, pp. 6085–6091, 1993.

[116] S. S. Andrews, "Methods for modeling cytoskeletal and DNA filaments," *Physical Biology*, vol. 11, no. 1, p. 011001, jan 2014. [Online]. Available: https://doi.org/10.1088/1478-3975/11/1/011001

[117] G. Chaudhary, A. Ghosh, N. A. Bharadwaj, J. G. Kang, P. V. Braun, K. S. Schweizer, and R. H. Ewoldt, "Thermoresponsive stiffening with microgel particles in a semiflexible fibrin network," *Macromolecules*, vol. 52, no. 8, pp. 3029–3041, 2019. [Online]. Available: https://doi.org/10.1021/acs.macromol.9b00124

APPENDIX A

VARIABLE SHEAR STIFFNESS PREDICTIONS

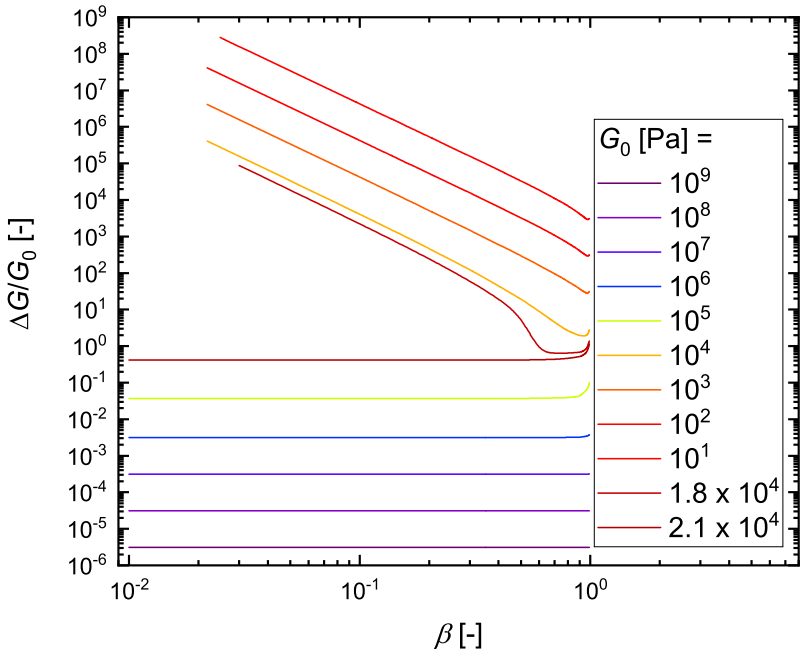

Figure A.1: The total variable shear stiffness, including contributions from the magnetic and elastic free energy of a MRE, with respect to G_0 and β. We are considering an isotropic distribution of particles $\alpha = 1$, $\phi = 0.05$, $M_s = 1582$ kA/m, $\mu_{ini} = 21.5$, and $B = 0.5$ T. This figure is created by finding the equilibrium strain using equation 3.24 and referencing equations 3.26 and 3.28 to find the variable shear stiffness.

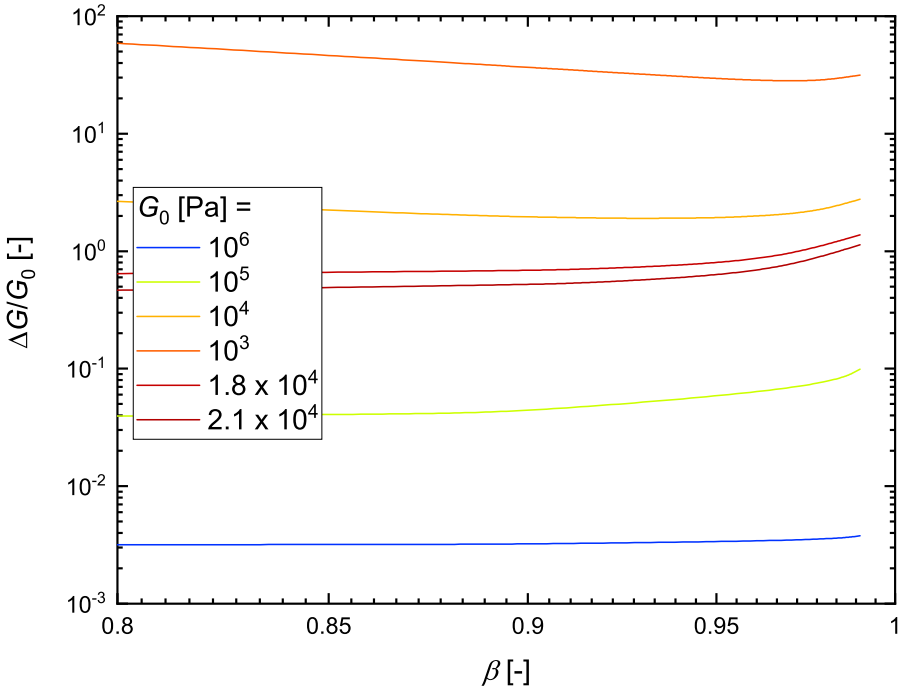

Figure A.2: The total variable shear stiffness, including contributions from the magnetic and elastic free energy of a MRE, with respect to G_0 and β. Large nonlinearities β are highlighted in this figure. We are considering an isotropic distribution of particles $\alpha = 1$, $\phi = 0.05$, $M_s = 1582$ kA/m, $\mu_{ini} = 21.5$, and $B = 0.5$ T. This figure is created by finding the equilibrium strain using equation 3.24 and referencing equations 3.26 and 3.28 to find the variable shear stiffness.

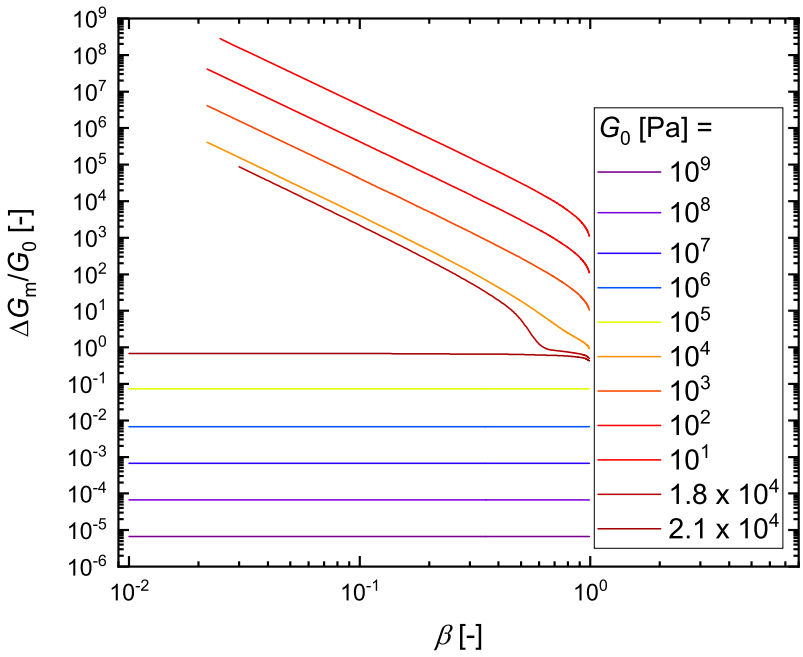

Figure A.3: The magnetic variable shear stiffness, with respect to G_0 and β, and with a constant ϕ, M_s, μ_{ini}, and B. We are considering an isotropic distribution of particles $\alpha = 1$, $\phi = 0.05$, $M_s = 1582$ kA/m, $\mu_{ini} = 21.5$, and $B = 0.5$ T. This figure is created by finding the equilibrium strain using equation 3.24 and referencing equations 3.13 and 3.29 to find the variable shear stiffness.

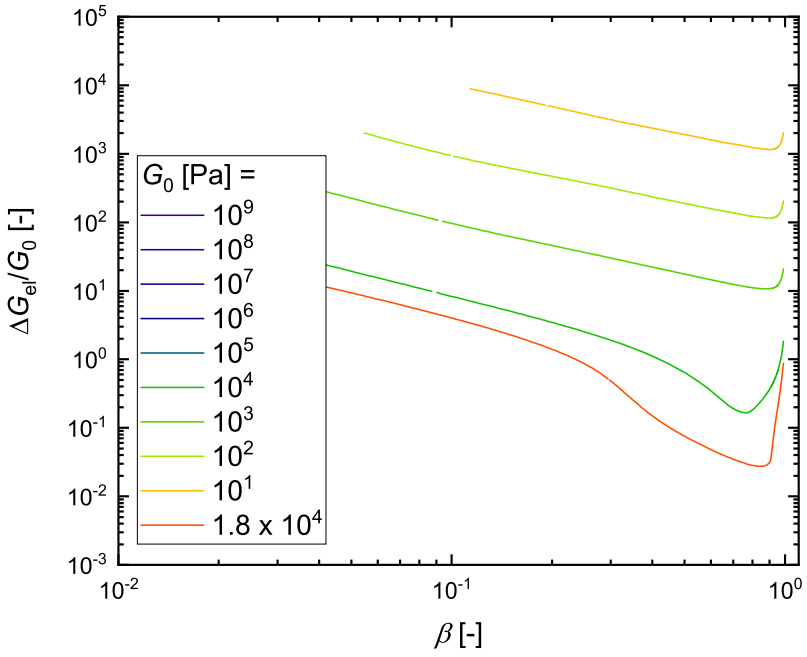

Figure A.4: A log-log representation of the elastic variable shear stiffness with respect to G_0 and β. We are considering an isotropic distribution of particles $\alpha = 1$, $\phi = 0.05$, $M_s = 1582$ kA/m, $\mu_{ini} = 21.5$, and $B = 0.5$ T. This figure is created by finding the equilibrium strain using equation 3.24 and referencing equations 3.22 and 3.30 to find the variable shear stiffness.